Fatigue of Structural and Additively Manufactured Steels: Damage Assessment and Modelling Techniques

by

Fredrik Bjørheim

Thesis submitted in fulfilment of
the requirements for the degree of
PHILOSOPHIAE DOCTOR
(PhD)

Faculty of Science and Technology
Department of Mechanical and Structural Engineering and Materials Science
2022

University of Stavanger
NO-4036 Stavanger
NORWAY
www.uis.no

ISBN: 978-82-8439-112-0
ISSN: 1890-1387
PhD Thesis UiS No. 659

Acknowledgements

This thesis is submitted in fulfilment of the requirements for the degree of Philosophiae Doctor at the University of Stavanger. The research presented herein was carried out in the Department of Mechanical and Structural Engineering and Materials Science, at the Faculty of Science and Technology from 2019 to 2022. This research was funded by the Ministry of Education and Research.

I would like to express my sincere gratitude to my supervisors, Professor Sudath C. Siriwardane and Professor Dimitrios G. Pavlou, for excellent guidance, support and advice throughout this work.

I would also thank all my colleagues at the Department of Mechanical and Structural Engineering and Materials Science during these three years, for providing a friendly and productive working environment. Especially, I would like to express my thanks to:

- Jørgen Grønsund, Emil S. Kristiansen and Caroline Einvik, for their assistance in fatigue machine maintenance and the preparation of specimens.
- Dr. Wakshum M. Tucho, for assistance regarding specimen preparation and microscopy.
- Mostafa A. Atteya and Prof. Vidar Hansen, for fruitful and pleasant discussions.
- Isabel M. La Torraca Lopez, for collaboration regarding research on additive manufacturing by Bound Metal Deposition.
- Jan-Tore Jakobsen, Johan A. Thorkaas and Mats Ingdal, for support during the experimental work of additive manufacturing.
- Prof. Tor Hemmingsen, for welcoming me to the department and for facilitating my work during the PhD project.
- John C. Grønli and Dr. Mona W. Minde, for providing funding for experimental work.

Abstract

The topics of damage assessment by in situ measurements before a macroscopic crack has been initiated, nonlinear damage modelling and additive manufacturing are herein discussed and researched from the perspective of the maintenance of ageing structures and mechanical equipment subjected to fatigue loading.

In relation to the aforementioned topics, the thesis can be categorized into three parts, all of which are related to the maintenance of ageing structures and mechanical equipment. These are: 1) Fatigue damage monitoring prior to macroscopic crack initiation, 2) Damage modelling based on S-N curves, and 3) Mechanical properties of additively manufactured steel.

1. Fatigue damage monitoring prior to macroscopic crack initiation

A conceptual framework is developed to select a method to assess small fatigue crack propagation and fatigue damage accumulation. The framework is focused on the underlying fatigue mechanism which is correlated with the measurable change for each of the identified parameters throughout the fatigue life, and how the parameter will change. The framework is based on the literature and is useful for both research and development communities, for those who are involved in structural integrity assessment.

An experimental study is also performed regarding the feasibility of adopting macroscopic hardness indentations and their correlation with fatigue damage accumulation. Both Brinell and Vickers were adopted, with Brinell being found to exhibit a more continuous change, in addition to being statistically significant.

2. Damage modelling based on S-N curves

A new damage function is proposed herein, based on the damage theory known as the theory of the S-N fatigue damage envelope. The work can be considered a framework to develop S-N curve-specific damage functions, as the underlying theory can be applied to any S-N curve for materials or structural details. Furthermore, the proposed damage function is compared with other recently proposed functions, including Miner's rule, using experimental data. The proposed function generally exhibits better prediction than Miner's rule and some of the other models.

A generalized expression/function for fatigue damage was also proposed by investigating the functional forms commonly adopted in the literature. The relation of the parameters or variables of the functional form can be represented in three dimensions, resulting in it being able to be evaluated in three dimensions with experimental data, where it will result in a surface. Herein, it is also shown that two special cases of the proposed function exist, where the parameters are reduced to a single ratio, which is subsequently evaluated based on experimental data.

3. Mechanical properties of additively manufactured steel

An experimental study is performed regarding the mechanical properties of additively manufactured steel printed by the technology of Bound Metal Deposition. Specimens were printed in various directions, which were subsequently tension tested to develop stress-strain curves. It was found that the printing technology would result in the final product exhibiting anisotropic behaviour correlated to a mesh of crack-like defects. The crack like defects also result in the conclusion that the printed specimens are expected to exhibit very poor fatigue capacity in comparison to their traditionally manufactured counterparts and also to exhibit anisotropic behaviour in relation to fatigue.

Keywords: *Fatigue damage assessment, hardness-based fatigue damage, nonlinear damage modelling, additively manufactured steel*

Table of Contents

List of Papers

Paper I: F. Bjørheim, S. C. Siriwardane, D. Pavlou, “Fatigue damage monitoring methods - current practices,” *5th International Conference on Offshore Renewable Energy – CORE*, Online, 2021, pp. 112-125.

Paper II: F. Bjørheim, S. C. Siriwardane, D. Pavlou, “A review of fatigue damage detection and measurement techniques,” *International Journal of Fatigue*, vol. 154, 2022, Art no. 106556, doi: 10.1016/j.ijfatigue.2021.106556.

Paper III: F. Bjørheim, D. Pavlou, S. C. Siriwardane, "Hardness measurements as a technique for measuring accumulated fatigue damage", *International Journal of Structural Integrity*, vol. ahead-of-print, no. ahead-of-print, 2022, doi: 10.1108/IJSI-04-2022-0061.

Paper IV: F. Bjørheim, D. G. Pavlou, S. C. Siriwardane, “Nonlinear fatigue life prediction model based on the theory of the S-N fatigue damage envelope,” *Fatigue & Fracture of Engineering Materials & Structures*, vol. 45, no. 5, pp. 1480-1493, 2022, doi:10.1111/ffe.13680.

Paper V: F. Bjørheim, S. C. Siriwardane, D. G. Pavlou, “S-N based fatigue damage modelling of offshore structures: Recent damage accumulation models and the way forward,” *8th European Congress on Computational Methods in Applied Sciences and Engineering*, 2022.

Paper VI: F. Bjørheim, I. M. La Torraca Lopez, “Tension testing of additively manufactured specimens of 17-4 PH processed by Bound Metal Deposition,” *IOP Conference Series: Materials Science and Engineering*, vol. 1201, no. 1, 2021, Art no. 012037, doi: 10.1088/1757-899X/1201/1/012037.

Abbreviations

AM	Additive manufacturing
BMD	Bound metal deposition
DED	Direct energy deposition
DFF	Design fatigue factor
DNV	Det Norske veritas
FM	Fracture mechanics
GOM	Gulf of Mexico
HCF	High cycle fatigue
ISO	International Organization for Standardization
PBF	Powder bed fusion
RBI	Risk based inspection
S-N	Stress life
S_e	Fatigue limit or knee-point stress
S_u	Ultimate tensile strength
σ_y	Yield strength

Part I – Thesis Summary

Chapter 1 Introduction

1.1 Background

An increasing number of offshore installations in the North Sea, on both the UK Continental Shelf and the Norwegian Continental Shelf, have surpassed and are continuously approaching their initial design life. In fact, since the discovery of the Ekofisk field in the Norwegian sector and the discovery of the Forties field in the UK sector, over 100 and 300 platforms, respectively, have been installed in the two sectors. Many of these have surpassed their initial design life, with over 50% of the offshore structures now effectively being in a life-extension phase [1, 2]. Furthermore, there is an increasing interest in and need for renewable energy, with the government aiming to encourage greater investment in offshore wind, to meet the rising demand for electric power emerging from the electrification of Norwegian society [3].

The long-term environmental loads acting on ageing offshore structures located in the North Sea commonly result in high cycle fatigue (HCF) being a major cause of failure [4]. In fact, one of the early drilling platforms, namely "Ocean Traveler", which was initially operated in the Gulf of Mexico (GOM) and later transported to the North Sea, was unable to endure the harsh environmental conditions in this region and subsequently needed to be repaired and strengthened [5]. This was a consequence of the platform being designed for the environmental loads related to the GOM, where cracking due to HCF is not as common [6].

The definition of fatigue can be considered "The progressive, localized, permanent structural change that occurs in materials subjected to fluctuating stresses and strains that may result in cracks or fracture after a sufficient number of fluctuations" [7]. For steels in non-corrosive environments, it is a requirement that the stresses and strains surpass a threshold level, commonly known as the knee-point stress or, alternatively, the fatigue limit. However, as the crack is formed and starts

to propagate, it will eventually reach a critical size, at which the structure will fail abruptly, without any further warning. This sudden failure after cyclic loading is commonly referred to by practising engineers as fatigue failure [8].

Although the topic of fatigue can be considered to have been researched for about two centuries now, if one defines the article "Uber Treibseile am Harz" published by Albert in 1837 [9] as the start, fatigue failure still occurs. A highly relevant example of this might be the Alexander Kielland accident in 1980, where fatigue failure of the oil rig claimed the lives of 123 people. In fact, the investigation determined that the cause of the structural collapse was a fatigue fracture in one of the bracings due to the mounting of a hydrophone. The report states that the initiating cause in this situation was the presence of a small crack after welding, as paint could be found inside the crack originating at the weld [10]. Furthermore, in March 2017 at the Gullfaks B installation, a 14.4-tonne boom of the pipe handling crane fell 10 metres down to the pipe deck while transferring materials from the pipe deck to the drill floor. The direct cause of this incident was found to be fatigue in the steel rope. Luckily, the incident did not result in any personal injuries, although the total financial cost was estimated at NOK 66 million [11]. Another recent accident occurred near Turøy, where an Airbus Helicopters EC 225 LP Super Puma lost its main rotor and thereafter impacted a small island, with all onboard being fatally injured. During the investigation, it was found that the cause of the accident was the structural/material degradation of a second-stage planet gear, where the fatigue fracture initiated from a surface micro-pit in the upper outer race of the bearing [12].

When it comes to the topic of fatigue, it can be found that a major cause of failure for bridges and offshore structures – especially those located in the North Sea – is fatigue [1, 4, 13]. For instance, in [1], it can be found that 38.3% damage cases related to bridges can be attributed to fatigue, whereas for offshore structures, this has been found to be 25%.

It has also been estimated that approximately 90% of all service failures of mechanical equipment [14].

Furthermore, Additive Manufacturing (AM) is gaining momentum within industry today. Motivations from industry are such as shorter supply chains for spare parts, i.e., being able to print spare parts either offshore or locally onshore, in order to transport the part a short distance. Effectively, instead of maintaining large storage of spare parts, i.e., "just in case" philosophy, the goal would be to have digital storage and local printing competence to result in a "just in time" maintenance philosophy. Furthermore, it is highlighted that AM technology can help both in a circular economy and in maintaining older equipment, where spare parts might not be available, resulting in the technology being considered "green" [15-17].

The increasing interest of offshore industries, such as petroleum or renewable energy, and the recent accidents related to fatigue damage mentioned herein highlight the need for further research within the domain of fatigue. In addition, as the field of AM is gaining momentum, especially for parts which will be used in mechanical equipment, it is highly important to gain further knowledge regarding the fatigue capacity of the resulting product. This is from the perspective that, as aforementioned, it has been estimated that 90% of all mechanical service failures occur due to fatigue.

1.2 Problem statements

Based on the current standards and recommended practices, with the aid of published research, the following problem statements are defined.

1. The common practice for damage assessment and life extension of ageing structures that are in service beyond the design life, is based upon the initiation and detection of a macroscopic crack and the subsequent evaluation of the crack in relation to fracture mechanics (FM). Fatigue damage monitoring techniques before initiation and detection are not available within the current standards and practices.

The common practice for life extension today is through the application of risk-based inspection (RBI) for cracks once the expected fatigue design life has been surpassed. This can be seen in standards such as NORSOK, both N-005 and N-006, in addition to the recommended practice by DNV RP-C203 [18-20]. The problem with such a methodology is that, as the expected fatigue design life is exceeded, a costly inspection programme must be initiated in the life extension phase. It should be acknowledged that a propagating macroscopic crack is certainly the strongest indicator of accumulated damage. However, it is well known that such a crack first occurs at the end of the total fatigue capacity [21-23], especially of those structural details which are subjected to high cycle fatigue, while it has been documented that significant measurable change does occur to the material before that stage [24].

2. The commonly used fatigue damage hypothesis in design standards does not accurately take into account the loading sequence effect. Consequently, this may result in uncertain estimate of the design life, by neglecting the fatigue mechanisms.

Offshore installations, bridges and other mechanical systems/equipment are subjected to fatigue damage due to the effect of variable amplitude

loading histories induced by random environmental loads, traffic, etc. [4, 25]. This damage is commonly accounted for in design by adopting the fatigue damage hypothesis commonly called the Palmgren-Miner rule [26, 27]. In fact, the adaptation of this hypothesis can be seen, for instance, in the industry standard EUROCODE 3 [28] and the recommended practice by DNV [20], which is referred to in NORSOK N-004 [29]. However, the Palmgren-Miner linear damage hypothesis is known to give unreliable results, as it does not accurately take into account the loading sequence effect [4, 30]. In fact, this was even presented by Miner, in his original article, in which he stated that the rule would give estimated damage in the range of 0.61-1.45 at failure [27, 31]. This may lead to the introduction of large design fatigue factors (DFF) in the standards.

3. The interest in the additive manufacturing of spare parts or components commonly adopted in mechanical equipment is increasing rapidly; however, the printing methods often result in defects like those of welding. This ultimately results in quite uncertain fatigue capacity.

Additive manufacturing (AM) is gaining momentum within industry today, where the motivations are such as shorter supply chains for spare parts, i.e., being able to print spare parts either offshore or locally onshore, in order to transport the part a short distance. The AM processes are often similar to those of welding, resulting in the production processes introducing pores, voids, surface roughness, cracking, delamination, residual stresses, deformation, etc. Subsequently, the components generally exhibit poor fatigue capacity in comparison to those produced by traditionally manufactured processes of casting and subtractive manufacturing [32, 33].

1.3 Research gaps

Much research has been carried out with the objective of overcoming the aforementioned problems. Hence, a literature survey of the previously performed research was performed, and the main findings are presented below, with the research gaps being identified and highlighted.

1. Lack of methods/techniques in design standards to predict the damage state/remaining life based on measurable change of physical quantities

The method of in situ damage assessment or measurement is commonly based on the detection of a macroscopic crack, as aforementioned. However, much research has been performed regarding the objective of measuring the accumulated fatigue damage before macroscopic crack propagation occur. Examples of this might be such methods as electric resistance [34-37], hardness [38-45], x-ray diffraction [46-50], thermometric [51-55], strain [21, 56, 57], positron annihilation [58-64], magnetic [65-68], and ultrasonic [69-72]. However, it is not yet practical at this time to adopt these measuring techniques for the assessment of remaining fatigue capacity on ageing structures, for a number of reasons, as discussed below.

Firstly, it should be highlighted that the method in question must be calibrated for the material which will be assessed or measured. It can be argued that, to some extent, this is the same as for crack propagation theories for life extension. In fact, the crack growth parameters and their statistical distribution must be known for the specific material in the case of such as RBI, etc.

Secondly, there is still more research to be done within the topic of fatigue damage measurement prior to macroscopic crack initiation. A few of the topics to be researched are (i) the feasibility of adopting macroscopic hardness measurements as a means of non-destructive damage assessment, in contrast to the commonly adopted micro hardness

techniques. This is from the perspective that these generally have more stringent requirements for surface preparation before the measurement is performed [73, 74]; (ii) whether the aforementioned non-destructive hardness can be considered non-destructive in relation to components subjected to fatigue or, alternatively, the possibility of removing the indented region; (iii) the feasibility of adopting positron annihilation as a method of determining whether fatigue damage has been accumulated or not, for structures operating near the fatigue limit, which can occur for structures subjected to high cycle fatigue where a high design fatigue factor is required. This is from the perspective that a rather distinctive initial change could be observed for the related parameters in research by Holzwarth and Schaaff [59, 60]; (iv) the feasibility of adopting damage assessment methods for welded details, as most of the research is performed on base material.

Furthermore, there is a lack of a clear framework categorizing the mentioned existing methods. As a result, it is difficult for the research and development communities to map what exists in the domain of fatigue damage assessment prior to crack initiation.

Finally, the highly scattered nature of results which has been found in this domain for seemingly similar tests should be highlighted. This might occur due to slight difference in the loading parameters or to the practical performance of the measurements taken. Therefore, it is important to emphasize that research papers in relation to damage measurement techniques should include a set of parameters, to make research more unified. This will result in research being more comparable and more knowledge gathering being achieved in future research.

2. Lack of accurate uniaxial fatigue damage models which can be adopted with the readily available S-N curves of design codes and standards

As aforementioned, the commonly adopted Miner's rule introduces further scatter to the fatigue life subjected to variable amplitude loading. In fact, Miner even stated that the rule would give estimated damage of 0.61-1.45 at failure [27, 31]. To overcome this issue, much work has been performed to better model the damage accumulation, which can be found in the literature. For instance, Fatemi and Yang [75] reviewed the cumulative damage theories for metals, with a focus on the models proposed between the early 1970s and the early 1990s. Thereafter, Hectors and De Waele [76] reviewed the nonlinear functions published after 1998, to extend the work of Fatemi and Yang. Early damage accumulation theory, in addition to that of Palmgren [26] and Miner [27], might be the improvements by, for instance, Marco and Starkey, who first proposed a nonlinear functional form which includes load-dependent damage progression, by adding an exponential term to the commonly adopted linear damage rule. Exactly what the functional form should be is not directly defined, whereas it is related to the current loading level [77]. Furthermore, Langer [78], followed by Grover [79], proposed the separation of the fatigue damaging process into two stages, each of which would adopt a linear damage summation. Based on this concept, Manson et al. developed and presented the double linear damage rule (DLDR) [80-82], which exhibited good results. Initially, the two phases were categorized as crack initiation and propagation, whereas this terminology was eventually changed to Phase I and Phase II. This is from the perspective that no measurable cracks could be observed after the first phase, whereas a difference between the phases was recognized. Shortly after, Manson and Halford proposed the damage curve approach (DCA), which was based on the functional form proposed by Marco and Starkey. However, it was highlighted that no functional form of the exponent had been presented; therefore, they derived an equation based

on the crack growth [83]. Later, Manson and Halford would also propose the double damage curve approach (DDCA) for the damaging effect a small cycle ratio would have on the reduction of capacity on the second loading block [84]. Many more functions have been proposed since that time. Examples of this might be such as the model proposed by Corten and Dolan, which depends on parameters m, r, and a. Another example might be the model by Lemaitre and Plumtree [85], and by Chaboche and Lesne [86], which depends upon several material parameters which have to be determined before it can practically be used. In fact, various proposed models can generally be categorized into such as: continuum damage mechanics, energy-based models, crack growth based, damage curve modifications, S-N curve modifications, etc.

Recently, researchers have also attempted to make damage functions for mechanical parameters which might change during the fatigue damaging process. This might be such as that of Ye et al. in [43-45] and Pavlou in [42], who developed damage functions in relation to the hardness evolution of steel and an aluminium alloy, respectively. Another example might be that of Shang and Yao [87], who proposed a damage model related to the exhaustion of ductility. Alternatively, the damage function proposed by Sun et al. in [35] depends on the change of electrical resistance during cycling. Although the models might achieve high accuracy, they all require further material testing and can only be related to the material which they are calibrated for, subsequently resulting in their being less feasible for practising engineers.

Models related to the S-N curve have also been presented, such as that of Mesmacque et al. [88], which is commonly called the sequential law, where the permissible stress is reduced until failure is expected to occur. However, the model states that it requires the full-range S-N curve. Other examples might be such as the isodamage lines, proposed by Subramanyan [89] and Hashin and Rotem [90], where improvements to make the functions more conservative have been proposed by, for instance, Rege and Pavlou [91]. Though all these proposals have been

made, the current versions of these models are difficult to use with bilinear or trilinear S-N curves, commonly found in the current codes and standards, which are not compatible with, for example, the damage functions of sequential law or the isodamage lines. Therefore, further improvement of these concepts and models is essential, to integrate with design practices.

Aeran et al. recently also stated that, although there are plenty of models available in the literature, they generally are not easily applicable to practising engineers. This is from the perspective that the presented theories often require additional material parameters, resulting in the need to perform additional, costly fatigue tests. Thereafter, the authors proposed a damage function which only depends on readily available S-N curves. The model accounts for the loading sequence effect, and a parameter was also proposed to adjust the effective number of cycles to account for the load interaction effect [92, 93]. However, it is still challenging to apply for random loading spectra, as the load interaction factor is applied on a cycle-to-cycle basis; hence, it will amplify the reduction or increase in effective cycles. Furthermore, the proposed function can also not be numerically estimated by a set of linear functions, which is required for nonlinear damage functions to be applicable to damage assessment on a cycle-to-cycle basis. Also, even though the model is based only on the S-N curves, it results in a somewhat difficult numerical procedure. Thus, there is a need for simple damage functions, which are based on the commonly used S-N curves, to more accurately estimate damage accumulation subjected to variable amplitude loading, than the commonly used Miner's rule.

3. Lack of research regarding the additive manufacturing method of Bound Metal Deposition and its fatigue capacity

AM is a rapidly evolving technology, in which it is well known that the resulting product of the material is directly correlated with the printing parameters. These parameters might be such as layer thickness, heat

input, scanning speed and strategy, amongst others. Furthermore, all these parameters will also be related to the printing technique which is adopted [32, 94-96]. As aforementioned in the problem statement, AM methods generally exhibit characteristics similar to those of welding, resulting in the production processes introducing pores, voids, surface roughness, cracking, delamination, residual stresses, deformation, etc. [32, 33]. In fact, two major groups of additive manufacturing of metals can be categorized as Direct Energy Deposition (DED) and Powder Bed Fusion (PBF). Generally, DED is the application of material by sending into a heat source either a wire or particles, which will melt and thereafter land on the part which is printed. PBF is performed by evenly distributing a layer of powder, then using a heat source such as a laser to selectively melt or sinter (i.e., selective laser melting (SLM) or selective laser sintering (SLS)) this layer. Thereafter, a new layer of powder is distributed, which again is selectively melted or sintered. As this process continues, the part will be built [32, 97]. However, there are also other methods of additive manufacturing. One of these is such as the bound metal deposition method (BMD), where the part is sintered in one step. In fact, the BMD manufacturing process can be described as having four steps, namely, (a) printing, (b) debinding, (c) sintering and (d) post processing. (a) Firstly, powder-filled wire of polymer wax binder is heated up and extruded layer by layer, to develop the generated and sliced geometry. (b) Thereafter, the printed specimen is put in a washer to go through a debinding process, to partly remove the binder. (c) After debinding has been performed, the specimen will be sintered to both remove the remaining binder and fuse the metal particles together, resulting in a solid metal part. The sintering process is performed by placing the specimen in a furnace, with a slow uniform heat development and subsequent cooling in an inert gas. (d) The last step is post processing, which might be such as machining or polishing, to achieve a better surface finish in regard to fatigue capacity, or, alternatively, hot isostatic pressing (HIP), to reduce pore structure or alter the microstructure [98, 99]. The fact that the printing method sinters the final

part as a whole in the last step results in the aforementioned common defects for such as DED or PBF being avoided. However, it was found that little research had been done on this printing method and mechanical performance, thus highlighting the need for further research on this printing technique and related mechanical properties.

1.4 Objectives

On the basis of the presented problem statements and the research gaps, the main objectives of this thesis are to improve the knowledge of in-situ fatigue damage assessment practices, to propose accurate fatigue damage models/theories and to assess the feasibility of additively manufactured steels in relation to their fatigue performance. These objectives are described in greater detail below.

1. Assess the currently proposed damage measurement techniques applicable prior to initiation of a macroscopic crack by identifying their relationship with the fatigue damaging phenomenon and by proposing a framework applicable to selecting a suitable technique. Furthermore, present recommendations for what is beneficial to document in relation to research within this domain. Finally, assess the feasibility of adopting Vickers, low-force Vickers and Brinell hardness measurements as a means of assessing accumulated fatigue damage.

2. Propose a method of adopting damage theories related to the S-N curve presented in the literature, to develop damage functions which more accurately take into account the loading sequence effect. The proposed model is to be easily applicable without further material testing and mathematically applicable to random loading.

3. Investigate the macroscopic material properties of steel printed by the bound metal deposition method with a focus on the anisotropic characteristics of the component, with respect to potential fatigue capacity.

1.5 Overview of the thesis

The thesis is separated into two parts. Part I consists of the following sections: Introduction, Research Outcomes and Conclusions. The background, problem statements, research gaps and objectives are presented in Chapter 1 “Introduction". Subsequently, the main research outcomes of the study are presented in Chapter 2 “Research Outcomes”. The conclusions and suggestions for future research are presented in Chapter 3 “Conclusions”. Part II of the thesis is comprised of the published journal and conference articles based on the research outcomes of this thesis/study.

Chapter 2 Research Outcomes

The research herein was carried out to fill or reduce the aforementioned research gaps. The research results/outcomes were presented in international journals and conferences and their proceedings. This thesis is therefore based on the published articles, which subsequently form the research outcomes from this study. The published articles are presented in a list below, then categorized in relation to their research gap in Table 1.

Paper I: F. Bjørheim, S. C. Siriwardane, D. Pavlou, "Fatigue damage monitoring methods - current practices," *5th International Conference on Offshore Renewable Energy – CORE*, Online, 2021, pp. 112-125.

Paper II: F. Bjørheim, S. C. Siriwardane, D. Pavlou, "A review of fatigue damage detection and measurement techniques," *International Journal of Fatigue*, vol. 154, 2022, Art no. 106556, doi: 10.1016/j.ijfatigue.2021.106556.

Paper III: F. Bjørheim, D. Pavlou, S. C. Siriwardane, "Hardness measurements as a technique for measuring accumulated fatigue damage", *International Journal of Structural Integrity*, vol. ahead-of-print, no. ahead-of-print, 2022, doi: 10.1108/IJSI-04-2022-0061.

Paper IV: F. Bjørheim, D. G. Pavlou, S. C. Siriwardane, "Nonlinear fatigue life prediction model based on the theory of the S-N fatigue damage envelope," *Fatigue & Fracture of Engineering Materials & Structures*, vol. 45, no. 5, pp. 1480-1493, 2022, doi:10.1111/ffe.13680.

Paper V: F. Bjørheim, S. C. Siriwardane, D. G. Pavlou, "S-N based fatigue damage modelling of offshore structures: Recent damage accumulation models and the way forward," *8th European Congress on Computational Methods in Applied Sciences and Engineering*, 2022.

Paper VI: F. Bjørheim, I. M. La Torraca Lopez, "Tension testing of additively manufactured specimens of 17-4 PH processed by Bound Metal Deposition," *IOP Conference Series: Materials Science and Engineering*, vol. 1201, no. 1, 2021, Art no. 012037, doi: 10.1088/1757-899X/1201/1/012037.

Table 1 Research gaps and corresponding published articles

1. Fatigue damage monitoring prior to macroscopic crack (Research gap 1, objective 1)	2. Damage modelling based on S-N curves (Research gap 2, objective 2)	3. Mechanical properties of additively manufactured steel (Research gap 3, objective 3)
Paper I Fatigue damage monitoring methods - current practices (CORE 2021)	**Paper IV** Nonlinear fatigue life prediction model based on the theory of the S-N fatigue damage envelope (Fatigue & Fracture of Engineering Materials & Structures 2022)	**Paper VI** Tension testing of additively manufactured specimens of 17-4 PH processed by Bound Metal Deposition (IOP Conf. Ser.: Mater. Sci. Eng 2021)
Paper II A review of fatigue damage detection and measurement techniques (International Journal of Fatigue 2022)	**Paper V** S-N Based fatigue damage modelling of offshore structures: Recent damage accumulation models and the way forward (ECCOMAS 2022)	
Paper III Hardness measurements as a technique for measuring accumulated fatigue damage (International Journal of Structural Integrity 2022)		

2.1 Framework for fatigue damage detection methods

Many methods have been proposed as damage monitoring methods for fatigue damage before a macroscopic crack has initiated. However, a systematic description of the various techniques, their strengths and weaknesses could not be found in the literature. Hence, both a conference paper [100] and journal article [101] were published on the topic in Papers I and II, respectively. The journal article was also expanded somewhat to include methods regarding crack measurement techniques. Overall, the journal article discusses the techniques for fatigue crack monitoring and fatigue damage monitoring, as presented in Table 2. The focus of the article is the underlying fatigue related damage mechanism which causes the change in the measured parameter, in addition to how the parameter changes as the material is subjected to fatigue loading.

Table 2 Methods discussed in Paper II

Category	Method
Fatigue crack monitoring	Potential drop Acoustic emission Ultrasonic
Fatigue damage monitoring	Electric resistance Hardness X-ray diffraction Thermometric Strain Positron annihilation Magnetic Ultrasonic

In addition to the discussion presented, another outcome of the journal article was a framework that can aid the research and development communities in selecting methods for performing damage monitoring during fatigue testing. In fact, the framework consists of a table, in which each method is briefly described by presenting the parameter in conjunction with the technique/phenomenon that is being monitored, the known limitations of the technique and a short discussion regarding the method. Furthermore, in the literature, some of the published articles were found to exhibit various results for seemingly similar experiments. However, these experiments usually lacked some information regarding the experimental setup. Hence, a table was proposed regarding what data should be included in experimental damage monitoring research. The table regarding data which should be reported for experimental damage monitoring research can be found in Table 3, while the framework for selecting the method for crack monitoring and damage monitoring can be seen in Table 4 and Table 5, respectively.

Table 3 Important information to document during damage measurement of fatigue

Material	The material used – with material characteristics Surface finish and processing of the material Microstructure (especially if unknown material)	
Load parameters	Cyclic loading	Spectrum loading
	Stress amplitude R - Ratio Frequency Number of cycles	Standard deviation Mean value Coefficient of variation of stress amplitude and R - Ratio
Measurement technique	Good explanation of the method used	
Criterion for fatigue failure	The criterion which is considered fatigue failure should be highlighted, as in first crack, through thickness crack or final fracture	

Table 4 Summary of crack monitoring based on the reviewed literature

Method	Parameter	Technique/Phenomenon	Limitations	Discussion
Electric	$\text{PDM} = 1 - \frac{V_0}{V}$	PDM: Change in potential (voltage) field due to discontinuity in the material (crack).	- From crack initiation. - Calibration curves must be developed.	The PDM method is well established in the monitoring of cracks via the calibration curves. However, such curves are geometry-dependent and must be developed for each case.
Acoustic emission	Amplitude; Counts; Duration; Energy; Risetime; Counts to Peak; Absolute Energy; Count rate $\log\left(\frac{dA}{dN}\right) = B\log(\Delta K) + \log(C)$	Elastic stress waves generated due to rapid release of energy from a localized source within a stressed material.	- Crack must be present. - Only measurable during propagation. - Signal processing/ interpretation. - Number of sensors defines accuracy and the information that can be obtained.	Generally, for in situ monitoring of various structures, in contrast to laboratory/specimen-scale testing. However, has a disadvantage in regard to unwanted noise and signal processing.
Ultrasonic method	Time of flight; Time of flight diffraction; Energy; Amplitude	Elastic stress waves, commonly generated by the use of a piezoelectric crystal, with the resulting reflection or diffraction.	- Crack or loss of material must be present.	Common method to apply for in situ inspection of various components. TOFD seems most reliable for crack sizing, with the advantage of also exhibiting good detectability.

Table 5 Summary of damage monitoring based on the reviewed literature

Method	Parameter	Technique/Phenomenon	Limitations	Discussion
Electric	Resistance = ΔR; $\frac{\Delta R}{R}$; $R = \frac{\rho L}{A} \rightarrow \Delta\rho$	Increased resistivity due to dislocations, point defects, micro and macroscopic crack propagation.	- Conductive materials. - Most significant near fracture. - Small measurement (μΩ). - Measurable outside operation.	Resistance seems more applicable to specimen testing, for additional information.
Hardness	Hv; Hb; $1 - \frac{H_D}{H_0}$; $H_D = C(1-D)k(\varepsilon + \varepsilon_H)^m$	Measurement of the surface hardening/softening due to cyclic microplasticity.	- Requires extensive polishing procedure before operation. - Requires microstructural analysis. - NDE perspective questionable. - Measurable outside operation.	Strong correlation with the fatigue damaging process. Disadvantage in regard to the polishing requirement. Furthermore, the method being non-destructive as regards fatigue is a subject for discussion.
X-ray diffraction	Halfwidth b; Integral width β; Fourier coefficients; Dislocation estimate $\bar{\rho} = \frac{\bar{\beta}^2}{9b^2}$	Broadening of the XRD peak due to micro stresses (dislocations) causing lattice distortion.	- Radiation penetration depth dictates the shape of the damage accumulation curve. - Measurable outside operation.	The penetration depth of the radiation used should be carefully considered. More towards laboratory testing in the literature.

Table 5 Summary of damage monitoring based on the reviewed literature, continued

Method	Parameter	Technique/Phenomenon	Limitations	Discussion
Thermometric	ΔT; $\frac{\Delta T}{\Delta N}$; R_θ ; $Q\left(\frac{kJ}{m^3 cycle}\right)$	Dissipation of heat energy due to internal friction (plastic deformation).	- Strongly stress- and frequency-dependent. - Has to be measured during operation/loading.	Strong relation to the accumulation of fatigue damage. Has limitations in practical applications. Consequently, cyclic loading must be applied to assess the damage. However, can easily be applied in parallel with fatigue testing, to obtain additional information.
Strain-based	Ratcheting: $\frac{\varepsilon_m-(\varepsilon_m)_{min}}{(\varepsilon_m)_{max}-(\varepsilon_m)_{min}}$ Inelastic strains: $\frac{\Delta\varepsilon^i-\Delta\varepsilon_0^i}{\Delta\varepsilon_f^i-\Delta\varepsilon_0^i}$	Ratcheting: Generated by the local deformation around voids, non-metallic precipitations and other defects within the material. Inelastic strains: Cyclic plasticity. Both cases: Measurement of the cyclic nonlinear deformation.	- Small measurement (magnitude around 10^{-4} or 10^{-3}). - Load must be applied to evaluate.	Can give increased information in contrast to the thermometric method, as in if the fatigue is due to ratcheting or inelastic strains. However, smaller measurable values.

Table 5 Summary of damage monitoring based on the reviewed literature, continued

Method	Parameter	Technique/Phenomenon	Limitations	Discussion
Positron annihilation	τ $S-\text{parameter}$ $=\frac{\text{The counts of }\gamma-\text{ray near central peak}}{\text{Total counts of }\gamma-\text{ray}}$	Measurement of time from birth to annihilation and the energy of the resulting photons. Caused due to the development of vacancies through the fatigue loading.	- Measurability drops once the amount of positron trapping sites saturates (mainly measurable early in the fatigue life). - Not applicable to materials exhibiting saturation of positron trapping sites in initial state. - Mainly applicable in laboratories. - Measurable without loading.	Applicability dependent on material characteristics. Due to the existence of initial positron traps, such as precipitates. The parameter is most significant early in the fatigue life. Might have the potential to monitor whether fatigue damage has accumulated or not, either in conservative designs with a high DFF or where "infinite" fatigue life is desired. Mainly for laboratory testing.
Magnetic	BHN: RMS (V); $\frac{V_n}{V_0}$ Magnetic hysteresis parameters	In both cases due to interaction of dislocation structures and the magnetic domain walls.	- Only works for ferromagnetic materials or through stress-induced phase change. - Not applicable if yield has been surpassed. - Often large plateaus. - Measurable without loading.	The magnetic methods have a strong relation to the microstructure, as can be seen in the cited literature. However, regarding monitoring fatigue damage, there are contradicting findings.
Ultrasonic	Nonlinear: $\beta \propto \frac{A_2}{A_1^2}$; $\%THD = \frac{A_2}{A_1} \times 100\%$ Linear: $\Delta V(\frac{m}{s})$; $\alpha(\mu s^{-1})$; $\frac{\Delta V}{V_0}$; $\frac{\Delta \alpha}{\alpha_0}$; $1-\frac{\bar{V}_L^2}{V_L^2}$; $1-\frac{\alpha}{\tilde{\alpha}}$	Nonlinear: Attributed to the nonlinearity of the propagation medium, commonly discussed as microcracks and dislocations, generating secondary harmonics. Linear: Dislocation dampening.	- Linear methods exhibit small change often with large plateaus. - Measurable without loading.	The nonlinear method exhibits a continuous noticeable increase throughout the reviewed literature. The linear methods are generally more questionable, with large sections of insignificant change.

2.2 Hardness measurements as a means of damage monitoring

Based on the reviewed literature, it was found that most methods for monitoring fatigue damage by hardness measurements were performed through the adoption of microhardness measurements, where either a Vickers or Berkovich indenter was adopted. The disadvantage of microhardness is, for example, the stringent surface preparations, which can be found, for instance, in the ISO standard ISO 6507-1:2005 [74], which states "Due to the small depth of Vickers microhardness indentations, it is essential that special precautions are taken during preparation. It is recommended to use a polishing/electropolishing process which is suitable for the material parameters". Thus, it was thought that macroscopic hardness measurements might be more suitable, while keeping in mind that the indenters might be detrimental to the fatigue life. Hence, this was investigated and published in Paper III [102].

Specimens subjected to tension-tension and tension-compression fatigue loading were continuously stopped, to monitor the change of surface hardness. For the tension-tension specimens, the Vickers hardness indenter was adopted with 1kg and 5kg loading, whereas, for the tension-compression specimens, Vickers 0.5kg and Brinell 1mm diameter with 20kgf and 40kgf, and 2.5mm diameter with 50kgf and 125kgf, were also adopted. The parameter analysed throughout the study was the damage evolution, with the functional form as presented in Eq. (1).

$$D = \frac{H_i - H_{min}}{H_{max} - H_{min}} \tag{1}$$

H_i is the current hardness value, H_{min} is the minimum hardness value and H_{max} is the maximum hardness value. H_{min} was usually experienced before any cycling had taken place, whereas H_{max} was generally the final measurement, as a hardening process was normally observed.

It was found that the tension-tension specimens would commonly exhibit ratcheting, which eventually resulted in the formation and propagation of fatigue Lüders bands, which can occur for steel which is cycled with a tensile mean stress [103]. Furthermore, it was found that the Vickers hardness generally did not exhibit a clear statistically significant change, whereas the Brinell hardness did, as can be seen in Figure 1, Figure 2 and Figure 3, being HV5, Brinell 2.5mm and Brinell 1.0mm, respectively.

In addition, during the experimental work, it was found that the indentations themselves would commonly promote crack initiation for tension-compression, whereas this was not found for the specimens subjected to tension-tension herein. Hence, the indentations' residual stress field and how it is affected by one tension-compression cycle was investigated by finite element analysis in the software Abaqus, where it was found that both the indentations of Vickers and Brinell will leave relatively high residual tensile stresses in the direction of applied stress. This will result in a local region effectively experiencing a high mean stress, thus promoting crack initiation. A detailed explanation of the analysis can be found in Paper III, Section 5, whereas figures displaying the resulting stress field after indentation, during a tensile cycle of 270 MPa and after one full tension-compression cycle, can be found in Figures 11 and 13 in Paper III for Vickers and Brinell, respectively.

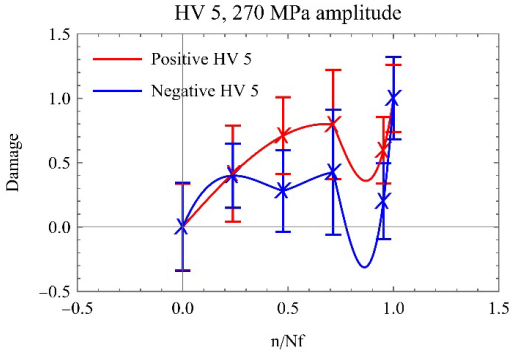

Figure 1 HV 5, 270 MPa amplitude tension-compression loading

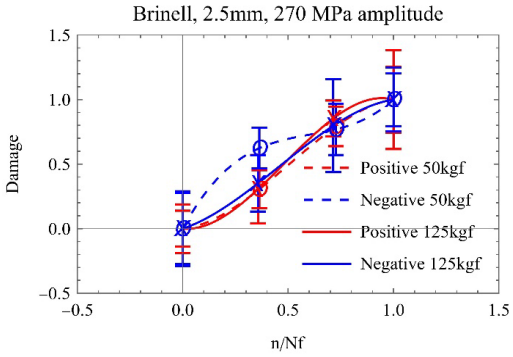

Figure 2 Brinell, 2.5mm, 270 MPa amplitude tension-compression loading

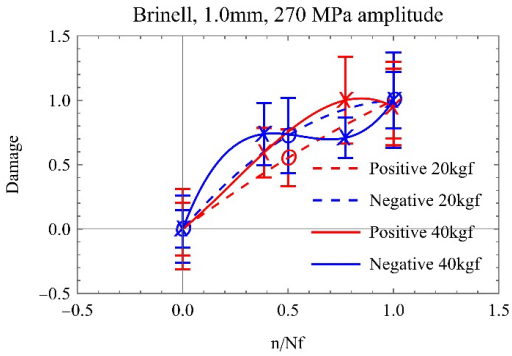

Figure 3 Brinell 1.0mm, 270 MPa amplitude tension-compression loading

2.3 Proposed uniaxial fatigue damage model

A nonlinear model is proposed in the light of the theory of isodamage curves, to assess the cumulative fatigue damage under variable amplitude loading, in Paper IV [104]. The proposed model is based on the theory of the S-N fatigue damage envelope proposed by Pavlou [105], in conjunction with a commonly adopted functional form for damage accumulation, which is presented in Eq. (2). The parameter n/N_f is the cycle ratio (i.e., the number of exhausted cycles n divided by the number of cycles to failure N_f), in addition to the exponential term $q(\sigma, m)$. It should be noted that the final expression of the exponential term and the number of material parameters *m* with their respective values depend on the theoretical or experimental method which is adopted to develop a function, as there are both theoretical and experimental methods for defining damage.

$$D = \left(\frac{n}{N_f}\right)^{q(\sigma,m)} \tag{2}$$

The advantage of having a numerical expression for the exponential term, in contrast to ratios which can commonly be seen in the literature, can be seen in Eqs. (3) and (4). In fact, by having a numerical expression

for the exponent, the continuous damage can be determined as presented in Eq. (3). However, if the damage formula can only be represented by a ratio, it must be performed in relation to the critical damage level D_c, which is often assumed to be one.

$$D_{tot} = \left(\left(\cdots \left(\left(\left(\frac{n_1}{N_{f1}} \right)^{\frac{q(\sigma_1,m)}{q(\sigma_2,m)}} + \frac{n_2}{N_{f2}} \right)^{\frac{q(\sigma_2,m)}{q(\sigma_3,m)}} + \frac{n_3}{N_{f3}} \right)^{\frac{q(\sigma_3,m)}{q(\sigma_4,m)}} + \cdots + \frac{n_{k-1}}{N_{f(k-1)}} \right)^{\frac{q(\sigma_{k-1},m)}{q(\sigma_k,m)}} + \frac{n_k}{N_{f(k)}} \right)^{q(\sigma_k,m)} \tag{3}$$

$$D = \left(\cdots \left(\left(\left(\frac{n_1}{N_{f1}} \right)^{\frac{q(\sigma_1,m)}{q(\sigma_2,m)}} + \frac{n_2}{N_{f2}} \right)^{\frac{q(\sigma_2,m)}{q(\sigma_3,m)}} + \frac{n_3}{N_{f3}} \right)^{\frac{q(\sigma_3,m)}{q(\sigma_4,m)}} + \cdots + \frac{n_{k-1}}{N_{f(k-1)}} \right)^{\frac{q(\sigma_{k-1},m)}{q(\sigma_k,m)}} + \frac{n_k}{N_{f(k)}} = 1 \tag{4}$$

2.3.1 The proposed damage function and damage transfer concept

A new damage function is herein proposed, as shown in Eq. (5)

$$D = \left(\frac{n}{N_f}\right)^{\frac{a(S_u - S_e)}{(\sigma - S_e)}} \tag{5}$$

where the cycle ratio is as aforementioned, whereas the parameters S_u, S_e and σ are the ultimate tensile strength, the fatigue limit or knee point stress and the stress amplitude. Furthermore, the functional form of the exponent, including the parameter a, is a result of the interpolation of the damage theory adopted, namely the S-N fatigue damage envelope proposed by Pavlou [105], which will be presented in the subsequent section. The parameter a was herein found to be six. Damage transfer between cycle blocks can be performed, as presented in Eq. (6).

$$D_1 = \left(\frac{n_1}{N_{f1}}\right)^{\frac{a(S_u - S_e)}{(\sigma_1 - S_e)}} = \left(\frac{n_2}{N_{f2}}\right)_{eq}^{\frac{a(S_u - S_e)}{(\sigma_2 - S_e)}} \rightarrow \left(\frac{n_2}{N_{f2}}\right)_{eq} = \left(\frac{n_1}{N_{f1}}\right)^{\frac{\sigma_2 - S_e}{\sigma_1 - S_e}} \tag{6}$$

It should be noted that, if this equation is adopted on a cycle-to-cycle basis, the exponential ratio will result in numerical errors. However, the nonlinear damage function can then be discretized into finite linear segments, which again makes it suitable for damage monitoring of real variable amplitude/random loading spectra. The discretization can be performed as follows in Eqs. (7) and (8) [106].

$$\omega_{ij} = \frac{D_j - D_{j-1}}{D_j^{1/q(\sigma_i)} - D_{j-1}^{1/q(\sigma_i)}} \tag{7}$$

$$\Delta D_{ij} = \omega_{ij} \frac{n_i}{N_i} \tag{8}$$

$D_j - D_{j-1}$ is the damage range for the specific band, $D_j^{1/q(\sigma_i)} - D_{j-1}^{1/q(\sigma_i)}$ is effectively the cycle ratio range for the specific damage band (consequently determining the rate of change dD/dn), which is determined for ω_{ij}, where i is the loading cycle/cycles and j is related to the damage band. It should be noted that, to adopt the numerical linearization of the nonlinear functions proposed, the damage function must have an expression for the exponent, to be able to directly calculate the various damage levels.

2.3.2 Framework for developing damage functions and verification

The methodology which was adopted to develop the damage function will be briefly described, as it will simultaneously express the methodology for developing other damage functions. As aforementioned, the theory for damage which will be adopted is the theory proposed by Pavlou regarding the S-N fatigue damage envelope. The damage envelope is developed by performing a heat transfer analysis of the normalized *S-N* curve, in finite element software. In fact, the abscissa and ordinate are normalized, as presented in Eqs. (9) and (10), respectively.

$$n_i^* = \frac{n_i}{N_e} \quad 0 \leq n_i^* \leq 1 \tag{9}$$

$$\sigma_i^* = \frac{\sigma_i - S_e}{S_u - S_e} \quad 0 \leq \sigma_i^* \leq 1 \tag{10}$$

The heat transfer analysis herein was performed on a generalized form of the S-N curve. In fact, it is a straight line, which intercepts the ultimate tensile strength and the fatigue limit or knee point stress. The heat transfer analysis by Pavlou and the evaluation of the heat transfer analysis with respective damage levels and cycle ratios can be seen in Figure 4 and Figure 5, respectively.

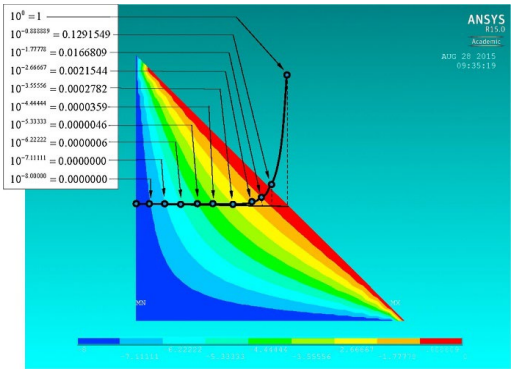

Figure 4 Damage envelope [105]

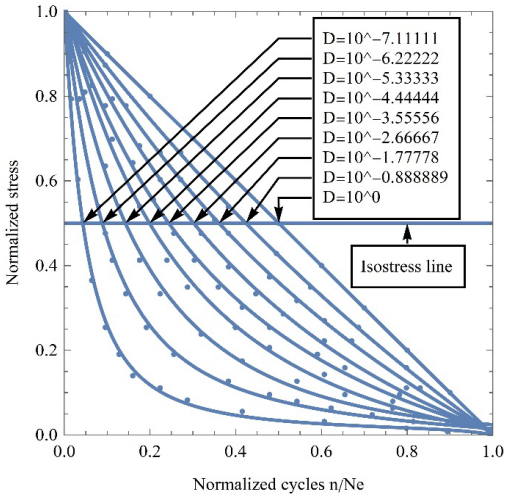

Figure 5 Numerical approximation of the damage envelope

Thereafter, the damage progression in relation to the cycle ratios can be extracted for a specific stress amplitude, which can again be interpolated. As aforementioned, this is an example based on the generalized form of the S-N curve, hence applicable to any S-N curve. Therefore, it was

compared with other models, C45, C35, 15HM, A387 GR 22, A336 GR 5 and Al-2024-T42 for two-stage loading, and Al 6082-T6 for multistage loading, where the function exhibited good results.

2.4 Common functional form of fatigue models and comparisons

The topics of fatigue damage models and modelling are discussed in Paper V [107]. In addition, a deterministic algorithm for nonlinear fatigue damage monitoring is presented and discussed. Furthermore, two commonly adopted functional forms for damage modelling are identified, and the adequacy of their functional form is directly investigated with the help of experimental data. Thereafter, nonlinear damage models proposed at the University of Stavanger were compared with the commonly adopted Miner's rule, using experimental data. The comparison was performed to check the accuracy of the nonlinear models in comparison to Miner's rule and whether the estimates are conservative. Finally, there is a discussion of how both the theory and deterministic algorithms now exist for adopting nonlinear functions in design if the expected loading sequence can be determined, whereas they can always be adopted for fatigue-based structural health monitoring.

It was found that a vast number of presented damage functions is based on the functional form presented in Eq. (11)

$$D = 1 - \left(1 - \left(\frac{n}{N_f}\right)^{\alpha}\right)^{\beta} \tag{11}$$

where n/N_f is the cycle ratio (i.e., the number of exhausted cycles divided by the fatigue capacity for the given stress amplitude), whereas the parameters α and β are based upon the theory adopted for damage monitoring and fatigue damaging parameters. In fact, it is well established that one of the parameters should be related to the stress amplitude. However, the functional form can be reduced to the following

functional forms, by determining one of the exponential terms as one which is presented in Eqs. (12) and (13) below.

$$\alpha = 1 \rightarrow D = 1 - \left(1 - \left(\frac{n}{N_f}\right)\right)^{\beta} \tag{12}$$

$$\beta = 1 \rightarrow D = \left(\frac{n}{N_f}\right)^{\alpha} \tag{13}$$

The damage modelling capabilities of the presented functional forms can be reduced to a single ratio by the damage transfer concept presented in Eq. (6). The resulting expressions can be seen in Eqs. (14) and (15).

$$\alpha = 1 \rightarrow 1 - \left(\frac{n_2}{N_{f2}} + 1 - \left(1 - \left(\frac{n_1}{N_{f1}}\right)\right)^{R_\beta}\right) = 0 \tag{14}$$

$$\beta = 1 \rightarrow 1 - \left(\frac{n_2}{N_{f2}} + \left(\frac{n_1}{N_{f1}}\right)^{R_\alpha}\right) = 0 \rightarrow \frac{n_2}{N_{f2}} + \left(\frac{n_1}{N_{f1}}\right)^{R_\alpha} = 1 \tag{15}$$

The resulting equations only depend on the first and second cycle ratios (i.e., n_1/N_{f1} and n_2/N_{f2}), in addition to the remaining exponential terms, which in fact are ratios R_β and R_α. Hence, these expressions can be compared with experimental data for two-stage loading at two constant stress amplitudes, for various cycle ratios. According to damage modelling theory, the exponential forms R_β and R_α should remain constant for two-stage loading. Herein, an evaluation was performed based on results published by Subramanyan in [89], where specimens made of C35 medium carbon steel were tested for two-stage loading. The material parameters were yield strength σ_y=324 MPa, ultimate tensile strength S_u=458 MPa and the knee-point stress S_e=255 MPa. The results can be seen in Figure 6 and Figure 7, where the notation 353-275 MPa means that the first and second stress amplitudes were 353 and 275 MPa, respectively.

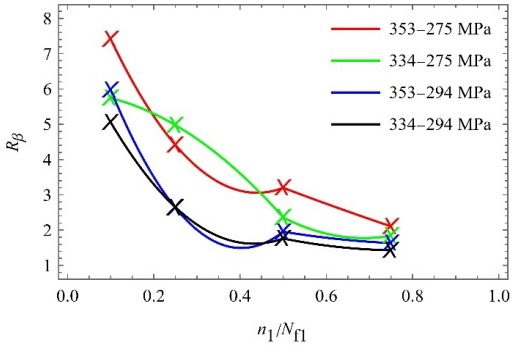

Figure 6 R_β ratios which make Eq. (14) true as a function of the first cycle ratio for C35

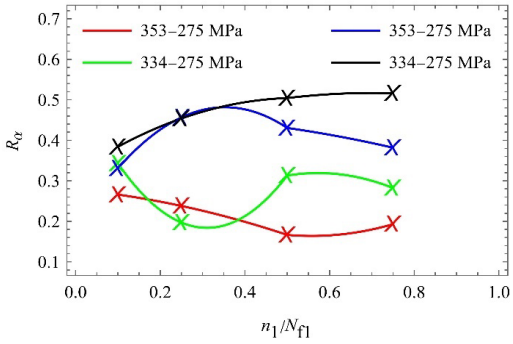

Figure 7 R_α ratios which make Eq. (15) true as a function of the first cycle ratio for C35

In addition, the equations were compared with another material, namely SAE 4130, the results of which were initially published by Manson et al. [80]. This dataset is often adopted to compare proposed fatigue damage models. The material parameters were yield strength 0.2 percent offset σ_y=113 ksi, ultimate tensile strength S_u=130 ksi, while the knee-point stress is unknown. The results can be seen in Figure 8 to Figure 11, where

the notation 140-120 ksi means that the first and second stress amplitudes were 140 and 120 ksi, respectively.

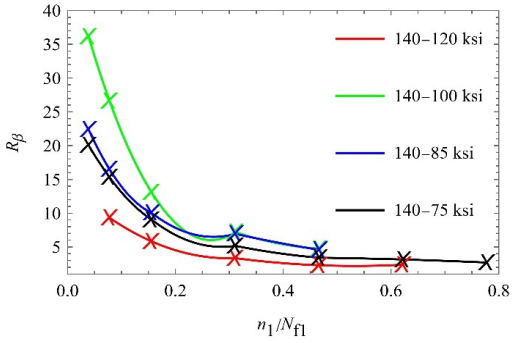

Figure 8 R_β ratios which make Eq. (14) true as a function of the first cycle ratio for SAE 4130

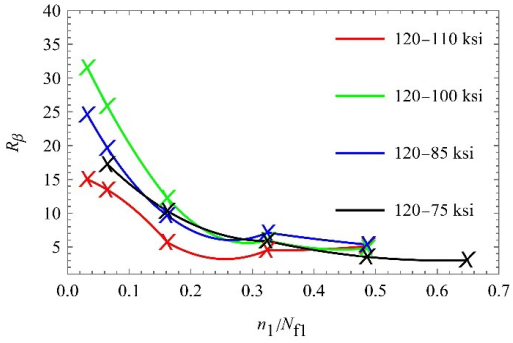

Figure 9 R_β ratios which make Eq. (14) true as a function of the first cycle ratio for SAE 4130

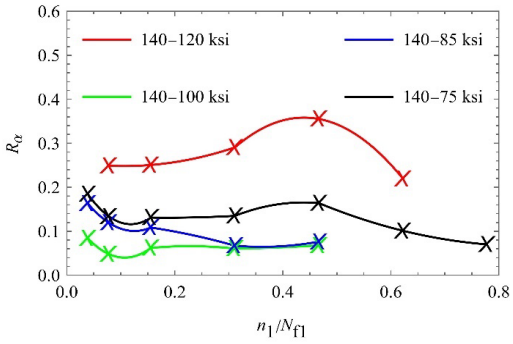

Figure 10 R_α ratios which make Eq. (15) true as a function of the first cycle ratio for SAE 4130

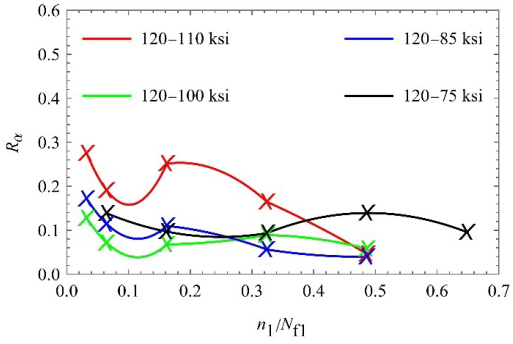

Figure 11 R_α ratios which make Eq. (15) true as a function of the first cycle ratio for SAE 4130

From the results, it can clearly be seen that especially Eq. (14), which is dependent on the ratio R_β, exhibits a very clear trend with number of cycles, which again indicates that the functional form is not adequate without either the exponential term being related to the cycle ratio or some correction, as presented by, for instance, Aeran et al. [92, 93]. When it comes to Eq. (15), it cannot clearly be defined that the functional

form is inadequate. From the plots, especially in Figure 7, there seems to be a possible trend, but, in relation to Figure 10 and Figure 11, it must also be acknowledged that fatigue is commonly known to have high scatter.

Furthermore, it was highlighted that a framework to adopt nonlinear damage functions now exists, in addition to emphasizing the higher accuracy and that the models exhibit more conservative results for several tests with various materials. The summary of the results for accuracy can be found in Table 6, where the resulting percentage is the percentage of times the models resulted in a number closer to the experimental result of remaining fatigue capacity, in comparison to the commonly adopted Miner's rule. Furthermore, the conservative nature of the models can be seen in Table 7, where the resulting percentage is the percentage of times the models underestimated the remaining fatigue capacity. The parentheses beneath the various materials display the number of test results which were available for each material subjected to fatigue testing. The tests were performed by two-stage loading, whereas the material Al-6082-T6 was subjected to multistage loading.

Table 6 Comparison of the accuracy of recent nonlinear models with Miner's rule

Models	C35 (22 tests) [89]	C45 (7 tests) [87]	Alloys (6 tests) [21]	Al-2024-T42 (6 tests) [42]	Al-6082-T6 (3 tests) [108]
Bjørheim [104]	100%	85.7%	50%	100%	100%
Rege [91]	100%	85.7%	50%	50%	100%
Aeran [93]	100%	71.4%	83.3%	100%	66.7%

Table 7 Comparison of the conservative nature of recent nonlinear models with Miner's rule

Models	C35 (22 tests) [89]	C45 (7 tests) [87]	Alloys (6 tests) [21]	Al-2024-T42 (6 tests) [42]	Al-6082-T6 (3 tests) [108]
Miner's rule	27.3%	42.9%	33.3%	50.0%	33.3%
Bjørheim [104]	63.6%	71.4%	33.3%	50.0%	0%
Rege [91]	81.8%	71.4%	33.3%	50.0%	0%
Aeran [93]	36.4%	57.1%	33.3%	50.0%	0%

2.5 Mechanical behaviour of additively manufactured steel printed by Bound Metal Deposition

The additive manufacturing process of Bound Metal Deposition (BMD) was assessed. Additively manufactured parts commonly exhibit defects like those of welding. Hence, it was thought that the BMD method might be advantageous, as the full part is sintered in the last step of the production method. Hence, an initial study was performed by tension testing and light microscopy, with the results being investigated and published in Paper VI [109].

2.5.1 Tensile test

From the results, it can be found that the printing method exhibited anisotropic mechanical properties in relation to the printing orientation. In fact, the specimens classified as XY-flat exhibited a significantly higher ultimate tensile strength and elongation at fracture, in comparison to the other specimens classed as XY-sided and ZX.

A total of nine specimens were printed, three of which were printed in each of the directions presented in Figure 13, where the classification of the specimens is as follows: (a) XY-flat, (b) XY-sided and (c) ZX. Furthermore, the stress-strain curves for the specimens can be seen in Figure 12, whereas the mechanical properties can be found in a tabulated form in Table 8.

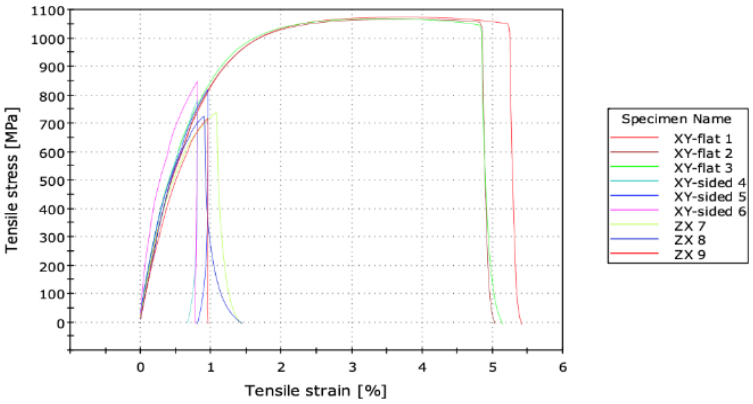

Figure 12 Stress-strain curves for the specimens

Table 8 Summary of mechanical properties

SPECIMEN	0.2% Yield Strength (MPa)	Ultimate Tensile Strength (MPa)	Young's Modulus (GPa)	Elongation at Break (%)
XY-flat 1	661.00	1072.00	136.74	5.24
XY-flat 2	764.30	1065.00	115.59	4.85
XY-flat 3	638.80	1067.00	161.53	4.84
XY-sided 4	699.80	780.80	135.54	0.81
XY-sided 5	637.60	817.50	145.63	0.96
XY-sided 6	613.30	846.70	286.87	0.80
ZX 7	579.40	737.70	139.73	1.09
ZX 8	656.60	725.50	128.68	0.91
ZX 9	610.10	717.20	123.83	0.95

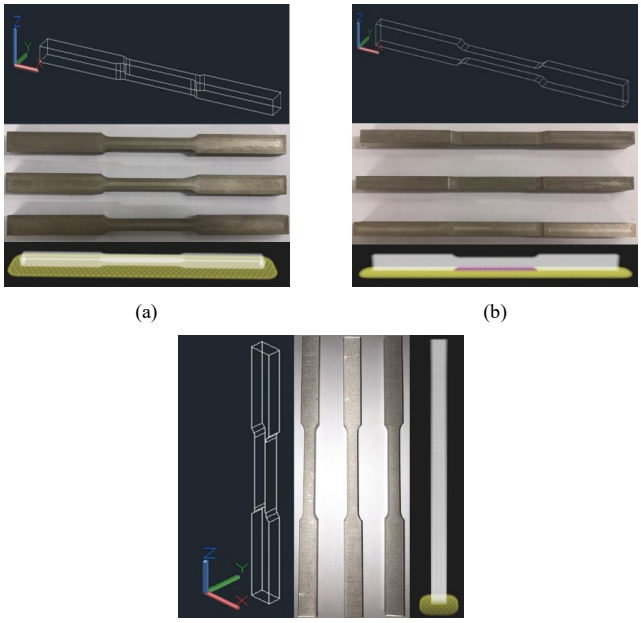

(a) (b)

(c)

Figure 13 Printed specimens (a) XY-flat, (b) XY-sided, (c) ZX

2.5.2 Fatigue performance

Herein, no fatigue tests were performed regarding the BMD printing method. However, a general comment regarding potential fatigue capacity should be made, considering some of the main industries motivated to use/introduce additive manufacturing, such as automotive, aerospace, energy oil and gas, mentioned in the introduction. This is from the perspective that the automotive, aerospace and energy oil and gas industries all commonly must consider dynamic loading.

From the tensile testing, it was clearly noted that the printed material exhibited anisotropic mechanical properties related to the printing

orientation. Furthermore, during the inspection of the material with light microscopy, it was found that a mesh of crack-like defects was present. In fact, the specimens were found to exhibit a systematic mesh of crack-like defects throughout, which can be correlated with the printing orientation. Images of the crack-like defects are presented in Figure 14, whereas a representation of how these defects are developed can be seen in Figure 15. The defects were found throughout the specimen, with a width in the range of 39-86 μm.

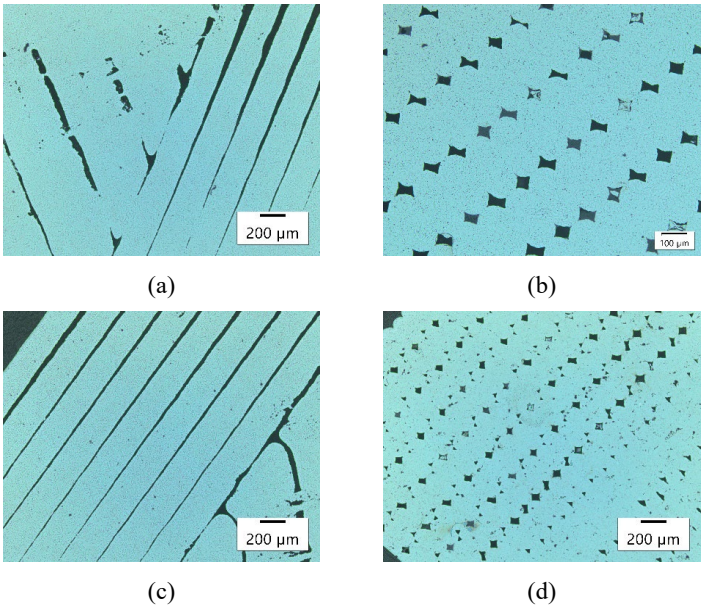

(a) (b)

(c) (d)

Figure 14 Images taken from optical light microscope (a) top view vertical printed, (b) side view vertical printed, (c) top view of horizontal print, (d) side view of horizontal print

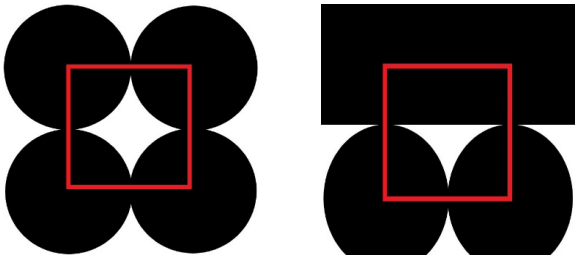

(a) (b)

Figure 15 Representations of defects found in the printed material (a) square defect, (b) triangle defect

Furthermore, it was also found that the printing scheme results in a high surface roughness, where the geometry can be found to be one half of the defect presented in Figure 15 a). An example of this can be seen in Figure 16. The measured distance from top to bottom of the grooves was in the range of 43-54µm. However, it should be noted that the surface condition mentioned here is only in regard to the iterative layers placed, and the surface will not be as rough along the grooves of the roughness/layers presented here. In fact, the direction into or out of Figure 16 will not exhibit a high surface roughness in relation to the printing scheme.

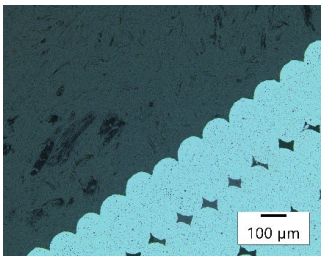

Figure 16 Surface condition of the printed specimens

Consequently, the following can be expected during fatigue loading:

1. The fatigue capacity will also be anisotropic.

2. The material/specimens printed in the XY-flat orientation might have a reasonable fatigue capacity; however, both the XY-sided and ZX specimens are expected to exhibit very poor fatigue capacity, in comparison to their traditionally manufactured counterparts. This is from the mesh of defects and surface roughness orientation to the applied cyclic loading.

Chapter 3 Conclusions

3.1 Summary

The topics of damage assessment by in situ measurements, nonlinear damage modelling and additive manufacturing are herein discussed and researched. Ageing mechanisms related to structures and mechanical equipment subjected to cyclical loading are associated with fatigue damage. Although much research has been performed within the domain of fatigue, failures are still occurring. Common practice for assessing structures which have surpassed their design life is by adopting a costly inspection programme. This is from the perspective that a macroscopic crack is certainly the strongest indicator of fatigue damage. Furthermore, the design codes and standards commonly adopt the linear damage rule known as Miner's rule, which increases the uncertainty in design, which again must be covered by the DFF factors, hence, reducing the time frame in which the structure can operate within the design life. Finally, it is well known that the ordering and logistics involved in acquiring spare parts for mechanical equipment can be time-consuming if not impossible, resulting in either large storage of spare parts, in relation to a "just in case" maintenance philosophy, which in turn is costly, or risking costly downtime.

In relation to the aforementioned common practice in damage monitoring, damage modelling and additive manufacturing, the thesis can be categorized as having three parts, as shown below.

1. Fatigue damage monitoring prior to macroscopic crack initiation

Based on the published literature, experimental methods to assess small fatigue crack propagation and fatigue damage accumulation of materials subjected to fatigue loading are researched and discussed. The focus of the research is the underlying damage mechanism which results in the change of the measured parameter, the damage expression commonly

used for each of the methods and how the parameters evolve as the material is subjected to fatigue. In addition, application areas for damage assessment by the various methods are also discussed, regarding whether they seem feasible in relation to in situ assessment, laboratory assessment and damage models. In this regard, it was on the basis of whether equipment exists and whether a measurement can be performed while the component/material is at rest (i.e., not subjected to cyclic loading).

The method of hardness is also further researched. It was found that much of the available literature for hardness methods is based on microhardness. The problem of microhardness is that it has stringent requirements for surface preparations, in contrast to macroscopic hardness measurements. Hence, macroscopic hardness was assessed by the use of both Vickers and Brinell with varying indenter loads. In addition, a finite element analysis was performed in Abaqus, to further investigate the stress field resulting from the indentation and the local cyclic stresses near the indentation.

2. Damage modelling based on S-N curves

A new uniaxial fatigue damage model is proposed, based on the damage theory of the S-N fatigue damage envelope. The damage envelope is a method of analysing the shape of the adopted S-N curve, which is expected to be a theory applicable to bilinear, trilinear or the full-range S-N curve. In relation to the proposed damage model, a generalization of the S-N curve was adopted, in which it was assumed that the curve is straight and intersects the stress axis at the ultimate tensile strength and the location of the knee-point stress, meaning that the resulting expression is in theory applicable to any S-N curve. The advantage of the proposed model in contrast to other models is that it does not depend on other material parameters when the model based upon the generalized S-N curve is adopted; it depends only on S-N data, which can be found in the standards. Consequently, the proposed model can be easily applied

by practising engineers. The model is verified and compared with damage functions which have similar prerequisites to the proposed function, in addition to Miner's rule for five materials, in which data for both two-stage loading and multistage loading is adopted.

In addition, it was found that the commonly adopted functional forms which are adopted in the literature can be generalized, to be a combined function with two exponential terms. The relation of the parameters or variables of the functional form can be represented in three dimensions, resulting in its ability to be evaluated in three dimensions; alternatively, it can be reduced to two functional forms, which are often adopted in the literature. These functional forms were subsequently reduced to a ratio which should be constant for two-stage loading, where the two stress amplitudes are maintained, whereas the cycle ratios used in the first and second block loading vary. These functional forms were subsequently compared with experimental data for two materials.

3. Mechanical properties of additively manufactured steel

The anisotropic properties of additively manufactured specimens of 17-4 PH by the printing method of Bound Metal Deposition were investigated. In fact, the specimens were printed in three different directions, with the mechanical properties from a tensile test revealing that the resulting product exhibits anisotropic behaviour. The cause of the anisotropic behaviour of the resulting product was thereafter investigated through light microscopy, as it was assumed that defects related to the printing method were the cause.

3.2 Concluding remarks

Based on the research outcomes of this project, the following major conclusions are made.

1. A framework is herein made for the research and development communities, when it comes to the topic of adopting methods to assess small fatigue crack propagation and fatigue damage accumulation before a macroscopic crack has initiated. The focus of the framework is the underlying cause of the measured change, which is correlated with the small fatigue crack propagation or fatigue damage accumulation. In addition, the evolution of the parameter for each of the methods as the material is continuously exposed to fatigue loading was a focus. The framework consists of two tables, one regarding small crack propagation (Table 4) and one regarding damage measurement techniques (Table 5). The reliability, advantages, weaknesses and case dependency are presented in the last two columns of the tables. The important information which should be included in fatigue damage measurement research, to make the literature more comparable, such as material, load parameters, measurement technique and failure criterion, was identified and is presented in Table 5 in Paper II.

2. Research into macroscopic hardness as a technique for measuring accumulated fatigue damage for structural steel was performed. It was found that the method of Brinell hardness measurements performed better than Vickers, in tension-compression loading. This is from the perspective that the measurement exhibited a more consistent change through the fatigue damage accumulation. In addition, the statistical significance of the parameter adopted for damage was more marked with Brinell than with Vickers. However, for tension-tension testing, the specimens would commonly exhibit the formation of fatigue

Lüders bands, thus making the assessment of fatigue damage by hardness measurements quite uncertain. Furthermore, it was found that the indentations left after macroscopic hardness measurements in tension-compression acted as crack-initiation locations, whereas this was not observed for tension-tension loading. Through the use of finite element analysis, it was found that the indentations of both Vickers and Brinell will leave relatively high residual tensile stresses in the direction of applied stress. For tension-compression, this will result in a local region which experiences the stress amplitude, amplified by the indentation, in addition to a local mean stress effect, thus promoting crack initiation. This results in the fact that it should not be considered non-destructive in regard to fatigue, unless the indentation and residual stress field can subsequently be removed.

3. A new damage model was proposed on the basis of the damage theory known as the theory of the S-N fatigue damage envelope and a commonly accepted functional form adopted within the domain of fatigue damage modelling. The resulting function was herein based on a generalized form of the S-N curve, resulting in it being a generalized damage function, which does not depend on any additional material parameters other than the readily available S-N curves. The work can also be considered a framework to develop S-N curve-specific damage functions, as the theory should be applicable to bilinear, trilinear and full-range S-N curves. The proposed damage function was compared with other damage functions which have similar requirements, in addition to Miner's rule, where the function generally exhibited better prediction than Miner's rule and some of the other models. In addition, the adopted damage theory was compared with commonly accepted relationships to the fatigue damaging process.

4. A discussion was also included, in relation to the fact that a fully functional framework now exists to be able to adopt nonlinear damage functions in design. It was found that the nonlinear damage functions recently proposed at the University of Stavanger generally exhibit higher accuracy and more conservative estimations, compared to the commonly adopted Miner's rule. In fact, the presented models exhibited more accurate and conservative estimates of the remaining fatigue capacity/life, with the exception of an aluminium alloy under multiblock loading, where the results were more accurate but slightly less conservative. Furthermore, it was also identified that the commonly adopted damage functions can be generalized to be a combined function with two exponential terms, as presented in Eq. (11). Herein, it is also shown that two special cases of the proposed function exist, where the parameters are reduced to a single ratio, which is subsequently evaluated based on experimental data. It was found that Eq. (12) does not seem adequate for damage modelling, whereas Eq. (13) remains uncertain.

5. The mechanical properties of additively manufactured steel printed by Bound Metal Deposition were researched. The material adopted was 17-4 PH; the printed specimens were found to exhibit anisotropic properties, which can be correlated to a mesh of crack-like defects associated with the printing strategy, resulting in the conclusion that the fatigue capacity is expected to be very poor, compared to traditional ways of manufacturing, and also to exhibit anisotropic properties. Consequently, the resulting material/part exhibits this initial mesh of microscopic cracks, which is expected to quickly propagate as cyclic loading is applied.

3.3 Suggestions for future work

There are still research gaps within the topics discussed herein; hence, suggestions for future research are mentioned below.

1. Herein, research into damage assessment by macroscopic hardness, before a macroscopic crack has been initiated, was performed by investigating the applicability of the load and hardness indenter type to hardness measurements. It was found that Brinell hardness was more successful in relation to monitoring a continuous change through the fatigue life. However, further research within this domain should be performed. For instance, if several specimens were subjected to fatigue, both at various stress amplitudes and at various percentages of the total fatigue capacity, a high number of hardness measurements could be performed on each specimen, which would increase confidence in the statistical mean value and distribution, while the results could also be adopted to develop damage functions. Furthermore, the feasibility of hardness amongst other techniques for damage assessment, as a means of damage evaluation during variable amplitude loading, is another topic for further research.
2. The damage function developed through the application of the theory of the S-N fatigue damage envelope was herein adopted only for a generalized form of the S-N curve. In fact, the generalized form adopted was a straight line through the ultimate strength and the knee-point stress amplitude. However, the theory should also be applicable to other curves, which is the advantage of the theory. Hence, further studies should be performed on bilinear S-N curves from the standards and codes, to further check the feasibility of such curves. In addition, the theory can also be applied to curves which are categorized as full-range S-N curves, with the work of Kohout and Vechet providing an example of such a curve [110].

3. The functional form commonly adopted within the domain of fatigue damage was also researched herein. Further research on this topic with a larger number of experimental results would be of interest, to both investigate the feasibility of the functional forms and further develop the domain of fatigue damage modelling.
4. Herein, additive manufacturing by Bound Metal Deposition (BMD) was performed. However, further research should be performed regarding the fatigue capacity of additively manufactured parts, from the aforementioned perspective that fatigue is a common cause of failure in mechanical parts, which is one of the main targeted areas of additive manufacturing. Further research might be the applicability of post processing of the resulting product, in addition to printing parameters, of which the resulting product is a function.

References

[1] G. Ersdal, J. V. Sharp, and A. Stacey, *Ageing and Life Extension of Offshore Structures: The Challenge of Managing Structural Integrity*. Newark: John Wiley & Sons, Incorporated, 2019.

[2] A. Stacey and J. V. Sharp, "Ageing and Life Extension Considerations in the Integrity Management of Fixed and Mobile Offshore Installations," in *ASME 2011 30th International Conference on Ocean, Offshore and Arctic Engineering*, 2011, vol. 3: Materials Technology, pp. 49-65, doi: 10.1115/omae2011-49090.

[3] P. M. Office. "Major initiative to promote offshore wind power." https://www.regjeringen.no/en/aktuelt/major-initiative-to-promote-offshore-wind-power/id2900436/ (accessed 27.05, 2022).

[4] I. Lotsberg, *Fatigue design of marine structures*. Cambridge: Cambridge University Press, 2016.

[5] H.-J. W. Weihe. "Ocean Traveler." in Store Norske Leksikon, snl.no. https://snl.no/Ocean_Traveler (accessed 27.05, 2022).

[6] A. Ghoneim, I. Lotsberg, H. Bratfos, L. Yang, and M. Moczulski, "Fatigue Calculations for Existing Gulf of Mexico Fixed Structures," Det Norske Veritas, TA&R 675, 2012. [Online]. Available: https://www.bsee.gov/tap-technical-assessment-program/tap-675aa

[7] H. E. Boyer, *Atlas of Fatigue Curves*. United States: ASM International, 1986.

[8] S. Suresh, *Fatigue of Materials*, 2 ed. Cambridge: Cambridge University Press, 1998.

[9] W. A. J. Albert, "Uber Treibseile am Harz," *Archiv für Mineralogie, Geognosie, Bergbau und Hüttenkunde,* vol. 10, pp. 215-234, 1837.

[10] "Riksrevisjonens undersøkelse av myndighetenes arbeid med Alexander L. Kielland-ulykken," Riksrevisjonen.no, Dokument 3:6 (2020–2021), 09.03 2021. [Online]. Available: https://www.riksrevisjonen.no/rapporter-mappe/no-2020-2021/undersokelse-av-myndighetenes-arbeid-med-alexander-l.-kielland-ulykken/

[11] A. M. Lie, R. Sune, G. W. Dunsæd, E. Sørensen, and S. Andreassen, "Undesirable incident with HTV Eagle pipehandling crane – Statoil Gullfaks B – 7 March 2017," Petroleumstilsynet, 2017. [Online]. Available: https://www.ptil.no/en/supervision/investigation-reports/2017/statoil-gullfaks-b-investigation-of-crane-incident/

[12] AIBN, "Report on the air accident near Turøy, Øygarden municipality, Hordaland county, Norway 29 April 2016 with Airbus Helicopters EC 225 LP, LN-OJF, operated by CHC Helikopter Service AS," Norwegian Safety Investigation Authority, SL 2018/04, 2018. [Online]. Available: https://www.nsia.no/Aviation/Published-reports/2018-04

[13] A. Almar-Næss, *Fatigue handbook : offshore steel structures*. Trondheim (Norway): Tapir Publishers, 1985.

[14] F. C. Campbell, *Elements of metallurgy and engineering alloys*, 1st ed. Materials Park: Materials Park: ASM International, 2008, pp. 667-667.

[15] M. Lorentzen. "Equinor støtter italienske 3D-printgründere: – Her går vi fra grav til vugge." E24. https://e24.no/teknologi/i/X8rLOB/equinor-stoetter-italienske-3d-printgrundere-her-gaar-vi-fra-grav-til-vugge (accessed 05.05, 2022).

[16] Equinor. "Equinor signs deals with startups from the Equinor and Techstars Energy Accelerator." https://www.equinor.com/news/archive/20210512-techstars-energy-accelerator (accessed 05.05, 2022).

[17] K. S. Grønnestad. "Equinor vil ha 3D-print av reservedeler." https://www.tu.no/artikler/equinor-vil-ha-3d-print-av-reservedeler/479443 (accessed 22.01, 2020).

[18] *NORSOK N-005:2017, In-service integrity management of structures and marine systems*, 2017.

[19] *NORSOK N-006:2015, Assessment of structural integrity for existing offshore load-breaing structures*, 2015.

[20] *DNV-RP-C203: Fatigue design of offshore steel structures, Recommended practice*, Det Norske Veritas, 2019.

[21] G. Socha, "Prediction of the fatigue life on the basis of damage progress rate curves," *International Journal of Fatigue,* vol. 26, no. 4, pp. 339-347, 2004, doi: 10.1016/j.ijfatigue.2003.08.019.

[22] H. Mughrabi, "Microstructural mechanisms of cyclic deformation, fatigue crack initiation and early crack growth," *Philosophical Transactions of the Royal Society A: Mathematical, Physical and Engineering Sciences,* vol. 373, no. 2038, 2015, Art no. 20140132, doi: doi:10.1098/rsta.2014.0132.

[23] A. V. Eremin, S. V. Panin, and Y. P. Sharkeev, "Fatigue behaviour of CG and UFG titanium: DIC and fractography studies," *IOP Conference Series: Materials Science and Engineering,* vol. 511, 2019, Art no. 012012, doi: 10.1088/1757-899x/511/1/012012.

[24] L. Yang and A. Fatemi, "Cumulative fatigue damage mechanisms and quantifying parameters: A literature review," *Journal of Testing and Evaluation,* vol. 26, no. 2, pp. 89-100, 1998.

[25] H. Xin and M. Veljkovic, "Residual stress effects on fatigue crack growth rate of mild steel S355 exposed to air and seawater environments," *Materials & Design,* vol. 193, 2020, Art no. 108732, doi: 10.1016/j.matdes.2020.108732.

[26] A. Palmgren, "Die Lebensdauer von Kugellagern," *Zeitschrift des Vereines Deutscher Ingenieure,* vol. 58, no. 14, pp. 339-341, 1924.

[27] M. A. Miner, "Cumulative damage in fatigue," *Journal of applied mechanics,* vol. 12, no. 3, pp. A159-A164, 1945.

[28] *Eurocode 3: Design of steel structures-Part 1–9: Fatigue*, NS-EN 1993-1-9:2005+NA:2010, European Committee for Standardization/Standard Norge, 2010.

[29] *NORSOK N-004:2021+AC, Design of steel structures*, 2021.

[30] N. E. Dowling, *Fatigue Failure Predictions for Complicated Stress-Strain Histories*. T. & A.M. Report no. 337. Department of theoretical and applied mechanics university of Illinois, 1971.

[31] N. M. Newmark, "A Review of Cumulative Damage in Fatigue," University of Illinois Engineering Experiment Station. College of Engineering. University of Illinois at Urbana-Champaign, Technical Report 1950. [Online]. Available: https://www.ideals.illinois.edu/handle/2142/13430

[32] T. DebRoy *et al.*, "Additive manufacturing of metallic components – Process, structure and properties," *Progress in Materials Science,* vol. 92, pp. 112-224, 2018, doi: 10.1016/j.pmatsci.2017.10.001.

[33] Z. Wang, W. Wu, G. Qian, L. Sun, X. Li, and J. A. F. O. Correia, "In-situ SEM investigation on fatigue behaviors of additive manufactured Al-Si10-Mg alloy at elevated temperature," *Engineering Fracture Mechanics,* vol. 214, pp. 149-163, 2019, doi: 10.1016/j.engfracmech.2019.03.040.

[34] H. Mao *et al.*, "Fatigue damage detection and location of metal materials by electrical impedance tomography," *Results in Physics,* vol. 15, 2019, Art no. 102664, doi: 10.1016/j.rinp.2019.102664.

[35] B. Sun, L. Yang, and Y. Guo, "A high-cycle fatigue accumulation model based on electrical resistance for structural steels," *Fatigue & Fracture of Engineering Materials & Structures,* vol. 30, no. 11, pp. 1052-1062, 2007, doi: 10.1111/j.1460-2695.2007.01175.x.

[36] B. Sun and Y. Guo, "High-cycle fatigue damage measurement based on electrical resistance change considering variable electrical resistivity and uneven damage," *International Journal of Fatigue,* vol. 26, no. 5, pp. 457-462, 2004, doi: 10.1016/j.ijfatigue.2003.10.004.

[37] J. Polák, "Electrical resistivity of cyclically deformed copper," *Czechoslovak Journal of Physics,* vol. 19, no. 3, pp. 315-322, 1969, doi: 10.1007/BF01712868.

[38] G. Drumond, B. Pinheiro, I. Pasqualino, F. Roudet, and D. Chicot, "High Cycle Fatigue Damage Evaluation of Steel Pipelines Based on Microhardness Changes During Cyclic Loads: Part II," in *ASME 2018 37th International Conference on Ocean, Offshore and Arctic Engineering*, 2018, vol. 4: Materials Technology, doi: 10.1115/omae2018-78752.

[39] G. Drumond, B. Pinheiro, I. Pasqualino, F. Roudet, D. Chicot, and X. Decoopman, "High Cycle Fatigue Damage Evaluation of Steel Pipelines Based on Microhardness Changes During Cyclic Loads," in *ASME 2017 36th International Conference on Ocean, Offshore and Arctic Engineering*, 2017, vol. 4: Materials Technology, doi: 10.1115/omae2017-62677.

[40] Š. Miroslav, C. Vladimír, and M. Kepka, "Possibility of fatigue damage detection by non-destructive measurement of the surface hardness," in *Procedia Structural Integrity*, 2017, vol. 7, pp. 262-267, doi: 10.1016/j.prostr.2017.11.087.

[41] X. Chen and S. M. Zhao, "Evaluation of fatigue damage at welded tube joint under cyclic pressure using surface hardness measurement," *Engineering Failure Analysis,* vol. 12, no. 4, pp. 616-622, 2005, doi: 10.1016/j.engfailanal.2004.08.001.

[42] D. G. Pavlou, "A phenomenological fatigue damage accumulation rule based on hardness increasing, for the 2024-T42 aluminum," *Engineering Structures,* vol. 24, no. 11, pp. 1363-1368, 2002, doi: 10.1016/S0141-0296(02)00055-X.

[43] D. Ye and Z. Wang, "Approach to investigate pre-nucleation fatigue damage of cyclically loaded metals using Vickers microhardness tests," *International Journal of Fatigue,* vol. 23, no. 1, pp. 85-91, 2001, doi: 10.1016/S0142-1123(00)00034-7.

[44] D. Ye, X. Tong, L. Yao, and X. Yin, "Fatigue hardening/softening behaviour investigated through Vickers microhardness measurement during high-cycle fatigue," *Materials Chemistry and Physics,* vol. 56, no. 3, pp. 199-204, 1998, doi: 10.1016/S0254-0584(98)00135-7.

[45] D. Y. Ye, D. J. Wang, and P. An, "Characteristics of the change in the surface microhardness during high cycle fatigue damage," *Materials Chemistry and Physics,* vol. 44, no. 2, pp. 179-181, 1996, doi: 10.1016/0254-0584(95)01669-L.

[46] B. Pinheiro, J. Lesage, I. Pasqualino, E. Bemporad, and N. Benseddiq, "X-ray diffraction study of microstructural changes during fatigue damage initiation in pipe steels: Role of the initial dislocation structure," *Materials Science and Engineering: A,* vol. 580, pp. 1-12, 2013, doi: 10.1016/j.msea.2013.05.042.

[47] B. Pinheiro, J. Lesage, I. Pasqualino, N. Benseddiq, and E. Bemporad, "X-ray diffraction study of microstructural changes during fatigue damage initiation in steel pipes," *Materials Science and Engineering: A,* vol. 532, pp. 158-166, 2012, doi: 10.1016/j.msea.2011.10.077.

[48] K. Vijayan, A. Mani, C. Balasingh, and A. K. Singh, "X-ray analysis of polycrystalline aluminium subjected to fatigue cycling," *Bulletin of Materials Science,* vol. 10, no. 3, pp. 205-216, 1988, doi: 10.1007/BF02744065.

[49] R. N. Pangborn, S. Weissmann, and I. R. Kramer, "Dislocation distribution and prediction of fatigue damage," *Metallurgical Transactions A,* vol. 12, no. 1, pp. 109-120, 1981, doi: 10.1007/BF02648515.

[50] M. Nagao and V. Weiss, "X-ray diffaction study of low cycle fatigue damage in plain carbon steel," *Journal of Engineering Materials and Technology,* vol. 99, no. 2, pp. 110-113, 1977, doi: 10.1115/1.3443418.

[51] A. Risitano and G. Risitano, "Determining fatigue limits with thermal analysis of static traction tests," *Fatigue & Fracture of Engineering Materials & Structures,* vol. 36, no. 7, pp. 631-639, 2013, doi: 10.1111/ffe.12030.

[52] P. Kucharczyk, A. Rizos, S. Münstermann, and W. Bleck, "Estimation of the endurance fatigue limit for structural steel in load increasing tests at low temperature," *Fatigue & Fracture of Engineering Materials & Structures,* vol. 35, no. 7, pp. 628-637, 2012, doi: 10.1111/j.1460-2695.2011.01656.x.

[53] M. Amiri and M. M. Khonsari, "Rapid determination of fatigue failure based on temperature evolution: Fully reversed bending load," *International Journal of Fatigue,* vol. 32, no. 2, pp. 382-389, 2010, doi: 10.1016/j.ijfatigue.2009.07.015.

[54] D. Wagner, N. Ranc, C. Bathias, and P. C. Paris, "Fatigue crack initiation detection by an infrared thermography method," *Fatigue & Fracture of Engineering Materials & Structures,* vol. 33, no. 1, pp. 12-21, 2010, doi: 10.1111/j.1460-2695.2009.01410.x.

[55] H. Wang, L. Jiang, P. K. Liaw, C. R. Brooks, and D. L. Klarstrom, "Infrared temperature mapping of ULTIMET alloy during high-cycle fatigue tests," *Metallurgical and Materials Transactions A,* vol. 31, no. 4, pp. 1307-1310, 2000, doi: 10.1007/s11661-000-0126-y.

[56] L. Dietrich and G. Socha, "Accumulation of Damage in A336 GR5 Structural Steel Subject to Complex Stress Loading," *Strain,* vol. 48, no. 4, pp. 279-285, 2012, doi: 10.1111/j.1475-1305.2011.00821.x.

[57] G. Socha, "Experimental investigations of fatigue cracks nucleation, growth and coalescence in structural steel," *International Journal of Fatigue,* vol. 25, no. 2, pp. 139-147, 2003, doi: 10.1016/S0142-1123(02)00068-3.

[58] Y. Uematsu, T. Kakiuchi, K. Hattori, N. Uesugi, and F. Nakao, "Non-destructive evaluation of fatigue damage and fatigue crack initiation in type 316 stainless steel by positron annihilation line-shape and lifetime analyses," *Fatigue & Fracture of Engineering Materials & Structures,* vol. 40, no. 7, pp. 1143-1153, 2017, doi: 10.1111/ffe.12572.

[59] U. Holzwarth and P. Schaaff, "On the non-destructive detection of fatigue damage in industrial aluminium alloys by positron annihilation," *Journal of Materials Science,* vol. 42, no. 14, pp. 5620-5628, 2007, doi: 10.1007/s10853-006-0993-8.

[60] U. Holzwarth and P. Schaaff, "Nondestructive monitoring of fatigue damage evolution in austenitic stainless steel by positron-lifetime measurements," *Physical Review B - Condensed Matter and Materials Physics,* vol. 69, no. 9, 2004, doi: 10.1103/PhysRevB.69.094110.

[61] Y. Kawaguchi and Y. Shirai, "Fatigue evaluation of type 316 stainless steel using positron annihilation lineshape analysis and β+-γ coincidence positron lifetime measurement," *Journal of Nuclear Science and Technology,* vol. 39, no. 10, pp. 1033-1040, 2002, doi: 10.1080/18811248.2002.9715291.

[62] P. Asoka-Kumar *et al.*, "Direct observation of carbon-decorated defects in fatigued type 304 stainless steel using positron annihilation spectroscopy," *Acta Materialia,* vol. 50, no. 7, pp. 1761-1770, 2002, doi: 10.1016/S1359-6454(02)00027-7.

[63] F. Hori and R. Oshima, "Positron annihilation study in the early stage of fatigue in type 304 stainless steel," *Physica Status Solidi (a),* vol. 191, no. 2, pp. 409-417, 2002, doi: 10.1002/1521-396X(200206)191:2<409::AID-PSSA409>3.0.CO;2-H.

[64] N. Maeda, N. Nakamura, M. Uchida, Y. Ohta, and K. Yoshida, "Application of positron annihilation line-shape analysis to fatigue damage for nuclear plant materials," *Nuclear Engineering and Design,* vol. 167, no. 2, pp. 169-174, 1996, doi: 10.1016/S0029-5493(96)01295-2.

[65] M. Teschke, J. R. Vasquez, L. Lücker, and F. Walther, "Characterization of damage evolution on hot flat rolled mild steel sheets by means of micromagnetic parameters and fatigue strength determination," *Materials,* vol. 13, no. 11, 2020, Art no. 2486, doi: 10.3390/ma13112486.

[66] I. Tomáš, O. Kovářík, J. Kadlecová, and G. Vértesy, "Optimization of fatigue damage indication in ferromagnetic low carbon steel," *Measurement Science and Technology,* vol. 26, no. 9, 2015, Art no. 095603, doi: 10.1088/0957-0233/26/9/095603.

[67] H. Kikuchi, K. Ara, Y. Kamada, and S. Kobayashi, "Effect of microstructure changes on Barkhausen noise properties and hysteresis loop in cold rolled low carbon steel," *IEEE Transactions on Magnetics,* vol. 45, no. 6, pp. 2744-2747, 2009, doi: 10.1109/TMAG.2009.2020545.

[68] S. P. Sagar, N. Parida, S. Das, G. Dobmann, and D. K. Bhattacharya, "Magnetic Barkhausen emission to evaluate fatigue damage in a low carbon structural steel," *International Journal of Fatigue,* vol. 27, no. 3, pp. 317-322, 2005, doi: 10.1016/j.ijfatigue.2004.06.015.

[69] A. Kumar, C. J. Torbet, T. M. Pollock, and J. Wayne Jones, "In situ characterization of fatigue damage evolution in a cast Al alloy via nonlinear ultrasonic measurements," *Acta Materialia,* vol. 58, no. 6, pp. 2143-2154, 2010, doi: 10.1016/j.actamat.2009.11.055.

[70] T. Ohtani, K. Nishiyama, S. Yoshikawa, H. Ogi, and M. Hirao, "Ultrasonic attenuation and microstructural evolution throughout tension-compression fatigue of a low-carbon steel," *Materials Science and Engineering A,* vol. 442, no. 1-2, pp. 466-470, 2006, doi: 10.1016/j.msea.2006.02.226.

[71] J. H. Liu, G. L. Li, X. Y. Hao, D. B. Zeng, and Z. H. Sun, "Ultrasonic measurement of fatigue damage of nodular cast iron," *Materials Letters,* vol. 50, no. 4, pp. 194-198, 2001, doi: 10.1016/S0167-577X(01)00224-5.

[72] P. B. Nagy, "Fatigue damage assessment by nonlinear ultrasonic materials characterization," *Ultrasonics,* vol. 36, no. 1-5, pp. 375-381, 1998, doi: 10.1016/S0041-624X(97)00040-1.

[73] *Metallic materials - Brinell hardness test - Part 1: Test method*, ISO 6506-1:2014, International Organization for Standardization, 2014.

[74] *Metallic materials - Vickers hardness test - Part 1: Test method*, ISO 6507-1:2005, International Organization for Standardization, 2005.

[75] A. Fatemi and L. Yang, "Cumulative fatigue damage and life prediction theories: A survey of the state of the art for homogeneous materials," *International Journal of Fatigue,* vol. 20, no. 1, pp. 9-34, 1998, doi: 10.1016/S0142-1123(97)00081-9.

[76] K. Hectors and W. De Waele, "Cumulative Damage and Life Prediction Models for High-Cycle Fatigue of Metals: A Review," *Metals,* vol. 11, no. 2, 2021, Art no. 204, doi: 10.3390/met11020204.

[77] S. M. Marco and W. L. Starkey, "A concept of fatigue damage," *Transactions of the ASME,* vol. 76, pp. 627-632, 1954.

[78] B. F. Langer, "Fatigue Failure From Stress Cycles of Varying Amplitude," *Journal of Applied Mechanics,* vol. 4, no. 4, pp. A160-A162, 2021, doi: 10.1115/1.4008807.

[79] H. J. Grover, "An Observation Concerning the Cycle Ratio in Cumulative Damage," in *Symposium on Fatigue of Aircraft Structures*. ASTM STP 274, American Society for Testing and Materials, Philadelphia, 1960, pp. 120-124.

[80] S. S. Manson, J. C. Freche, and C. R. Ensign, "Application of a double linear damage rule to cumulative fatigue," *Fatigue crack propagation. ASTM STP 415,* pp. 384-412, 1967, doi: 10.1520/STP47237S.

[81] S. S. Manson, "Interfaces between fatigue, creep, and fracture," *International Journal of Fracture Mechanics,* vol. 2, no. 1, pp. 327-363, 1966, doi: 10.1007/BF00188825.

[82] S. S. Manson, A. J. Nachtigall, C. R. Ensign, and J. C. Freche, "Further Investigation of a Relation for Cumulative Fatigue Damage in Bending," *Journal of Engineering for Industry,* vol. 87, no. 1, pp. 25-35, 1965, doi: 10.1115/1.3670753.

[83] S. S. Manson and G. R. Halford, "Practical implementation of the double linear damage rule and damage curve approach for treating cumulative fatigue damage," *International Journal of Fracture,* vol. 17, no. 2, pp. 169-192, 1981, doi: 10.1007/BF00053519.

[84] S. S. Manson and G. R. Halford, "Re-examination of cumulative fatigue damage analysis—an engineering perspective," *Engineering Fracture Mechanics,* vol. 25, no. 5-6, pp. 539-571, 1986, doi: 10.1016/0013-7944(86)90022-6.

[85] J. Lemaitre and A. Plumtree, "Application of damage concepts to predict creep-fatigue failures.," *Journal of Engineering Materials and Technology,* vol. 101, no. 3, pp. 284-292, 1979.

[86] J. L. Chaboche and P. M. Lesne, "A non-linear contineous fatigue damage model," *Fatigue & Fracture of Engineering Materials & Structures,* vol. 11, no. 1, pp. 1-17, 1988, doi: 10.1111/j.1460-2695.1988.tb01216.x.

[87] D.-G. Shang and W.-X. Yao, "A nonlinear damage cumulative model for uniaxial fatigue," *International Journal of Fatigue,* vol. 21, no. 2, pp. 187-194, 1999, doi: 10.1016/S0142-1123(98)00069-3.

[88] G. Mesmacque, S. Garcia, A. Amrouche, and C. Rubio-Gonzalez, "Sequential law in multiaxial fatigue, a new damage indicator," *International Journal of Fatigue,* vol. 27, no. 4, pp. 461-467, 2005, doi: 10.1016/j.ijfatigue.2004.08.005.

[89] S. Subramanyan, "A Cumulative Damage Rule Based on the Knee Point of the S-N Curve," *Journal of Engineering Materials and Technology,* vol. 98, no. 4, pp. 316-321, 1976, doi: 10.1115/1.3443383.

[90] Z. Hashin and A. Rotem, "A cumulative damage theory of fatigue failure," *Materials Science and Engineering,* vol. 34, no. 2, pp. 147-160, 1978, doi: 10.1016/0025-5416(78)90045-9.

[91] K. Rege and D. G. Pavlou, "A one-parameter nonlinear fatigue damage accumulation model," *International Journal of Fatigue,* vol. 98, pp. 234-246, 2017, doi: 10.1016/j.ijfatigue.2017.01.039.

[92] A. Aeran, S. C. Siriwardane, O. Mikkelsen, and I. Langen, "An accurate fatigue damage model for welded joints subjected to variable amplitude loading," *IOP Conference Series: Materials Science and Engineering,* vol. 276, 2017, Art no. 012038, doi: 10.1088/1757-899x/276/1/012038.

[93] A. Aeran, S. C. Siriwardane, O. Mikkelsen, and I. Langen, "A new nonlinear fatigue damage model based only on S-N curve parameters," *International Journal of Fatigue,* vol. 103, pp. 327-341, 2017, doi: 10.1016/j.ijfatigue.2017.06.017.

[94] J. Milewski, "Additive Manufacturing of Metals: From Fundamental Technology to Rocket Nozzles, Medical Implants, and Custom Jewelry," *Additive Manufacturing of Metals,* 2017.

[95] D. Herzog, V. Seyda, E. Wycisk, and C. Emmelmann, "Additive manufacturing of metals," *Acta Materialia,* vol. 117, pp. 371-392, 2016, doi: 10.1016/j.actamat.2016.07.019.

[96] P. D. Nezhadfar *et al.*, "Fatigue crack growth behavior of additively manufactured 17-4 PH stainless steel: Effects of build orientation and microstructure," *International Journal of Fatigue,* vol. 123, pp. 168-179, 2019, doi: 10.1016/j.ijfatigue.2019.02.015.

[97] B. Blakey-Milner *et al.*, "Metal additive manufacturing in aerospace: A review," *Materials & Design,* vol. 209, 2021, Art no. 110008, doi: 10.1016/j.matdes.2021.110008.

[98] Markforged. "Metal X System." https://markforged.com/3d-printers/metal-x (accessed 13.09.2021, 2021).

[99] Desktop-metal. "Deep Dive: Bound Metal Deposition (BMD)." https://www.desktopmetal.com/resources/deep-dive-bmd (accessed 13.09.2021, 2021).

[100] F. Bjørheim, S. C. Siriwardane, and D. Pavlou, "Fatigue Damage Monitoring Methods - current practices," in *International Conference on Offshore Renewable Energy - CORE*, Online, 2021, pp. 112-125.

[101] F. Bjørheim, S. C. Siriwardane, and D. Pavlou, "A review of fatigue damage detection and measurement techniques," *International Journal of Fatigue,* vol. 154, 2022, Art no. 106556, doi: 10.1016/j.ijfatigue.2021.106556.

[102] F. Bjørheim, D. G. Pavlou, and S. C. Siriwardane, "Hardness measurements as a technique for measuring accumulated fatigue damage," *International Journal of Structural Integrity,* vol. ahead-of-print, no. ahead-of-print, 2022, doi: 10.1108/IJSI-04-2022-0061.

[103] D. Pilo, W. Reik, P. Mayr, and E. Macherauch, "Cyclic induced creep of a plain carbon steel at room temperature," *Fatigue & Fracture of Engineering Materials & Structures,* vol. 1, no. 3, pp. 287-295, 1979, doi: 10.1111/j.1460-2695.1979.tb00385.x.

[104] F. Bjørheim, D. G. Pavlou, and S. C. Siriwardane, "Nonlinear fatigue life prediction model based on the theory of the S-N fatigue damage envelope," *Fatigue & Fracture of Engineering Materials & Structures,* vol. 45, no. 5, pp. 1480-1493, 2022, doi: 10.1111/ffe.13680.

[105] D. G. Pavlou, "The theory of the S-N fatigue damage envelope: Generalization of linear, double-linear, and non-linear fatigue damage models," *International Journal of Fatigue,* vol. 110, pp. 204-214, 2018, doi: 10.1016/j.ijfatigue.2018.01.023.

[106] D. Pavlou, "A deterministic algorithm for nonlinear, fatigue-based structural health monitoring," *Computer-Aided Civil and Infrastructure Engineering,* vol. 37, pp. 809-831, 2021, doi: 10.1111/mice.12783.

[107] F. Bjørheim, S. C. Siriwardane, and D. G. Pavlou, "On the topic of fatigue damage modelling of offshore structures and the way forward," in *ECCOMAS Congress 2022 VII European Congress on Computational Methods in Applied Sciences and Engineering*, 2022.

[108] A. Aid, A. Amrouche, B. B. Bouiadjra, M. Benguediab, and G. Mesmacque, "Fatigue life prediction under variable loading based on a new damage model," *Materials & Design,* vol. 32, no. 1, pp. 183-191, 2011, doi: 10.1016/j.matdes.2010.06.010.

[109] F. Bjørheim and I. M. La Torraca Lopez, "Tension testing of additively manufactured specimens of 17-4 PH processed by Bound Metal Deposition," *IOP Conference Series: Materials Science and Engineering,* vol. 1201, no. 1, 2021, Art no. 012037, doi: 10.1088/1757-899x/1201/1/012037.

[110] J. Kohout and S. Věchet, "A new function for fatigue curves characterization and its multiple merits," *International Journal of Fatigue,* vol. 23, no. 2, pp. 175-183, 2001, doi: 10.1016/S0142-1123(00)00082-7.

Part II – Papers

Paper I

Fatigue Damage Monitoring Methods – current practices

Conference Paper
5th International Conference on Offshore Renewable Energy
CORE 2021
Online

Paper II

A Review of Fatigue Damage Detection and Measurement Techniques

Journal Paper
International Journal of Fatigue
January 2022, Volume 154, Article 106556

International Journal of Fatigue 154 (2022) 106556

Contents lists available at ScienceDirect

International Journal of Fatigue

journal homepage: www.elsevier.com/locate/ijfatigue

A review of fatigue damage detection and measurement techniques

Fredrik Bjørheim, Sudath C. Siriwardane, Dimitrios Pavlou *

University of Stavanger, Department of Mechanical and Structural Engineering and Materials Science, Stavanger N-4036, Norway

ARTICLE INFO

Keywords:
Fatigue
Damage
Measurement
NDT
Diagnostics

ABSTRACT

A vast amount of research has been carried out towards the goal of quantifying changes related to the fatigue damaging process in materials throughout the fatigue life. However, no recommended practice has been developed for the experimental measurement of fatigue damage before a macroscopic crack has been initiated. Therefore, this paper reviews the existing fatigue damage detection and measurement techniques on the basis of both momentum within the research field and their being considered non-destructive. The techniques are separated into two categories, namely, fatigue crack monitoring and fatigue damage monitoring. The parameters of these techniques, which quantify the physical and mechanical changes of the materials during the fatigue life, were critically reviewed in regard to the mechanism behind the change, limitations, shortcomings, etc. The acoustic emission, hardness, ultrasonic, magnetic and potential drop methods are applicable for in-situ measurements while positron annihilation and X-ray diffraction are more suitable for laboratory assessments. Even though all the revived methods are applicable for metals, acoustic emissions, X-ray diffraction, ultrasonic, strain-based and thermometric methods are also suitable for composites. The reliability, advantages, weaknesses, case/material dependency and applicability of each method are compared and tabulated for making a framework for choosing suitable technique for fatigue crack or damage detection of material or components.

1. Introduction

The iterative deterioration caused by the cyclic loading of a component or material, which eventually leads to crack initiation and, shortly after, final fracture, is generally known as “fatigue” by practising engineers. The current methodology to prevent this catastrophic failure is commonly based upon statistical analysis, with the addition of a damage accumulation rule, which is known to introduce further scatter. Furthermore, it can be seen in DNVGL-RP [1] and in a paper by Keprate and Ratnayake [2] that the common methodology for life extension involves estimating crack growth through statistical analysis and initiating an inspection program. The intervals of such an inspection program must be short enough for a detectable crack to not reach a critical size between inspections, to ensure safety during the life extension period. Consequently, the methodology in itself is fairly conservative, as the formation of a crack is certainly the simplest yet strongest indication of fatigue damage. However, the issue comes down to the fact that the crack propagation phase is commonly short, compared to the total fatigue life [3]. This results in a frequent and costly inspection program being initiated, from the time that conservative estimations of the fatigue life have been surpassed, until the point of decommissioning or, alternatively, retrofitting.

Fatigue occurs as a result of localized microstructural deformations due to cyclic loading, where the density of dislocations produced is significantly higher than for monotonic loading. The dislocations will under continued cycling form dislocation structures, such as well-defined cell structures and eventually persistent slip bands. Thereafter, microcrack initiation, coalescence and macroscopic crack propagation occurs [4,5]. Therefore, crack initiation remains the only sound methodology for assessing the remaining fatigue life, as it arises from the characteristics of the fatigue phenomenon [6,7]. This from the perspective that, detecting, measuring and assessing the fatigue damage prior to macroscopic crack initiation is quite challenging, due to the inherent nature of the phenomenon. However, the mechanisms before crack initiation will for example increase the surface hardness, generate heat, and nonuniformly deform the surface crystals, consequently resulting in the hardness-based, thermometric and X-ray diffraction methods which will be reviewed.

Regardless of the difficulties related to detecting and quantifying the accumulated fatigue damage, a vast number of researchers have performed experimental work and found several indicators of fatigue damage [8]. These indicators have contributed to the perspectives of

* Corresponding author.
E-mail address: dimitrios.g.pavlou@uis.no (D. Pavlou).

https://doi.org/10.1016/j.ijfatigue.2021.106556
Received 14 June 2021; Received in revised form 8 September 2021; Accepted 19 September 2021
Available online 22 September 2021

both better understanding the fatigue phenomenon and better predicting the remaining fatigue capacity. Even though much research has been performed, with varying degrees of success, a common practice/method/indicator has yet to be established for quantifying the accumulated damage prior to macroscopic crack initiation. Therefore, it is essential to critically review these methods from the viewpoint of accuracy, limitations, advantages, disadvantages, applicability, etc.

The objectives of this paper are to discuss the non-destructive quantifiable changes in material physical and mechanical properties throughout the fatigue life and to review the relevant detection and measurement techniques. Hence, most reliable parameters and methods are identified for investigating the related research/knowledge gaps which indicate the direction for future research.

2. Damage evaluation parameters/methods

A number of both mechanical parameters and physical measures have been proposed to be correlated with the microstructural change throughout the fatigue damaging process. The methods listed in Table 1 are chosen on the basis of both momentum within the research field and their being considered non-destructive. Momentum within the research field, is herein considered as that a number of articles from different research groups have been published regarding the method/phenomenon. The perspective of the method/phenomenon being non-destructive and having a relation to the damaging process was also considered. Furthermore, the methodologies are separated into two categories, namely, fatigue crack monitoring and fatigue damage monitoring. Fatigue crack monitoring is here considered to be the methodologies applicable after a crack has initiated, whereas fatigue damage monitoring is considered to be the phase before the aforementioned stage.

3. Crack monitoring

3.1. The potential drop method

The potential drop method (PDM) is an electric method, based on sending an electric current through the material or component and measuring the subsequent potentials at specific locations in relation to a crack. It is commonly used to either continuously or instantaneously monitor a crack in a conductive material. The methodology is based upon the fact that a crack which disrupts the continuous conductive material will significantly change the electrical potential field within the component. Therefore, crack propagation can be monitored by developing calibration curves for various crack scenarios [9]. Regarding the methodology, one can commonly discuss DC-PDM and AC-PDM; DC-PDM is the most commonly used method, whereas AC-PDM, with a high frequency current, has been observed to be more sensitive to surface cracks, due to the "skin effect" [10]. When it comes to defining calibration curves, one commonly talks about analytic, empirical and numerical methods. Gandossi et al. [11] demonstrated that finite element modelling can be used as a numerical method to develop the calibration curve with good accuracy. Spitas et al. [12] investigated the application of PDM during mixed-mode cracking, demonstrating that the application of a third sensing electrode, in contrast to the commonly used two, would result in the ability to estimate the crack angle. An example of the phenomenon can be seen in Fig. 1, developed through numerical methods, to display how the potential field is affected by the crack. Additionally, the direct current electric potential method (DC-EPM) has been considered in regard to the case of multiple small internal cracks, caused under creep-fatigue conditions, as can be seen, for example, in a paper by Tada et al. [13], which concluded that the accumulated damage could be measurable at about half the lifetime, given that the voltmeter used can measure a change of 1 percent in the potential difference.

Some examples of the accuracy of the methodology and practical examples might be such as a paper by Sonsino [14], where he compared various design concepts for the structural durability assessment of welded offshore K-nodes. In fact, the DC-PDM was adapted to define fatigue life to the initiation of a crack with a depth of about 1 mm. First detectable crack under laboratory conditions was 0.5 mm, whereas 1.0 mm for practical conditions. In [15] Černý also performed experiments on full-scale models, while monitoring the crack initiation and growth with the DC-PDM method, at elevated temperatures, also specifying that the precision of the crack length was within ±1 mm. Oppermann et al. considered in [16] the possibility of adapting DC-PDM as a means to evaluate weld seams in pipework, as a permanent installation, to reduce radiation exposure during inspection of nuclear powerplants. Herein, the perspective of achievable accuracies in monitoring is deeply discussed, from the perspective of initial length of the crack, initial crack depth and the wall thickness and length between measuring probes will affect the detectability.

Table 1
Quantifiable parameters and methods.

Category	Chapter	Method/phenomenon
Fatigue crack monitoring	3.1	Potential drop method
	3.2	Acoustic emission technique
	3.3	Ultrasonic methods
Fatigue damage monitoring	4.1	Electric resistance
	4.2	Hardness-based method
	4.3	X-ray diffraction method
	4.4	Thermometric
	4.5	Strain-based
	4.6	Positron annihilation
	4.7	Magnetic methods
	4.8	Ultrasonic methods

3.2. Acoustic emission technique

Acoustic emission (AE) is a non-destructive evaluation (NDE) method which has recently received increasing attention. The method is based on measuring the elastic stress waves, which are generated due to the rapid release of energy from a localized source within a stressed material. Thus, it is a passive methodology of NDE. Some examples of generators of elastic stress waves are plastic deformation, creep, fatigue crack nucleation and propagation, fracture and decohesion of inclusions [17,18]. It should be highlighted, however, that there are also unwanted sources of AE, such as grating between fracture surfaces, rubbing and fretting of moving parts, hammering, vibrating, rain and wind [19]. The issue of unwanted AE sources results in the application of signal

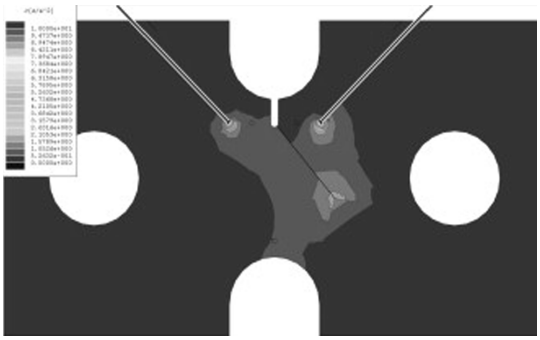

Fig. 1. Numerical methodology to develop the constant current density contours for specimen with 6.0-mm crack at 40° [12]. (Reprinted from Measurement, Volume 43, Issue 7, V. Spitas, C. Spitas, P. Michelis, A three-point electrical potential difference method for in situ monitoring of propagating mixed-mode cracks at high temperature, Pages 950–959, Copyright 2010, with permission from Elsevier.)

processing, which can be seen in works such as [20–22].

When it comes to the AE signal, it can commonly be characterized as having features such as those shown in Table 2 [20], where it can be noted that the parameters are in regard to a threshold crossing. The threshold is commonly set as a means to remove noise, by only monitoring or recording signals which exceed a certain acoustic pressure level (in dB), which in turn already highlights a weakness in the AE method. Consequently, setting the threshold too low will result in a lot of noise which is not related to the damaging process, while setting it too high might result in neglecting important signals. Thus, the threshold must be set at the "correct" level, which again is case-dependent.

As previously mentioned, the AE methodology has the advantage of being a passive method, in which the sensors detect elastic stress waves. This results both in it being applicable for continuous structural health monitoring (SHM) and that a complete scanning of the structure is not required: only a suitable number of sensors to detect the generated signals is necessary. An example of the number of sensors can be seen, for example, in [23], where it was estimated that 28 sensors were adequate to detect damage, whereas 72 would be required for damage localization for a 45.7-m-long wind turbine blade.

The AE methodology has also been investigated as a means to predict remaining fatigue life and crack extension. This can be seen in the work of Berkovits and Fang [24], who concluded that AE is an excellent tool to define initiation, and that the stress intensity factor threshold can be determined through AE, with comparable results. Furthermore, they argued that although the methodology might be complicated for estimating crack propagation, they were open to the possibility of doing so through parametric discrimination during postprocessing. Work in respect of estimating crack propagation through the use of AE signals can be seen in research by, for instance, Roberts and Talebzadeh [17,25], where an empirical relation between acoustic emission count rate and crack propagation was used. The tests were performed by extracting the count rate for the upper 5% and 10% of the applied load, with the experimental work revealing a close correlation. Similar work was also performed by Yu et al. in [26], where AE data below 80% of the peak load was removed from the dataset, and crack extension and fatigue life prediction were performed on the basis of count rate and absolute energy rate. Also to be mentioned is the study of Keshtgar and Modarres [27], who performed similar work, but using the top 40% of the peak load. All the aforementioned models on count rate and absolute energy rate follow Eq. (1):

$$\log\left(\frac{dA}{dN}\right) = B\log(\Delta K) + \log(C) \tag{1}$$

where parameter (dA/dN) is count rate, absolute energy rate or, alternatively, crack growth rate from Paris law, whereas B and C are empirical constants, depending on the methodology being used. An example of crack propagation monitoring through AE can be seen in Fig. 2, comparing the relations da/dN, dη/dN and dU/dN, being crack growth rate, count rate and absolute energy rate, respectively.

The experimental application of AE in the field can be found in, for example, detecting defects in vessels and offshore structures [18], SHM of bridges [19,28–30], wind turbine blades [23] and rail tracks [31,32], to mention a few.

Table 2
Definitions of AE time features [20].

AE Time Features	Definition
Amplitude	Peak voltage of the AE waveform
Counts	Number of threshold crossings
Duration	Time difference between the first and the last threshold crossings
Energy	Integral of the rectified voltage signal over the duration
Risetime	Time difference between the first threshold crossing and peak voltage
Counts to peak	Number of threshold crossings from first threshold to peak voltage
Absolute energy	Integral of the square voltage signal divided by the reference resistance over the entire duration

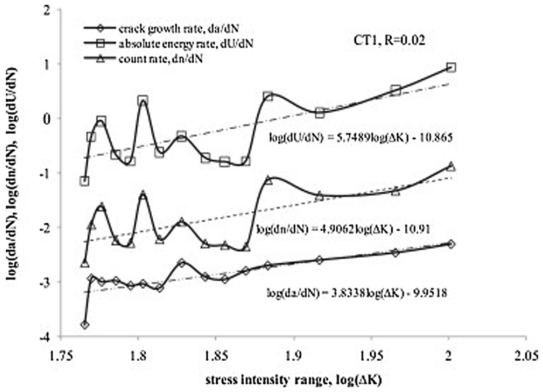

Fig. 2. Tests and regression for a CT specimen regarding the relation between da/dN, dη/dN and dU/dN, being crack growth rate, count rate and absolute energy rate, respectively, with the stress intensity range ΔK [26]. (Reprinted from Journal of Constructional Steel Research, Volume 67, Issue 8, Jianguo Yu, Paul Ziehl, Boris Zárate, Juan Caicedo, Prediction of fatigue crack growth in steel bridge components using acoustic emission, Pages 1254–1260, Copyright 2011, with permission from Elsevier.)

3.3. Ultrasonic method

The ultrasonic method is based upon sending ultrasonic waves into the material or component which is being tested, also called ultrasonic testing (UT). The ultrasonic wave is commonly generated by the use of piezoelectric transducers, whereas the non-contact technique of adapting electro-magnetic acoustic transducers (EMAT) should also be noted. As an ultrasonic wave propagate through the specimen, it will interact with discontinuities, such as cracks, which will reflect, or alternatively diffract the signal at the crack tips. Consequently, resulting in that the location and size of the crack can be determined through the sound velocity in the material and time [33].

The methods of pulse-echo and through transmission are commonly discussed in ultrasonic testing. The pulse-echo technique can be performed with either one or more ultrasonic probes, with access to one side of the part being tested. In fact, it is commonly performed by the use of an ultrasonic probe, emitting a short signal, for then to measure the subsequently reflected signal. The reflected signal will be the reflection originating from the backwall, with the addition of the signal reflected from the defect, if present. Furthermore, the intensity and arrival time of each signal will also be displayed. Consequently, resulting in that the depth to the defect, size and thickness of the specimen can be found. The through transmission technique requires both a transmitter and a receiver, with the addition of access to both sides of the specimen being tested. The transmitter will transmit a signal on one side of the specimen, which will be received by the receiver, located at the other side. If a crack or other defect is present within the scanned volume, the received signal will exhibit a lower intensity. However, the technique does not have the possibility to estimate the depth from the surface to the defect [34,35].

There are various techniques to size defects through the application of ultrasonics. Two examples might be such as the amplitude of the reflected signal from a flaw, or the time related technique of time-of-flight-diffraction (TOFD). However, it is generally accepted that the TOFD methodology is both easier to apply and more robust than the amplitude-based techniques. This from the perspective that the amplitude-based techniques commonly depend upon test pieces with

known reflectors. The test pieces should match the investigated specimen when it comes to such as material, surface finish, attenuation size and coupling conditions. Consequently, making the technique time-consuming and prone to failure if there is any difference in the reference setup and test setup. Whereas the TOFD technique is based upon the wave velocity and the diffracted signal to locate the crack tip. However, with the drawbacks of the fact that the diffracted signal will be weaker, reducing sensitivity, and that if the crack has a near surface crack-tip, the diffracted signal might coincide with the lateral signal in a commonly used pitch-catch configuration [36,37].

Examples of what has been done in regard to the TOFD technique might be such as Nath et al. who reported the possibility of sizing cracks from the outer surface in solid steam rotor shafts in [38] by the manual ultrasonic TOFD technique. Subsequently, they developed experimental probability of detection (POD) and probability of sizing (POS) curves for the complex geometry in [39]. Habibpour-Ledari and Honarvar discussed in [40] the weakness of TOFD being a two-dimensional technique. Subsequently proposing a method to locate and size defects in three dimensions, through the use of more transmitters and receivers with theoretical methods currently being used in radar systems. In fact, two algorithms were tested and compared, showing promising results. In [41] Chang and Hsieh proposed a double-probe TOFD imaging method to detect nonhorizontal flaws which could not be detected by the use of the common pulse-echo technique. Baskaran et al. Proposed in [35] the shear-wave time-of-flight-diffraction (S-TOFD) with the objective of achieving higher accuracy during near-surface inspection. Furthermore, the signal processing technique called Embedded Signal Identification Technique (ESIT) [42] was adapted to further increase accuracy. It was found that an EDM notch of 0.5 mm was sized to 0.52 mm through the combined method of S-TOFD and ESIT. Furthermore, for a fatigue crack of 2.63 mm, the application of S-TOFD alone sized it to 2.57, whereas the combination of S-TOFD and ESIT resulted in a sizing of 2.64 mm. Subbaratnam et al. highlights the limitation of TOFD for thinner sections [43]. Subsequently, proposing a technique of immersion TOFD for thin sections. This is from the perspective that immersion helps to provide sufficient time delay. The investigated material had a thickness of 3 mm, with artificial flaws down to 0.09 mm depth which were measured with good accuracy.

In [44] Masserey and Fromme investigated the application of high frequency guided waves to monitor the development of fatigue cracks at fastener holes in aircrafts. Concluding that a fatigue crack of 0.8 mm^2, which corresponded to about 1 mm depth could reliably be detected. Another study regarding sensitivity for the ultrasonic methods has been reported by Grubisic and Sonsino [45]. Crack initiation was detected by continuous ultrasonic measurements with several fixed 45°-US-sender/receivers; under laboratory conditions first detectable crack depth a = 0.25 mm, whereas under practical conditions a = 0.5 mm.

4. Damage monitoring

4.1. Electric resistance

The methodology for damage monitoring through electrical measurements has the same fundamental application as the methodology for crack monitoring. However, the parameter for damage monitoring is the change in resistance. The argument for the increased resistivity comes from cases such as dislocations, point defects, micro and macroscopic crack propagation [46]. However, there are other factors which might also affect the resistivity of the specimen, such as elongation, temperature or reduction of cross section, resulting in the fact that other changes which can influence the measurement must be eliminated or accounted for [47]. Starke et al. demonstrated how the resistivity can be used as a means to reveal initial material condition within a group of specimens made from the same material in [48], as can be seen in Fig. 3. Consequently, as the initial resistivity and the number of cycles to failure were in good correlation, higher initial resistance was attributed to a higher number of initial defects. Furthermore, it was demonstrated that resistivity can be applied to estimate the stress amplitude at the knee-point of the Woehler-line through a load increase test (LIT). Germann et al. applied resistance monitoring during common fatigue tests of three different steels in [49], revealing that the materials would exhibit an initial reduction in resistance, before then having a sharp increase towards failure. Both the maximum decrease and the following maximum resistance depend upon the applied stress amplitude. The initial reduction of resistance was also investigated through the application of scanning electron microscopy (SEM), revealing that the cause was closure of microcracks. Mao et al. proposed and demonstrated a method for damage detection and damage localization in [50], through the use

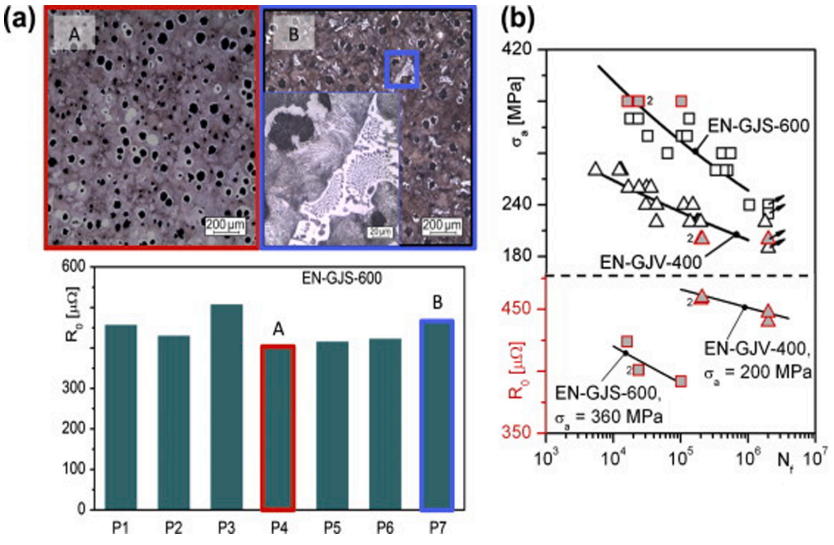

Fig. 3. Initial resistivity with the respective microstructures for cast iron EN-GJS-600 (ASTM 80-55-06) (a) and S-N curves, as well as initial resistivity-lifetime relation for EN-GJV-400 and EN-GJS-600 (ASTM 80-55-06) (b) [48]. (Reprinted from International Journal of Fatigue, Volume 82, Part 2, P. Starke, D. Eifler, C. Boller, Fatigue assessment of metallic materials beyond strain measurement, Pages 274–279, Copyright 2015, with permission from Elsevier.)

of a suitable number of electrodes and the application of an equipotential lines back-projection algorithm. However, the drawback is that accuracy is a function of measurement electrodes used. Klein and Eifler investigated the fatigue strength of different manufacturing processes, through the application of simultaneous measurements of temperature, resistivity and plastic strain amplitude, demonstrating that the change in both resistance and temperature is a better early warning sign, compared to plastic strain [51].

The parameter of resistivity has also resulted in the development of an accumulative damage model by Sun et al. [47,52]. However, it was not checked for variable amplitude loading. Furthermore, it could be seen that this material did not exhibit an initial decrease in the resistance, in contrast to the aforementioned research, highlighting the material dependence of the resistance method. Several other studies have also been performed, reporting similar results [53–57].

4.2. Hardness-based method

The argument for using hardness measurements as a means to evaluate fatigue damage originates from the crack initiation stage, commonly discussed as a surface phenomenon which is due to microplasticity at the free surface.

An early study of the correlation of fatigue damage with changes in the surface hardness can be found in [58]. In this work, there is experimental evidence that the fatigue damage accumulation until crack initiation can be reflected by changes in the surface Vickers hardness for aluminium specimens. In 2002, these findings were utilized to derive a nonlinear fatigue damage accumulation rule of the damage function D versus the stress amplitude and number of loading cycles [59]. The proposed model was verified in two-stage variable loading experimental results, showing very good accuracy.

Correlation of hardness change with the fatigue damage has also been carried out by Ye et al. [60,61], who worked on the microhardness level with a Vickers indentation, revealing that the statistical mean of the microhardness for both ferrite and pearlite would change throughout the fatigue life. In fact, both phases would display an initial hardening, stabilizing and then decreasing until failure, as can be seen in Fig. 4, including the full range of scatter bars. Furthermore, Ye and Wang argued [62] that the hardness measurement is a stochastic variable, then concluded that the damage variable should be a probabilistic

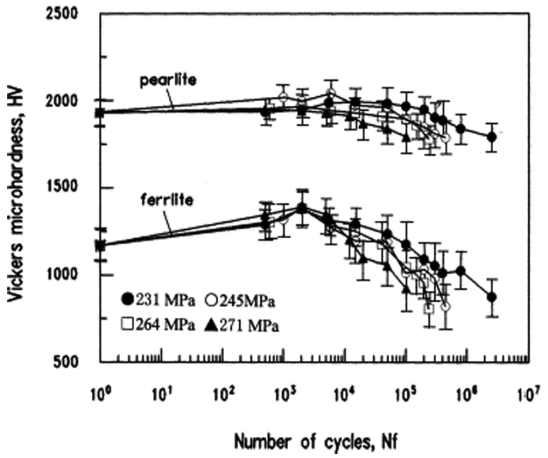

Fig. 4. Change and error bars with the total range of microhardness in ferrite and pearlite during fatigue loading [62]. (Reprinted from International Journal of Fatigue, Volume 23, Issue 1, Duyi Ye, Zhenlin Wang, An approach to investigate pre-nucleation fatigue damage of cyclically loaded metals using Vickers microhardness tests, Pages 85–91, Copyright 2001, with permission from Elsevier.)

function, subsequently adapting the normal distribution function to represent the probabilistic accumulated damage throughout the fatigue life.

Drumond et al. [63–65] investigated the microhardness evolution in API 5L X65 for both annealed and as-received specimens throughout the fatigue life, by the use of a Berkovich indentation. The findings were that, early in the fatigue life, the annealed specimens would initially harden, then soften, whereas the specimens in the as-received state would initially soften, then harden, highlighting the important role of initial material condition, as in dislocation structure. Furthermore, the results show that the change is certainly more prominent at the surface, as indentation depths of 2, 4 and 6 μm were measured, with the most significant change in hardness being observed for the 2 μm measurements.

Additionally, Miroslav et al. [66] investigated the microhardness evolution, through the use of Vickers indentations, and the hardness evolution, through Brinell of a S355J0 steel, which also followed the aforementioned described change. This highlights the applicability of Brinell measurements, which do not require the same level of surface preparations as in the case of the aforementioned Vickers microhardness test. Furthermore, the perspective of what qualifies as a good diagnostic method for the changes in the mechanical properties of the surface material was discussed, in which it was stated that the diagnostic method should:

- Be simple, and allow for use in operational conditions
- Target the surface layer of the material
- Have minimal influence on the material

In light of this, it should be mentioned that the methodology of hardness evolution throughout the fatigue life might be fairly applicable in regard to the understanding of the accumulated fatigue damage. However, its application as a diagnostic tool for in situ measurements might be questionable. This comes from the perspective that the fatigue phenomenon is known to be sensitive regarding notches or other discontinuities of material that cause stress concentrations, consequentially resulting in the fact that hardness measurements might not be a non-destructive method. The microhardness methodology might be more applicable in respect of the fact that it is a less intrusive indentation; thus, it can be argued that it actually is non-destructive. However, it comes with another disadvantage. In fact, Ye et al. [60] specify that the prerequisites for microhardness measurements are such that the specimens must be polished by an electro-chemical method, before being etched to reveal the microstructures; this must be performed before fatigue cycling is applied, as polishing a fatigue-damaged specimen would partly, if not fully, remove the strain-hardened/softened surface grains.

4.3. X-ray diffraction method

The X-ray diffraction (XRD) methodology is commonly applied for two reasons: (a) to determine residual stresses (macro stresses), through the $SIN^2\Psi$ method, or (b) to determine the dislocation density (micro deformations), through different methods of characterizing diffraction profile broadening [67]. Fig. 5 depicts the two observed changes to the peak of an XRD due to macro stresses and micro deformations, resulting in a peak shift and a peak broadening, respectively. The most common way to evaluate peak broadening is through the full width at half maximum (FWHM), due to its simplicity. However, maintaining comparable sensitivity to the integral method, with the exception of the early stages, was demonstrated by Vijayan et al. [68]. Nagao and Weiss investigated low cycle fatigue of plain carbon steel in [69] through XRD. The material had three different initial conditions: strain aged, 20% prestrained and as received, to investigate the effect of initial conditions for low cycle fatigue (LCF), concluding that after 10% of the fatigue life, the materials were independent of the initial condition. Pangborn et al. [70] investigated the dislocation density-depth profile in single crystals of

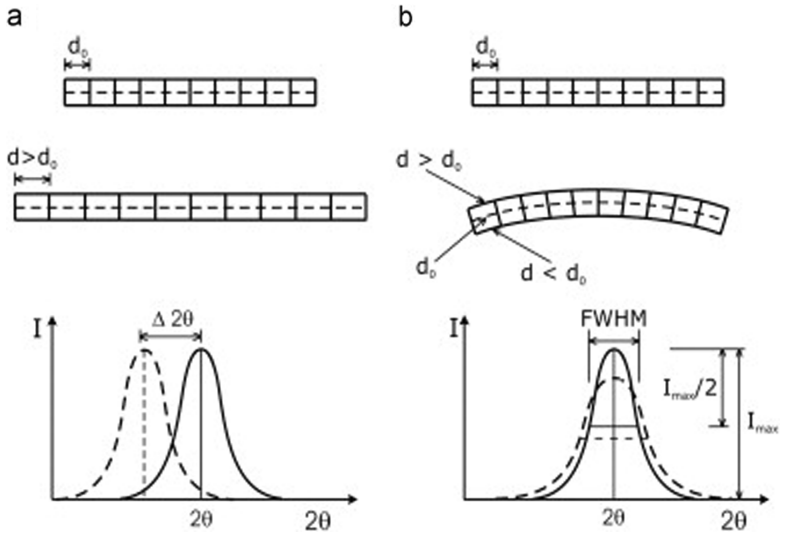

Fig. 5. Influence of (a) macro stresses (uniform deformation) and (b) micro deformations (nonuniform deformation) on X-ray diffraction peak [72]. (Reprinted from Materials Science and Engineering: A, Volume 580, B. Pinheiro, J. Lesage, I. Pasqualino, E. Bemporad, N. Benseddiq, X-ray diffraction study of microstructural changes during fatigue damage initiation in pipe steels: Role of the initial dislocation structure, Copyright 2013, with permission from Elsevier.)

aluminium, silicon, gold and polycrystalline Al-2024, after monotonically inducing a plastic strain. It was found that the dislocation distribution for monotonically loaded specimens exhibited a high number of dislocations at the surface, whereas it dropped continuously before converging towards the bulk material. However, the cyclically loaded specimens of polycrystalline aluminium, in addition, exhibited a minimum at a depth of about 100 μm, which was more marked with continued cycling. An important conclusion from the work, however, was that the three-stage sequence commonly observed in the fatigue damage evolution curve, through the use of XRD, is due to the application of low penetrating radiation, combined with early saturation of the surface. Thus, the application of deep penetrating molybdenum radiation in contrast to copper was applied, finding that the molybdenum resulted in a fairly linear increase of excess dislocation density throughout the fatigue life, subsequently demonstrating that XRD has the capability to estimate remaining fatigue life with good accuracy for a specimen previously subjected to four block loads of increasing amplitude. Kramer et al. continued this work on determining the dislocation density in depth of steels, aluminium and brass in [71]. In contrast to the findings for aluminium, the steel only exhibited a minimum in the dislocation-depth profile for the early stages of fatigue damage. In fact, the profile was similar to the monotonically loaded specimens, where

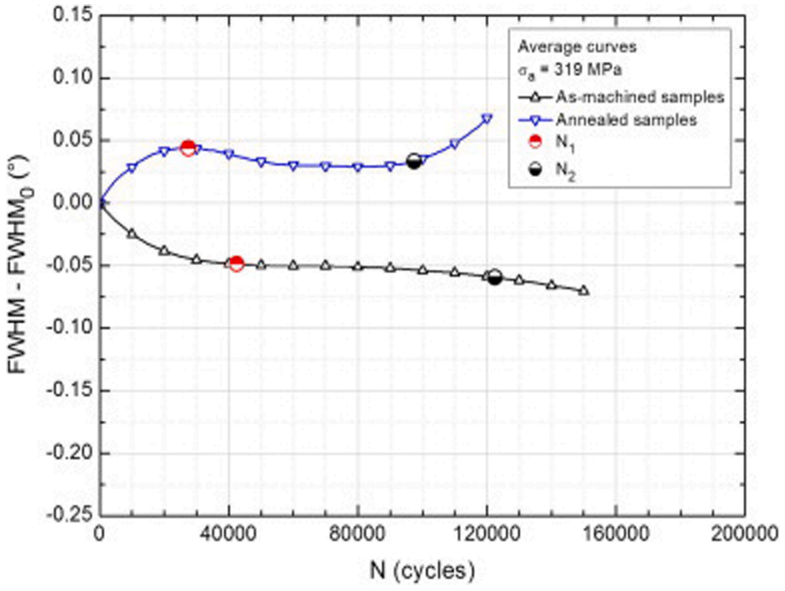

Fig. 6. Change of FWHM under fatigue cycling for as-machined and annealed samples of API 5L X60 at a stress amplitude of 319 MPa (R = −1) [72]. (Reprinted from Materials Science and Engineering: A, Volume 580, B. Pinheiro, J. Lesage, I. Pasqualino, E. Bemporad, N. Benseddiq, X-ray diffraction study of microstructural changes during fatigue damage initiation in pipe steels: Role of the initial dislocation structure, Copyright 2013, with permission from Elsevier.)

the conversion value of the bulk density increased towards the surface density with continued cycling. Pinheiro et al. [67,72] investigated pipeline steel with a ferritic-pearlitic microstructure, with the initial conditions as-machined and annealed states, under cyclic loading through the FWHM method. The radiation used was Cr-Kα radiation, which has a penetration depth of 5.8 μm for the ferritic-pearlitic steels at a tilt angle of 0, resulting in a three-stage sequence in the damage accumulation. However, the results highlight the effect of initial dislocation structure, as can be observed in Fig. 6. In fact, the as-machined specimens exhibited a reduction in peak width, whereas the annealed specimens exhibited the commonly discussed peak broadening.

4.4. Thermometric

The thermometric method is based on the absorbed hysteresis energy during fatigue cycling, where most of the energy (80–100%) is dissipated into the surroundings as heat, whereas a small portion increases the internal energy [73,74]. It is commonly agreed that a typical temperature-cycles curve will exhibit three stages, namely, increase, stabilization and failure [75,76]. When it comes to application of the thermometric methodology, a number of researchers have investigated and concluded that the energy dissipated as thermal energy can be used to determine the stress amplitude at the knee-point [77–81] and the fatigue curve [82–86], commonly based on temperature monitoring. An example of how the stress amplitude at the knee-point can be assessed in regard to thermal readings is presented in Fig. 7, where the commonly accepted stabilization temperature is exploited. In the aforementioned literature, for both the thermometric and the resistance-based methods, the knee-point is discussed as the fatigue limit or endurance limit. However, it is well documented that neither an endurance limit nor a corresponding threshold stress intensity exists [87,88]. Thus, it should be acknowledged that the knee-point stress amplitude can be found, whereas it also defines a limitation of the methodology, in regard to stress/strain amplitude domain.

Meneghetti investigated the dissipated energy in a unit volume of a material per cycle, concluding that the parameter is only dependent on load ratio and the applied stress, in contrast to surface temperature, which is also dependent on specimen geometry, test frequency and the thermal boundary conditions [89]. Boulanger et al. [90] separately identified the dissipative and thermoelastic sources, allowing the measurement of very low dissipation in comparison to the thermoelastic sources. Furthermore, the parameter of temperature is commonly very sensitive, in comparison to factors such as plastic strains. This can be seen in the aforementioned literature, where temperature and plastic strains are simultaneously monitored, but they were also explicitly mentioned by, for instance, Luong in [79] and Weber in [74]. Weber also included a practical example, in which a specimen cycled to 5×10^6 cycles at 37 Hz exhibited a temperature change of 10 Kelvin, while exhibiting a plastic strain of magnitude 10^{-4}. However, care should be taken in regard to frequency and stabilization temperature. An example of this can be seen in a paper by Liaw et al. [91], in which it was stated that the significantly higher stabilization temperature could contribute to the reduction of fatigue curves developed by 1000 Hz, in comparison to 20-Hz cycling.

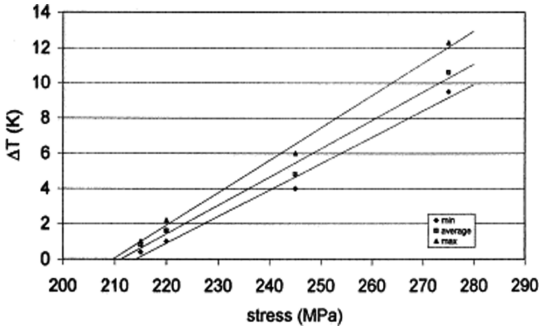

Fig. 7. Knee-point estimation through the use of the stabilization temperature [77]. (Reprinted from International Journal of Fatigue, Volume 22, Issue 1, G La Rosa, A Risitano, Thermographic methodology for rapid determination of the fatigue limit of materials and mechanical components, Pages 65–73, Copyright 1999, with permission from Elsevier.)

Furthermore, Amiri and Khonsari proposed the temperature-rise angle as a good candidate for fatigue damage indicator in [92]. They measured this by inserting cool-down periods within the fatigue loading test, before then measuring the new raise angle. Liakat and Khonsari proposed a method to evaluate the remaining fatigue life of damaged material in [93], with the aforementioned raise angle parameter, subsequently verifying the methodology for a two-stage loading from low to high and high to low with reasonable accuracy. It should be highlighted, however, that the parameter has a high load condition dependence, resulting in the fact that the stress range, mean stress and frequency must be defined to monitor the raise angle.

4.5. Strain-based

The strain-based methodologies can be separated into two different categories, namely, inelastic strains and ratcheting, as can be seen in Fig. 8 and Fig. 9, respectively. Ratcheting is commonly attributed to local deformation around voids, non-metallic precipitations and other defects within the material [94–96].

Dietrich and Radziejwska investigated the damage development in a cast Al-Si-Cu alloy through strain measurements in [94]. It was found that the main mechanism for fatigue damage for this material is ratcheting, justified through the fairly constant inelastic strains, with a continuous increase in mean strain. Damage accumulation curves were developed for the material, highlighting its nonlinearity and that the marked change in the parameter is observed early in the fatigue life.

Socha investigated the inelastic strains throughout the fatigue life of a structural steel under fully reversed cyclic loading for different stress amplitudes in [97], separately identifying the three commonly discussed fatigue damage accumulation stages: (a) elastic work of undamaged material, (b) micro crack initiation and growth, followed by (c) dominating crack propagation. This ended in a proposed method for fatigue life prediction, in light of the aforementioned stages, as the sum of Miner's rule, change of inelastic strains and macroscopic crack propagation. Socha also investigated three other structural steels in [98], with the introduction of damage progress rate curves, and proposed a formula for fatigue life prediction. The validity of the formula was checked, revealing good accuracy for two-stage loading from high to low and low to high, with the exception of one of the steels exhibiting high scatter for the high to low scenario. The scatter was attributed to early formation of Lüders bands.

Furthermore, the methodology of strain measurements has been used as a means to continuously monitor for crack initiation in regard to notches. This can be seen for instance in a paper by Sonsino [99] where the effect of cold forming was investigated for the cyclically softening steel Fe E 47 and the cyclically hardening aluminium alloy AlCuMg2 under low cycle fatigue. First detectable crack depth was $a = 0.25$ mm.

4.6. Positron annihilation

Positron annihilation spectroscopy has its basis in sending positrons into the material and registering the subsequent annihilation. The methodology has many applications. The main concepts which are applied in regard to non-destructively investigating fatigue damage accumulation are the time for a positron to annihilate and the energy distribution between the two resulting photons, commonly discussed as positron annihilation lifetime (PALS) and line shape analysis, the latter of which might be evaluated through the S-parameter, as seen in Eq. (2).

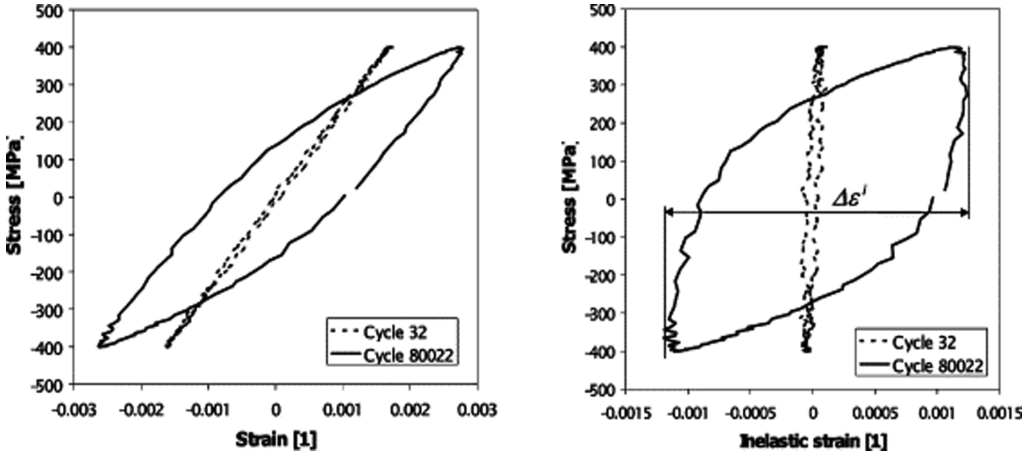

Fig. 8. Example of hysteresis loop recorded for cycle numbers 32 and 80,022 in structural steel A10, according to a Polish standard PN-73/H-84026, with a stress amplitude of 400 MPa [97]. (Reprinted from International Journal of Fatigue, Volume 25, Issue 2, G. Socha, Experimental investigations of fatigue cracks nucleation, growth and coalescence in structural steel, Pages 139–147, Copyright 2002, with permission from Elsevier.)

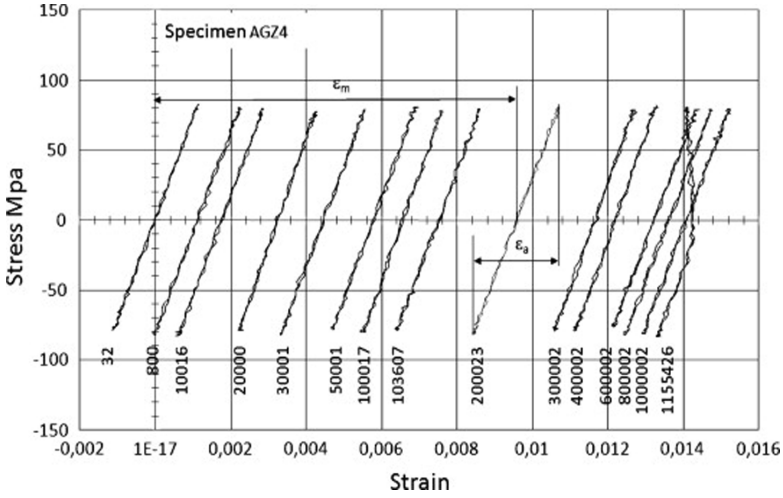

Fig. 9. The stress–strain curves of selected cycles in a cast Al-Si-Cu alloy specimen tested under stress amplitude equal to 80 MPa (The comma represents the decimal) [94]. (Reprinted from Materials & Design, Volume 32, Issue 1, Lech Dietrich, Joanna Radziejewska, The fatigue damage development in a cast Al–Si–Cu alloy, Pages 322–329, Copyright 2010, with permission from Elsevier.)

The increased time from birth to annihilation of a positron comes from the perspective that annihilation is a stochastic process, where the positron annihilation rate, or the probability of annihilation per unit time, is related to the local electron density. Furthermore, the resulting photon energy distribution comes from the fact that the positron-electron pair is not at rest, meaning that the momentum also has to be carried away by the radiation. The density and momentum of electrons commonly seen at positron trapping sites are observed to be lower, resulting in a longer lifetime and a sharper energy distribution curve. A positron trapping site is an open volume defect, such as vacancies, grain boundaries, precipitate, to mention a few [100–102]. Furthermore, a representation of the birth to annihilation for a positron can be seen in Fig. 10, both for the case of annihilation in the bulk and a positron trap.

$$\mathrm{S-parameter} = \frac{\text{The counts of } \gamma-\text{ray near central peak}}{\text{Total counts of } \gamma-\text{ray}} \quad (2)$$

Throughout the following reviewed literature, it can be seen that both dislocations and vacancies are discussed as positron trapping sites. However, in a review paper on positron annihilation spectroscopy by Čížek [101], it was discussed that the dislocations are shallow positron traps with a binding energy less than 0.1 eV. Thereafter, a generally accepted concept is mentioned of a two-step process, where the positrons at first are trapped in the dislocation core, before diffusing along the dislocation line, eventually being trapped at vacancies anchored in the elastic field of the dislocation, resulting in a slightly shorter lifetime than for a monovacancy, as the anchored vacancies will be compressed due to the elastic stress field of the dislocation. In light of this, it should also be mentioned that other researchers also highlight the development of vacancies through plastic deformation and fatigue [100,103,104].

Uematsu et al. investigated the possibility of using positron annihilation as a means of crack detection for 316 SS in [105], finding that the lifetime analysis is suitable for detecting crack initiation, whereas the line-shape analysis could not. However, it was highlighted that both parameters are capable of detecting fatigue damage, exhibiting a

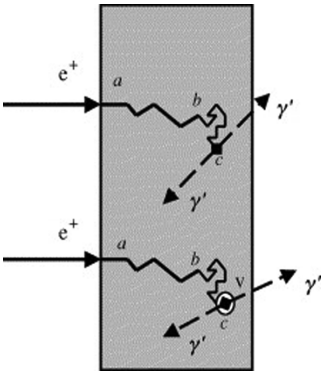

Fig. 10. Schematic view of possible fates of positrons implanted in a solid. Upper track: implantation (a), slowing-down (a to b), thermal diffusion (b to c), annihilation at c with a bulk electron and emission of two photons (γ′). Lower track: same as above from a to c, trapping at c in a vacancy (v), annihilation in v and emission of two photons (γ′) [100]. (Reprinted from Acta Materialia, Volume 52, Issue 16, A. Dupasquier, G. Kögel, A. Somoza, Studies of light alloys by positron annihilation techniques, Pages 4707–4726, Copyright 2004, with permission from Elsevier.)

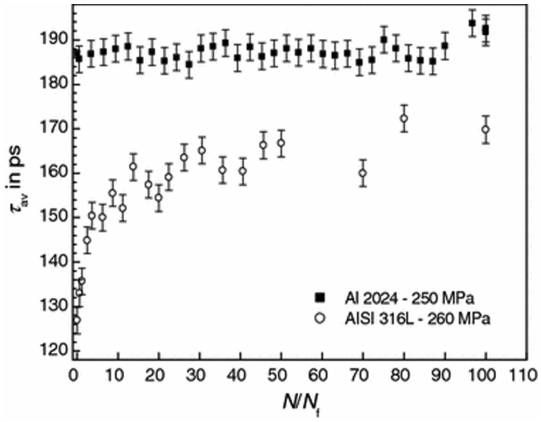

Fig. 11. Comparison of the evolution of average positron lifetime τ_{av} during stress-controlled fatigue experiments between stainless steel AISI 316 L and the aluminum alloy 2024. The number of fatigue cycles N is normalized to number at failure N_f. The error bars denote the accuracy of the positron lifetime measurement of ±3 ps [111]. (Reprinted by permission from Springer Nature, Journal of Materials Science, On the non-destructive detection of fatigue damage in industrial aluminium alloys by positron annihilation, Holzwarth, U., Schaaff, P., Copyright 2007.)

continuous increase throughout the fatigue life of the specimen.

Kawaguchi et al. investigated 316 SS for both low stress and low strain through the S-parameter, highlighting its increase throughout the fatigue life, and how the evolution depends on whether the test is stress or strain controlled [106]. Furthermore, Kawaguchi and Shirai investigated the different components of the lifetime spectra, highlighting that the lifetime of the different defect types changes little, whereas the relative intensity increases, subsequently highlighting that, in contrast to line shape analysis, the PALS has the advantage of identifying defects [107].

Although several researchers document a continuous increase in PALS and continuous sharpening of the S-parameter, it should be highlighted that the methodology sometimes exhibits saturation before fatigue failure, thus possibly being more applicable to early-stage fatigue. Examples of this can be seen in such as [108] for 316 SS, reporting a significant change in the S-parameter from 0% to 10% of the fatigue life, whereas a very small increase from 10% to 100%. Furthermore, in [104], it was reported that the positron lifetime did not exhibit significant change after 50% of the lifetime in the SS 316L. Similar studies reporting early saturation have also been performed on SS 304 [109,110].

Holzwarth and Schaaff investigated the applicability of PALS for industrial aluminium alloys, concluding that there was no significant change in the measured PALS throughout the fatigue life, attributed to the high density of precipitates which mask the accumulated fatigue damage in respect of PALS, as can be seen in Fig. 11. This essentially highlighted the importance of microstructure in regard to the methodology [111]. Furthermore, in [103], the same authors investigated AISI-316 L under both stress and strain control conditions, highlighting how the methodology is much more pronounced in the earlier stages of fatigue damage accumulation.

4.7. Magnetic methods

Within the field of magnetic methods of determining accumulated fatigue damage for ferromagnetic materials, methods such as Barkhausen noise (BHN) or magnetic hysteresis are commonly discussed. The fundamental argument for the magnetic methods is the strong relation between the magnetization process and the microstructure [112], commonly attributed to the fact that the magnetization process is through movement of the domain walls within the material, which will be affected by different microstructural characteristics [113–115]. Several studies have been performed on how the magnetic methods might be affected by such characteristics as grain boundaries [116], inclusions [117] and dislocations [118,119], amongst others [120,121]. However, in the light of fatigue damage, it is commonly the accumulated dislocation structure which is discussed.

4.7.1. Barkhausen noise

Lindgren and Lepistö investigated the application of a new sensor which could continuously monitor BHN during the fatigue life, in which the dimensional changes of the specimen took care of the magnetization (mechanical BHN) [122]. Furthermore, they investigated the fatigue of a mild steel specimen which was loaded in bending, while investigating the BHN in different directions in comparison to the commonly used loading direction. They concluded that measuring BHN in only one direction might result in misevaluation of the fatigue damage. In fact, the most prominent changes observed were at approximately a 45° angle, as presented in Fig. 12 [123].

Soultan et al. also investigated the mechanical BHN in iron specimens in [124], finding that the root mean square (RMS) of the mechanical BHN is load frequency dependent and would not have an initial increase for stress amplitudes beneath the fatigue knee-point stress amplitude. Furthermore, it was noted that the variation in BHN throughout the fatigue life could be divided into three stages, namely, a transient stage, a stationary stage and a reduction, ending in fracture. The observed stationary stage linearly increased with applied stress amplitude up to the fatigue knee-point stress amplitude, whereas it started to saturate as the stress amplitude exceeded the knee-point stress amplitude of the material.

Palma et al. investigated the magnetic BHN of AISI 8620, a ferritic pearlitic steel, subjected to rotating bending fatigue, and axially loaded with R = 0 [125]. They found that no change was observed with amplitudes beneath the knee-point stress amplitude, whereas small changes could be observed slightly above this knee-point stress amplitude. Furthermore, the parameter was more marked with higher amplitude loading, whereas it was significantly reduced in axial testing if the maximum stress surpassed yielding, as observed in Fig. 13. Thus, they concluded that the methodology was not applicable for stresses above the yield limit.

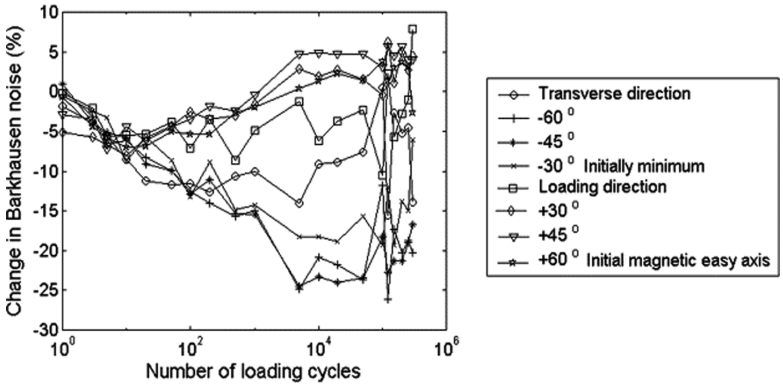

Fig. 12. Change in Barkhausen noise in different measuring directions through the fatigue life with a strain amplitude of 1000 μ Strain [123]. (Reprinted from NDT & E International, Volume 36, Issue 6, M. Lindgren, T. Lepistö, Effect of cyclic deformation on Barkhausen noise in a mild steel, Pages 401–409, Copyright 2003, with permission from Elsevier.)

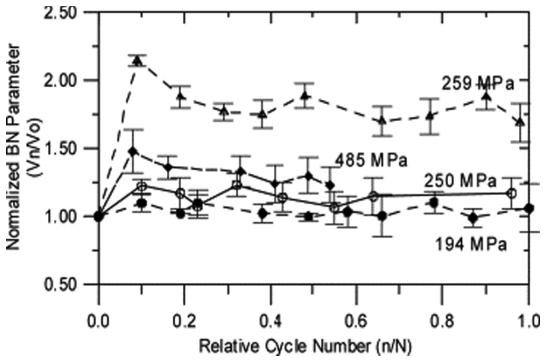

Fig. 13. Change of the normalized Barkhausen noise rms value in AISI 8620 steel specimens through the relative cycle number - axial machine (R = 0) [125]. (Reprinted from International Journal of Fatigue, Volume 27, Issue 6, E. S. Palma, T.R. Mansur, S. Ferreira Silva, A. Alvarenga, Fatigue damage assessment in AISI 8620 steel using Barkhausen noise, Pages 659–665, Copyright 2004, with permission from Elsevier.)

Sagar et al monitored the magnetic BHN peak voltage of a low carbon structural steel in [126], with the addition of microstructural analysis through transmission electron microscopy (TEM). They defined a three-stage process: (a) peak voltage increase due to the rearrangements and formation of dislocation cell structures, (b) a decrease in peak voltage, due to a reduction in cell size, increased dislocation density and formation of slip bands, and (c) an increase due to the initiation and growth of macro-cracks.

4.7.2. Hysteresis loops

In addition to the work performed in regard to BHN, researchers have also directly investigated the magnetic properties of materials. For example, Morishita et al. investigated the magnetic properties of A533B low alloy steel, under both plastic deformations and fatigue loading. They found that the residual magnetic flux density decreased continuously throughout the fatigue cycling. However, they also reported that there was no change in the coercive force throughout the investigation [127]. Gao et al. monitored the coercivity of the same type of steel, under the initial conditions of pre-strained and non-pre-strained, finding that they exhibited a reduction and increase in coercivity, respectively, in [128]. This might be due to the fact that Morishita's fatigue tests were performed with zero-tension cyclic load, and well within the high cycle fatigue (HCF) domain, whereas Gao's tests are very close to the LCF domain, with tension and compression fatigue tests. Gilanyi et al. found that the strongest property changes of the hysteresis loops related to fatigue damage were the remanent induction of the material [129]. Chen et al. performed a comparison of magnetic hysteresis and the magnetic Barkhausen effect in [130] for the same type of material. They concluded that the hysteresis parameters typically would not exhibit much change before the last 10–20% of the fatigue life, whereas the BHN signal amplitude would continuously decrease with the increasing number of loading cycles. Grimberg et al. investigated SAE 4130 under two different stress amplitudes and found, through the incremental magnetic permeability method, that the coercive force increased with an increasing number of fatigue cycles, reaching a level of about 595 A/m at failure for both load amplitudes. They concluded that the methodology could be used to predict the fatigue damage for SAE 4130 [131].

4.7.3. Deformation-induced phase transformation

Furthermore, it should be mentioned that there is also a magnetic method which exploits the deformation-induced phase transformation in austenitic stainless steels to martensite. In this regard, it is commonly the magnetic content in comparison to number of cycles which is used as damage parameter [132].

4.8. Ultrasonic methods

The commonly used ultrasonic methods for crack detection in materials are not sensitive enough to detect microstructural defects generated in the early stages of fatigue, as the defects are shorter than the wave length normally used in ultrasonics [133]. However, it has been shown by several researchers that parameters such as attenuation, velocity and secondary harmonics can be exploited to characterize the microstructural damage. These are commonly discussed as the nonlinear ultrasonic method and linear or attenuation and velocity methods.

4.8.1. Nonlinear ultrasonic method

The nonlinear ultrasonic method has its basis in the fact that, as an ultrasonic wave propagates through the nonlinear material, the signal will be distorted, and secondary harmonics will be developed. Thus, nonlinear behaviour is attributed to the microstructural nonlinearity of the propagation medium, which is commonly discussed in light of both microcracks and dislocations [134]. An example of this can be seen in Fig. 14 by Palit Sagar et al., who investigated in [5] the development of the secondary harmonic and compared it to the dislocation structure of different specimens of a low carbon structural steel, which had been fatigued to various percentages of the total fatigue life. Furthermore, the amplitude of the fundamental and secondary harmonic of the resulting

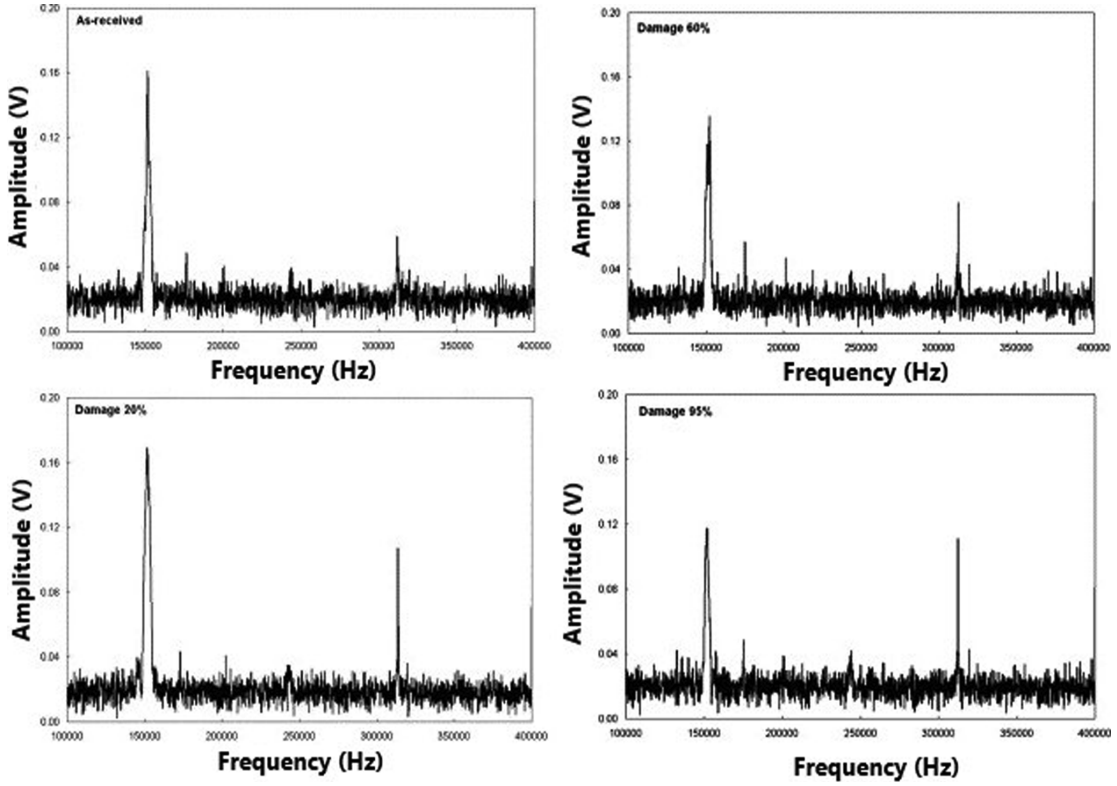

Fig. 14. Power spectrum of received signals during various stages of fatigue damage [5]. (Reprinted from Scripta Materialia, Volume 55, Issue 2, S. Palit Sagar, S. Das, N. Parida, D.K. Bhattacharya, Non-linear ultrasonic technique to assess fatigue damage in structural steel, Pages 199–202, Copyright 2006, with permission from Elsevier.)

power spectrum was compared in the form, total harmonic distortion (THD) given by $\%THD = \frac{A_2}{A_1}$, revealing a damage progression of first increasing, then plateauing, before further increasing. Cantrell and Yost investigated AA2024-T4 in [135] through the nonlinearity parameter β defined as $\beta \propto \frac{A_2}{A_1^2}$, A_1 and A_2 being the amplitude of the fundamental and second harmonic, respectively, revealing a monotonic increase with an increasing number of fatigue cycles. Kumar et al. investigated the possibility of in situ measurements during very high cycle fatigue (VHCF) damage accumulation in [136,137], by analysing the feedback signal of a closed-loop ultrasonic fatigue system. They highlighted the possibility of achieving additional information through ultrasonic fatigue testing, such as initial hardening/softening and crack initiation. Shui et al. discussed and demonstrated a method for and advantages of using low voltage generated Rayleigh waves, in the view of reducing instrumentation nonlinearity, being a single-sided, surface sensitive method which can be performed over large distances [138]. Jhang proposed a new method to measure β through bispectral analysis to remove noise, and investigated the nonlinear and linear parameters for mild steels (SS41 and SS45) in [139], revealing the proportionality of the nonlinear parameter with the applied load amplitude and the number of fatigue cycles. Furthermore, Jhang concluded that the velocity and attenuation did not exhibit any noticeable change. Nagy investigated both nonlinear and linear parameters for plastics, metals, composites and adhesives in [133], revealing the material dependence in metals on the evolution of the nonlinearity, and that the nonlinear parameter is fairly sensitive for all the aforementioned materials, whereas, in comparison, the linear parameters commonly exhibited small variation.

4.8.2. *Linear or attenuation and velocity methods*

It has been documented that a change also exists in the parameters of attenuation and velocity, although not as marked as in the nonlinear method. In [140], Ogi et al. investigated the attenuation and velocity change of 99 wt pct pure polycrystalline copper as a uniaxial stress state was applied, demonstrating that both longitudinal and shear waves are sensitive to dislocations, whereas the latter wave exhibits higher sensitivity. Ohtani et al. continuously monitored the change of attenuation and velocity in two annealed low carbon steels with 0.21 and 0.15 mass % C through the EMAR method in [141,142]. The experimental work also included TEM images and a discussion of the different stages observed. Both the investigated materials exhibited small regions of significant change and large regions with insignificant change. Liu et al. [143] measured the change in velocity and attenuation in nodular cast iron, finding that the attenuation parameter is a more pronounced parameter than speed for the specified material. Furthermore, through the graphs, it can be noted that this material, in contrast to the aforementioned material, exhibits a more continuous form, even though it exhibits a plateau for both parameters around half of the fatigue life. In [144], Yamagashi and Fukuhara monitored several mechanical parameters through the use of the ultrasonic shear wave and longitudinal wave velocities of extruded pure magnesium. However, the plots for the change of velocities are included in the paper, revealing a strong dependency on the domain of fatigue, as in if it is within the LCF, HCF or very high cycle fatigue (VHCF), consequently highlighting the stress/strain amplitude dependency. Kenderian et al. applied the Granato and Lücke [145,146] dislocation damping theory, to perform a relative estimation of the dislocation density and loop length in rail steel [147]. The study revealed a drastic change in the parameters within the first

10% of the fatigue life, before then showing a monotonic increasing or decreasing trend. Furthermore, a relaxation phenomenon due to paused cycling was discovered in regard to the parameter. The parameters would, however, quickly retrieve the previous value upon continued cycling.

5. Discussion

In light of the reviewed literature, two discussions and a section regarding comments on the way forward can be developed: one discussion from the perspective of general damage measurement and a second, focused on the case-dependent damage assessment.

5.1. General damage measurement

When it comes to the topic of applying a damage parameter to assess the accumulated damage through measurements, there are several considerations to be made.

It is evident that both the material in question and its initial dislocation structure will play a crucial part in the measurability of the accumulated damage and progression, respectively. In the review, it can be seen that methodology is material-dependent, for example in the case of positron annihilation. In fact, it was found that positron annihilation was not applicable for Al-2024, attributed to the initial presence of positron trapping sites, consequently masking the fatigue damage. Furthermore, it was noted that the initial dislocation structure will influence the parameter used for damage progression. This was seen in regard to both the X-ray diffraction and the hardness methodology, where the progression of the parameter in question would strongly depend on the initial dislocation structures resulting from as-machined/received, in contrast to annealed, specimens.

Applicability and measurability dependence, in regard to applied stress/strain with its accompanying stress/strain ratio and frequency, is an important factor to consider. In regard to the thermometric review, it was highlighted, for instance, that the dissipated energy in a unit volume per cycle has a stress/strain and ratio dependence, which could also be noted through the raise angle methodology for damage assessment. Furthermore, it can be seen that the reduction of the ultrasonic linear parameters exhibits vastly different degradation/damage curves for LCF, HCF and VHCF, consequently highlighting the damage progression dependence on the stress/strain range.

The desired region of the fatigue damage progression should be considered, as regards whether it is early or late in the fatigue life. Throughout the review, it is clear that most of the methodologies do not exhibit high measurability throughout the fatigue damage process, with the possible exception of X-ray diffraction with a carefully selected penetration depth. For instance, positron annihilation commonly exhibits the largest change early in the fatigue life, before then either converging or reaching saturation, resulting in a reduction or termination of measurability, respectively. However, methodologies such as electric resistance and strain-based methods seem to be more prominent in the late stages of fatigue, consequently resulting in different applicability. Positron annihilation could potentially be used in the early stages of fatigue, where the stresses are rather close to the knee-point stress amplitude, to signal whether or not damage has been introduced, whereas the electric resistance method will be more applicable towards the end of the fatigue life, although earlier than the initiation of a macroscopic crack.

Furthermore, the geometry in combination with the resulting local stress field has to be considered in light of the adapted measurement technique. This from the perspective that the measurement should preferably be performed in the same location to obtain comparable results, of the parameters change through cycling, or alternatively, in a location with similar stress gradients. For instance, when the hardness methodology is adapted, a measurement cannot be performed in the exact same location twice, consequently resulting in that a similar stress field should be measured. It should be noted that the measurement location and location of similar stress gradients also has to be the location or field of highest cyclic stress. Consequently, as it is commonly the location of crack initiation/failure.

The perspective of how the measurement itself is performed should also be considered, in regard to both whether the measurements have to be performed during operation and whether the measurement can be performed in situ. For instance, AE has the advantage of being focused on in-situ measurements, but these must be in the situation of a propagating crack, as in during operation, whereas the XRD and positron annihilation methods seem generally more applicable in laboratory experiments. However, the hardness, ultrasonic and magnetic parameters have the potential to be measured in situ.

5.2. Case-dependent damage assessment

The previous section ended with a short discussion regarding how the measurement itself is performed, as well as its applicability. In this section, methods are classified into three categories, based on the limitations of the applicability, as shown in Table 3. It is highlighted that the parameters applicable for in situ assessment can also be performed in a laboratory, and the parameters which can be laboratory assessment can also be good to develop a damage model. However, the table is simply constructed from the perspective of practical applications, not from that of accuracy, nor from the perspective of exhibiting continuity throughout the fatigue life. Furthermore, it can be noted that for damage assessment, access to the potentially damaged material is a requirement for the reviewed methods.

For damage assessment of structures in situ, the acoustic emission, hardness, ultrasonic, magnetic and potential drop methods were selected. This is from the perspective that portable equipment exists. The acoustic emission method would require to be monitored passively during loading of the component/structure, consequently meaning during operation. Furthermore, the hardness, ultrasonic, magnetic and potential drop methods do not depend on present cycling, meaning that the measurements can be performed when the component is at rest. However, if a nonzero nominal stress were present in the measured state, it should be accounted for. This is due to the fact that the four aforementioned methods are known to be influenced by the presence of stress/strain in the material. Furthermore, the electrical PDM method seems to be applicable within the category of in situ inspections, from the perspective of crack detection.

To the authors' knowledge, there is yet no commercially available portable equipment for positron annihilation and X-ray diffraction, feasible to perform in situ inspections. That said, there might be the potential for such equipment in the future. However, when it comes to the perspective of investigations of mechanical equipment, which can either be performed in a laboratory or even disassembled, their applications seem viable in the view of damage assessment.

The electrical resistance, strain and thermometric methods were not included for in situ or laboratory investigations. The thermometric methods were not included as it is a requirement to induce further damage to the component to evaluate the current damage state, consequently making it less attractive. Furthermore, the electrical resistance revealed that a large number of electrodes would be required to properly map the accumulated fatigue damage.

Table 3
Applicability of methods.

In situ assessment	Laboratory assessment	Damage model
Acoustic emission	Positron annihilation	Electric resistance
Hardness	X-ray diffraction	Strain-based
Ultrasonic		Thermometric
Magnetic		
Potential drop method		

Regarding laboratory experiments, from the perspective of better understanding and developing models for fatigue damage accumulation, all the different methods have their advantages and disadvantages as regards damage measurement, as highlighted in Section 5.1.

In addition, the various methods were categorized in regard to groups of materials, as can be seen in Table 4.

Furthermore, in Section 5.1, the topic of stress field and gradients were mentioned. This should also be considered regarding case-dependent damage assessment. This is from the perspective that notched specimens will commonly exhibit both stress concentrations, with high gradients, and a multiaxial stress state. Consequently, resulting in that the measurement techniques might not be comparable to the measured change under a uniaxial stress state. Furthermore, if it is assumed that there is an equivalent stress which will under the multiaxial cyclic stress be equivalent to the uniaxial cyclic stress, the measurement might still be challenging. This from the perspective that the measurement themselves might have to be performed over a variety of the stress contours, due to the area required to be measured, consequently not measuring one damage zone, but instead a vast number of damage zones. An example of this might be such as the hardness methodology, where an area has to be indented, regardless of which hardness testing method is applied. Consequently, resulting in that the indentation might cover a vast number of areas which have experienced different cyclic stress.

The topic of continuous measurements, or alternatively measurability during continuous operation should be considered. From the perspective of crack monitoring, the methods of potential drop method, acoustic emissions, and ultrasonics seems feasible. However, from the perspective of damage monitoring, the methods recommended for continuous monitoring is strain, thermometric, ultrasonic and magnetic.

6. Conclusions

The main conclusions and reflections regarding future work within the field of damage measurement are presented in this section. Additionally, the relevant key information and findings of reviewed fatigue damage detection and measurement techniques are clearly presented in Tables 5, 6 and 7.

Fatigue damage measurement through the discussed methods is commonly a rather time-consuming task. This is because each specimen has to be fatigue tested while also continuously being monitored, to achieve a single test result. Furthermore, it has been found that there are several test parameters which might affect the observed change throughout the fatigue life, as previously discussed, which further complicates the experimental work, subsequently resulting in the fact that exhaustive research is not necessarily an achievable task for a small research group alone. In light of this, it should be highlighted that extensive descriptions in experimental work will make the different work more comparable, which can result in better “knowledge gathering”. Some parameters considered as important to make the works more comparable can be found in Table 5, while a discussion on the various parameters is presented in Section 5.1.

Table 4
Applicability in regard to groups of material.

Metals	Composites
Potential drop method	Acoustic emissions
Electric resistance	X-ray diffraction
Acoustic emissions	Ultrasonic
Hardness-based	Strain-based
X-ray diffraction	Thermometric
Positron annihilation	
Magnetic	
Ultrasonic	
Thermometric	
Strain-based	

Table 5
Important information to document during damage measurement of fatigue.

Material	The material used – with material characteristics Surface finish and processing of the material Microstructure (especially if unknown material)	
Load parameters	Cyclic loading Stress amplitude R - Ratio Frequency Number of cycles	Spectrum loading Standard deviation Mean value Coefficient of variation of stress amplitude and R - Ratio
Measurement technique	Good explanation of the method used	
Criterion for fatigue failure	The criterion which is considered as fatigue failure should be highlighted, as in first crack, through thickness crack or final fracture	

Table 6
Summary of crack monitoring based on the reviewed literature.

Method	Parameter	Technique/ Phenomenon	Limitations	Discussion
Electric	$PDM = 1 - \frac{V_0}{V}$	Change in potential (voltage) field due to discontinuity in the material (Crack).	- From crack initiation. - Calibration curves must be developed.	The PDM method is well established in the monitoring of cracks via the calibration curves. However, such curves are geometry-dependent and must be developed for each case.
Acoustic emission	Amplitude; Counts; Duration; Energy; Risetime; Counts to Peak; Absolute Energy; Count rate $\log\left(\frac{dA}{dN}\right) = B\log(\Delta K) + \log(C)$	Elastic stress waves generated due to rapid release of energy from a localized source within a stressed material.	- Crack must be present. - Only measurable during propagation. - Signal processing/ interpretation. - Number of sensors defines accuracy, and the information that can be obtained.	Generally, for in situ monitoring of various structures, in contrast to laboratory/ specimen-scale testing. However, has a disadvantage in regard to unwanted noise and signal processing.
Ultrasonic method	Time of flight, Time of flight diffraction, energy, amplitude.	Elastic stress waves, commonly generated by the use of a piezoelectric crystal, with the resulting reflection or diffraction.	- Crack or loss of material must be present.	Common method to apply for in situ inspection of various components. TOFD seems most reliable for crack sizing, with the advantage of exhibiting good detectability as well.

As previously noted, some of the methodologies are more applicable from the perspective of obtaining additional information during common fatigue tests and, therefore, more applicable from the perspective of developing damage laws. However, for the methodologies where the

Table 7
Summary of damage monitoring based on the reviewed literature.

Method	Parameter	Technique/Phenomenon	Limitations	Discussion
Electric	Resistance $= \Delta R$; $\frac{\Delta R}{R}$; $R = \frac{\rho L}{A} \rightarrow \Delta\rho$	Increased resistivity due to dislocations, point defects, micro and macroscopic crack propagation.	- Conductive materials. - Most significant near fracture. - Small measurement ($\mu\Omega$). - Measurable outside operation.	Resistance seems more applicable to specimen testing, for additional information.
Hardness	Hv; Hb; $1 - \frac{H_D}{H_0}$; $H_D = C(1-D)k(\varepsilon + \varepsilon_H)^m$	Measurement of the surface hardening/softening due to cyclic microplasticity.	- Requires extensive polishing procedure before operation. - Requires microstructural analysis. - NDE perspective questionable. - Measurable outside operation.	Strong correlation with the fatigue damaging process. Disadvantage in regard to the polishing requirement. Furthermore, the method being non-destructive in view of fatigue is a subject for discussion.
X-ray diffraction	Halfwidth b; Integral width β; Fourier coefficients; Dislocation estimate $\overline{\rho} = \frac{\overline{\beta}^2}{9b^2}$	Broadening of the XRD peak due to micro stresses (dislocations) causing lattice distortion.	- Radiation penetration depth dictates the shape of the damage accumulation curve. - Measurable outside operation.	The penetration depth of the radiation used should be carefully considered. More towards laboratory testing in the literature.
Thermometric	ΔT; $\frac{\Delta T}{\Delta N}$; R_θ; $Q\left(\frac{kJ}{m^3 cycle}\right)$	Dissipation of heat energy due to internal friction (plastic deformation)	- Strongly stress- and frequency-dependent. - Has to be measured during operation/loading.	Strong relation to the accumulation of fatigue damage. Has limitations in practical applications. Consequently, cyclic loading must be applied to assess the damage. However, can easily be applied in parallel with fatigue testing, to obtain additional information.
Strain-based	Ratcheting: $\frac{\varepsilon_m - (\varepsilon_m)_{min}}{(\varepsilon_m)_{max} - (\varepsilon_m)_{min}}$ Inelastic strains: $\frac{\Delta\varepsilon^i - \Delta\varepsilon^i_0}{\Delta\varepsilon^i_f - \Delta\varepsilon^i_0}$	Ratcheting: Generated by the local deformation around voids, non-metallic precipitations and other defects within the material. Inelastic strains: Cyclic plasticity Both cases: Measurement of the cyclic nonlinear deformation	- Small measurement (magnitude around 10^{-4} or 10^{-3}) - Load must be applied to evaluate	Can give increased information in contrast to the thermometric method, as in if the fatigue is due to ratcheting or inelastic strains. However, smaller measurable values.
Positron annihilation	τ; S − parameter $=$ $\frac{\text{The counts of } \gamma - \text{ray near central peak}}{\text{Total counts of } \gamma - \text{ray}}$	Measurement of time from birth to annihilation and the energy of the resulting photons. Caused due to the development of vacancies through the fatigue loading.	- Measurability drops once the amount of positron trapping sites saturates (mainly measurable early in the fatigue life). - Not applicable for materials exhibiting saturation of positron trapping sites in initial state. - Mainly applicable in laboratories.	Applicability dependent on material characteristics. Due to the existence of initial positron traps such as, for instance, precipitates. The parameter is most significant early in the fatigue life. Might have the potential to monitor whether fatigue damage has accumulated or not, in either conservative designs with a high DFF or where "infinite" fatigue life is desired. Mainly for laboratory testing.
Magnetic	BHN: RMS (V); $\frac{V_n}{V_0}$ Magnetic hysteresis parameters	In both cases due to interaction of dislocation structures and the magnetic domain walls.	- Measurable without loading. - Only works for ferromagnetic materials or through stress-induced phase change. - Not applicable if yield has been surpassed. - Often large plateaus. - Measurable without loading.	The magnetic methods have a strong relation to the microstructure, as can be seen in the cited literature. However, in regard to monitoring fatigue damage, there are contradicting findings.
Ultrasonic	Nonlinear: $\beta \propto \frac{A_2}{A_1^2}$; %THD $= \frac{A_2}{A_1} \times 100\%$ Linear: $\Delta V(\frac{m}{s})$; $\alpha(\mu s^{-1})$; $\frac{\Delta V}{V_0}$; $\frac{\Delta\alpha}{\alpha_0}$; $1 - \frac{V_L^2}{V_L^2}$; $1 \frac{-\alpha}{\alpha}$	Nonlinear: Attributed to the nonlinearity of the propagation medium, commonly discussed as microcracks and dislocations, generating secondary harmonics. Linear: Dislocation dampening.	- Linear methods exhibit small change often with large plateaus. - Measurable without loading.	The nonlinear method exhibits a continuous noticeable increase throughout the reviewed literature. The linear methods are generally more questionable, with large sections of insignificant change.

goal is to develop a diagnostic tool for the remaining fatigue life before a macroscopic crack has been initiated, it would be of importance to also consider factors such as bolted and welded joints, as fatigue failure is commonly associated with such details, due to the higher local stresses and often multiaxial fatigue in both categories, with the addition of mean stress/residual stresses, the presence of microcracks and the potential for unfavourable microstructure for welded details.

The methods are classified in the Table 3 based on the usage of laboratory and in-situ assessments. Table 4 categorized the applicability of the methods for metal and composites. Tables 6 and 7 summarized the parameters, phenomenon and limitations of all the crack monitoring and damage monitoring separately. The reliability, advantages, weaknesses and case dependency are presented at the last column of the tables. The important information such as material, load parameters, measurement technique and failure criterion, which should be investigated before monitoring, and relevant guidelines are presented in the Table 5. Therefore, these tables can be considered as a framework for choosing suitable technique for fatigue crack or damage detection of material or components and this is one of the main outcomes of the review paper.

Furthermore, validation of methods in regard to such as variable

amplitude loading (VAL) should be made. In the review, it was noted that both the thermometric and XRD method achieved reasonable accuracy for determining the remaining fatigue life during two and four stage block loadings. However, variable amplitude loadings and block loadings is not equivalent.

At last, it should be noted that even though microstructural changes throughout the fatigue life can be measured, it does not necessarily define the consumed nor remaining fatigue life. In fact, the only common practice to estimate remaining life through measurements, is by crack detection and crack propagation. Consequently, as it is the strongest and simplest indicator for fatigue damage. However, the continued research towards the field of damage measurement, through microstructural changes for the crack initiation phase, helps both in the understanding of fatigue mechanisms and developing damage accumulation rules. This from the perspective that the parameters adapted for damage measurements, are closely related to the microstructural progression of fatigue damage.

Declaration of Competing Interest

The authors declare that they have no known competing financial interests or personal relationships that could have appeared to influence the work reported in this paper.

Acknowledgement

The authors are grateful for the financial support provided by the Norwegian Ministry of Education during this project. Furthermore, the group wishes to thank the publishers for allowing the reuse of figures.

References

[1] DNVGL. RP-C203: Fatigue design of offshore steel structures; 2014.
[2] Keprate A, Ratnayake RMC. Fatigue and fracture degradation inspection of offshore structures and mechanical items: The state of the art. Proceedings of the International Conference on Offshore Mechanics and Arctic Engineering - OMAE. 2015.
[3] Wang QY, Berard JY, Rathery S, Bathias C. Technical note High-cycle fatigue crack initiation and propagation behaviour of high-strength sprin steel wires. Fatigue Fract Eng Mater Struct 1999;22(8):673–7.
[4] Suresh S. Fatigue of materials. 1st paperback ed. (with corrections and exercises). Cambridge solid state science series, vol. 8. Cambridge: Cambridge University Press; 1992.
[5] Palit Sagar S, Das S, Parida N, Bhattacharya DK. Non-linear ultrasonic technique to assess fatigue damage in structural steel. Scr Mater 2006;55(2):199–202.
[6] Lukáš P, Kunz L. Specific features of high-cycle and ultra-high-cycle fatigue. Fatigue Fract Eng Mater Struct 2002;25(8–9):747–53.
[7] Pippan R, Zelger C, Gach E, Bichler C, Weinhandl H. On the mechanism of fatigue crack propagation in ductile metallic materials. Fatigue Fract Eng Mater Struct 2011;34(1):1–16.
[8] Yang L, Fatemi A. Cumulative fatigue damage mechanisms and quantifying parameters: A literature review. J Test Eval 1998;26(2):89–100.
[9] Ritchie RO, Garrett GG, Knott JP. Crack-growth monitoring: Optimisation of the electrical potential technique using an analogue method. Int J FractMech 1971;7(4):462.
[10] Tada N. Application of direct-current potential difference method to evaluation of various damages in conductive materials. American Society of Mechanical Engineers, Pressure Vessels and Piping Division (Publication) PVP. 2008.
[11] Gandossi L, Summers SA, Taylor NG, Hurst RC, Hulm BJ, Parker JD. The potential drop method for monitoring crack growth in real components subjected to combined fatigue and creep conditions: Application of FE techniques for deriving calibration curves. Int J Press Vessels Pip 2001;78(11–12):881–91.
[12] Spitas V, Spitas C, Michelis P. A three-point electrical potential difference method for in situ monitoring of propagating mixed-mode cracks at high temperature. Meas J Int Meas Confeder 2010;43(7):950–9.
[13] Tada N, Hayashi Y, Kitamura T, Ohtani R. Analysis on the applicability of direct current electrical potential method to the detection of damage by multiple small internal cracks. Int J Fract 1997;85(1):1–9.
[14] Sonsino CM. Comparison of different local design concepts for the structural durability assessment of welded offshore K-nodes. Int J Fatigue 2012;34(1):27–34.
[15] Černý I. The use of DCPD method for measurement of growth of cracks in large components at normal and elevated temperatures. Eng Fract Mech 2004;71(4):837–48.
[16] Oppermann W, Hofstötter P, Keller HP. Long-term installations of the DC-potential drop method in four nuclear power plants and the accuracies thereby obtained for monitoring of crack initiation and crack growth 1 This paper was presented at the 21st MPA Seminar, Stuttgart, 5th–6th October 1995.1. Nucl Eng Des 1997;174(3): 287–92.
[17] Roberts TM, Talebzadeh M. Acoustic emission monitoring of fatigue crack propagation. J Constr Steel Res 2003;59(6):695–712.
[18] Anastasopoulos A, Kourousis D, Botten S, Wang G. Acoustic emission monitoring for detecting structural defects in vessels and offshore structures. Ships Offshore Struct 2009;4(4):363–72.
[19] Yu J, Ziehl P, Matta F, Pollock A. Acoustic emission detection of fatigue damage in cruciform welded joints. J Constr Steel Res 2013;86:85–91.
[20] Mazur K, Wisner B, Kontsos A. Fatigue damage assessment leveraging nondestructive evaluation data. JOM 2018;70(7):1182–9.
[21] Sedlak P, Hirose Y, Enoki M. Acoustic emission localization in thin multi-layer plates using first-arrival determination. Mech Syst Sig Process 2013;36(2):636–49.
[22] Bai F, Gagar D, Foote P, Zhao Y. Comparison of alternatives to amplitude thresholding for onset detection of acoustic emission signals. Mech Syst Sig Process 2017;84:717–30.
[23] Tang J, Soua S, Mares C, Gan TH. An experimental study of acoustic emission methodology for in service condition monitoring of wind turbine blades. Renew Energy 2016;99:170–9.
[24] Berkovits A, Fang D. Study of fatigue crack characteristics by acoustic emission. Eng Fract Mech 1995;51(3). 401–9, 411–6.
[25] Roberts TM, Talebzadeh M. Fatigue life prediction based on crack propagation and acoustic emission count rates. J Constr Steel Res 2003;59(6):679–94.
[26] Yu J, Ziehl P, Zrate B, Caicedo J. Prediction of fatigue crack growth in steel bridge components using acoustic emission. J Constr Steel Res 2011;67(8):1254–60.
[27] Keshtgar A, Modarres M. Acoustic emission-based fatigue crack growth prediction. Proceedings - Annual Reliability and Maintainability Symposium. 2013.
[28] Yuyama S, Yokoyama K, Niitani K, Ohtsu M, Uomoto T. Detection and evaluation of failures in high-strength tendon of prestressed concrete bridges by acoustic emission. Constr Build Mater 2007;21(3):491–500.
[29] Nair A, Cai CS. Acoustic emission monitoring of bridges: Review and case studies. Eng Struct 2010;32(6):1704–14.
[30] Yu L, Momeni S, Godinez V, Giurgiutiu V, Ziehl P, Yu J. Dual mode sensing with low-profile piezoelectric thin wafer sensors for steel bridge crack detection and diagnosis. Adv Civ Eng 2012;2012.
[31] Bruzelius K, Mba D. An initial investigation on the potential applicability of Acoustic Emission to rail track fault detection. NDT E Int 2004;37(7):507–16.
[32] Kuang KSC, Li D, Koh CG. Acoustic emission source location and noise cancellation for crack detection in rail head. Smart Struct Syst 2016;18(5):1063–85.
[33] van der Horst MP, Kaminski ML, Puik E. Methods for Sensing and Monitoring Fatigue Cracks and Their Applicability for Marine Structures; 2013.
[34] Manjula K, Vijayarekh K, Venkatrama B. Weld Flaw Detection Using Various Ultrasonic Techniques: A Review. J Appl Sci 2014;14:1529–35.
[35] Baskaran G, Balasubramaniam K, Lakshmana Rao C. Shear-wave time of flight diffraction (S-TOFD) technique. NDT E Int 2006;39(6):458–67.
[36] Felice MV, Fan Z. Sizing of flaws using ultrasonic bulk wave testing: A review. Ultrasonics 2018;88:26–42.
[37] Moles M, Robertson LB, Sinclair T. Developments in Time-Of-Flight Diffraction (TOFD); 2012.
[38] Nath SK, Balasubramaniam K, Krishnamurthy CV, Narayana BH. Sizing of surface-breaking cracks in complex geometry components by ultrasonic Time-of-Flight Diffraction (TOFD) technique. Insight: Non-Destruct Test Cond Monit 2007;49(4):200–6.
[39] Nath SK, Balasubramaniam K, Krishnamurthy CV, Narayana BH. Reliability assessment of manual ultrasonic time of flight diffraction (TOFD) inspection for complex geometry components. NDT E Int 2010;43(2):152–62.
[40] Habibpour-Ledari A, Honarvar F. Three Dimensional Characterization of Defects by Ultrasonic Time-of-Flight Diffraction (ToFD) Technique. J Nondestr Eval 2018;37(1):14.
[41] Young-Fo C, Cheng IH. Time of flight diffraction imaging for double-probe technique. IEEE Trans Ultrason Ferroelectr Freq Control 2002;49(6):776–83.
[42] Baskaran G, Balasubramaniam K, Krishnamurthy CV, Rao CL. Ultrasonic TOFD flaw sizing and imaging in thin plates using embedded signal identification technique (ESIT). Insight: Non-Destruct Test Cond Monit 2004;46(9):537–42.
[43] Subbaratnam R, Abraham ST, Venkatraman B, Raj B. Immersion and TOFD (I-TOFD): A Novel Combination for Examination of Lower Thicknesses. J Nondestr Eval 2011;30(3):137.
[44] Masserey B, Fromme P. In-situ monitoring of fatigue crack growth using high frequency guided waves. NDT E Int 2015;71:1–7.
[45] Grubisic V, Sonsino CM. Fatigue strength of high-pressure vessels for novel manufacturing processes. Fraunhofer Inst. for Structural Durability LBF, Report No. 148; 1979.
[46] Polák J. Electrical resistivity of cyclically deformed copper. Czech J Phys 1969;19(3):315–22.
[47] Sun B, Guo Y. High-cycle fatigue damage measurement based on electrical resistance change considering variable electrical resistivity and uneven damage. Int J Fatigue 2004;26(5):457–62.
[48] Starke P, Eifler D, Boller C. Fatigue assessment of metallic materials beyond strain measurement. Int J Fatigue 2016;82:274–9.
[49] Germann H, Starke P, Eifler D. Resistivity-based evaluation of the fatigue behavior of cast irons. Metall Mater Trans A 2012;43(8):2792–8.

[50] Mao H, Yi X, Mao H, Tang W, Huang Z, Li X, et al. Fatigue damage detection and location of metal materials by electrical impedance tomography. Res Phys 2019;15.

[51] Klein M, Eifler D. Influences of the manufacturing processes on the surface integrity and the resulting fatigue behavior of quenched and tempered SAE 4140. Procedia Eng 2010.

[52] Sun B, Yang L, Guo Y. A high-cycle fatigue accumulation model based on electrical resistance for structural steels. Fatigue Fract Eng Mater Struct 2007;30(11):1052–62.

[53] Balle F, Huxhold S, Wagner G, Eifler D. Damage monitoring of ultrasonically welded aluminum/CFRP-joints by electrical resistance measurements. Procedia Eng 2011.

[54] Walther F, Eifler D. Cyclic deformation behavior of steels and light-metal alloys. Mater Sci Eng, A 2007;468–470(SPEC. ISS.):259–66.

[55] Starke P, Klein M, Eifler D. Resistivity - A characteristic fingerprint of fatigue induced changes in the microstructure of metallic materials. Procedia Eng 2011.

[56] Walther F, Eifler D. Fatigue life calculation of SAE 1050 and SAE 1065 steel under random loading. Int J Fatigue 2007;29(9–11):1885–92.

[57] Kucharczyk P, Rizos A, Münstermann S, Bleck W. Estimation of the endurance fatigue limit for structural steel in load increasing tests at low temperature. Fatigue Fract Eng Mater Struct 2012;35(7):628–37.

[58] Pavlou DG, Prediction of Fatigue Damage Accumulation under Real Loading Spectra. University of Patras; 1994.

[59] Pavlou DG. A phenomenological fatigue damage accumulation rule based on hardness increasing, for the 2024–T42 aluminum. Eng Struct 2002;24(11):1363–8.

[60] Ye DY, Wang DJ, An P. Characteristics of the change in the surface microhardness during high cycle fatigue damage. Mater Chem Phys 1996;44(2):179–81.

[61] Ye D, Tong X, Yao L, Yin X. Fatigue hardening/softening behaviour investigated through Vickers microhardness measurement during high-cycle fatigue. Mater Chem Phys 1998;56(3):199–204.

[62] Ye D, Wang Z. Approach to investigate pre-nucleation fatigue damage of cyclically loaded metals using Vickers microhardness tests. Int J Fatigue 2001;23(1):85–91.

[63] Drumond G, Pinheiro B, Pasqualino I, Roudet F, Chicot D, Decoopman X. High Cycle Fatigue Damage Evaluation of Steel Pipelines Based on Microhardness Changes During Cyclic Loads. ASME 2017 36th International Conference on Ocean, Offshore and Arctic Engineering. 2017.

[64] Drumond G, Pinheiro B, Pasqualino I, Roudet F, Chicot D. High Cycle Fatigue Damage Evaluation of Steel Pipelines Based on Microhardness Changes During Cyclic Loads: Part II. ASME 2018 37th International Conference on Ocean, Offshore and Arctic Engineering. 2018.

[65] Drumond G, Roudet F, Chicot D, Pinheiro B, Pasqualino I. A damage criterion to predict the fatigue life of steel pipelines based on indentation measurements. J Offshore Mech Arct Eng 2021;143(1).

[66] Miroslav Š, Vladimír C, Kepka M. Possibility of fatigue damage detection by non-destructive measurement of the surface hardness. Procedia Structural Integrity. 2017.

[67] Pinheiro B, Lesage J, Pasqualino I, Benseddiq N, Bemporad E. X-ray diffraction study of microstructural changes during fatigue damage initiation in steel pipes. Mater Sci Eng, A 2012;532:158–66.

[68] Vijayan K, Mani A, Balasingh C, Singh AK. X-ray analysis of polycrystalline aluminium subjected to fatigue cycling. Bull Mater Sci 1988;10(3):205–16.

[69] Nagao M, Weiss V. X-ray diffraction study of low cycle fatigue damage in plain carbon steel. American Society of Mechanical Engineers (Paper); 1976(76 -WA/Mat-10).

[70] Pangborn RN, Weissmann S, Kramer IR. Dislocation distribution and prediction of fatigue damage. Metall Trans A 1981;12(1):109–20.

[71] Kramer IR, Feng CR, Wu B. Dislocation-depth distribution in fatigued metals. Mater Sci Eng 1986;80(1):37–48.

[72] Pinheiro B, Lesage J, Pasqualino I, Bemporad E, Benseddiq N. X-ray diffraction study of microstructural changes during fatigue damage initiation in pipe steels: Role of the initial dislocation structure. Mater Sci Eng, A 2013;580:1–12.

[73] Teng Z, Wu H, Boller C, Starke P. A unified fatigue life calculation based on intrinsic thermal dissipation and microplasticity evolution. Int J Fatigue 2020;131.

[74] Harig H, Weber M. Estimation of crack initiation in plain carbon steels by thermometric methods. In: Sih GC, Provan JW, editors. Defects, Fracture and Fatigue. Dordrecht: Springer; 1983.

[75] Wang H, Jiang L, Liaw PK, Brooks CR, Klarstrom DL. Infrared temperature mapping of ULTIMET alloy during high-cycle fatigue tests. Metall Mater Trans A 2000;31(4):1307–10.

[76] Wagner D, Ranc N, Bathias C, Paris PC. Fatigue crack initiation detection by an infrared thermography method. Fatigue Fract Eng Mater Struct 2010;33(1):12–21.

[77] La Rosa G, Risitano A. Thermographic methodology for rapid determination of the fatigue limit of materials and mechanical components. Int J Fatigue 2000;22(1):65–73.

[78] Curà F, Curti G, Sesana R. A new iteration method for the thermographic determination of fatigue limit in steels. Int J Fatigue 2005;27(4):453–9.

[79] Luong MP. Infrared thermographic scanning of fatigue in metals. Nucl Eng Des 1995;158(2–3):363–76.

[80] Luong MP. Fatigue limit evaluation of metals using an infrared thermographic technique. Mech Mater 1998;28(1–4):155–63.

[81] Risitano A, Risitano G. Determining fatigue limits with thermal analysis of static traction tests. Fatigue Fract Eng Mater Struct 2013;36(7):631–9.

[82] Teng Z, Wu H, Boller C, Starke P. Thermography in high cycle fatigue short-term evaluation procedures applied to a medium carbon steel. Fatigue Fract Eng Mater Struct 2020;43(3):515–26.

[83] Fargione G, Geraci A, La Rosa G, Risitano A. Rapid determination of the fatigue curve by the thermographic method. Int J Fatigue 2002;24(1):11–9.

[84] Amiri M, Khonsari MM. Rapid determination of fatigue failure based on temperature evolution: Fully reversed bending load. Int J Fatigue 2010;32(2):382–9.

[85] Wu H, Bäumchen A, Engel A, Acosta R, Boller C, Starke P. SteBLife – A new short-time procedure for the evaluation of fatigue data. Int J Fatigue 2019;124:82–8.

[86] Starke P. StressLifetc – NDT-related assessment of the fatigue life of metallic materials. Materialpruefung/Mater Test 2019;61(4):297–303.

[87] Sonsino CM. Course of SN-curves especially in the high-cycle fatigue regime with regard to component design and safety. Int J Fatigue 2007;29(12):2246–58.

[88] Newman JC. Fatigue and Crack-growth Analyses under Giga-cycle Loading on Aluminum Alloys. Procedia Eng 2015;101:339–46.

[89] Meneghetti G. Analysis of the fatigue strength of a stainless steel based on the energy dissipation. Int J Fatigue 2007;29(1):81–94.

[90] Boulanger T, Chrysochoos A, Mabru C, Galtier A. Calorimetric analysis of dissipative and thermoelastic effects associated with the fatigue behavior of steels. Int J Fatigue 2004;26(3):221–9.

[91] Liaw PK, Wang H, Jiang L, Yang B, Huang JY, Kuo RC, et al. Thermographic detection of fatigue damage of pressure vessel steels at 1,000 Hz and 20 Hz. Scr Mater 2000;42(4):389–95.

[92] Amiri M, Khonsari MM. Nondestructive estimation of remaining fatigue life: Thermography technique. J Fail Anal Prev 2012;12(6):683–8.

[93] Liakat M, Khonsari MM. An experimental approach to estimate damage and remaining life of metals under uniaxial fatigue loading. Mater Des 2014;57:289–97.

[94] Dietrich L, Radziejewska J. The fatigue damage development in a cast Al-Si-Cu alloy. Mater Des 2011;32(1):322–9.

[95] Moćko W, Grzywna P, Kowalewski ZL, Radziejewska J. An influence of cyclic loading on the form of constitutive relationship for DP500 steel. Mater Des 2016;103:183–93.

[96] Moćko W. The influence of stress-controlled tensile fatigue loading on the stress-strain characteristics of AISI 1045 steel. Mater Des 2014;58:145–53.

[97] Socha G. Experimental investigations of fatigue cracks nucleation, growth and coalescence in structural steel. Int J Fatigue 2003;25(2):139–47.

[98] Socha G. Prediction of the fatigue life on the basis of damage progress rate curves. Int J Fatigue 2004;26(4):339–47.

[99] Sonsino CM. The influence of coldforming on the low cycle fatigue behaviour of the finegrained structural steel Fe E 47 and the age-hardened aluminium alloy AlCuMg2. Int J Fatigue 1984;6(3):173–83.

[100] Dupasquier A, Kögel G, Somoza A. Studies of light alloys by positron annihilation techniques. Acta Mater 2004;52(16):4707–26.

[101] Čížek J. Characterization of lattice defects in metallic materials by positron annihilation spectroscopy: A review. J Mater Sci Technol 2018;34(4):577–98.

[102] Puska MJ, Nieminen RM. Theory of positrons in solids and on solid surfaces. Rev Mod Phys 1994;66(3):841–97.

[103] Holzwarth U, Schaaff P. Nondestructive monitoring of fatigue damage evolution in austenitic stainless steel by positron-lifetime measurements. Phys Rev B Condens Matter Mater Phys 2004;69(9).

[104] Nagoshi T, Kozu S, Inoue Y, O'Rourke BE, Harada Y. Fatigue damage assessment of SUS316L using EBSD and PALS measurements. Mater Charact 2019;154:61–6.

[105] Uematsu Y, Kakiuchi T, Hattori K, Uesugi N, Nakao F. Non-destructive evaluation of fatigue damage and fatigue crack initiation in type 316 stainless steel by positron annihilation line-shape and lifetime analyses. Fatigue Fract Eng Mater Struct 2017;40(7):1143–53.

[106] Kawaguchi Y, Nakamura N, Yusa S. Non-destructive evaluation of fatigue damage in type 316 stainless steel using positron annihilation lineshape analysis. Mater Trans 2002;43(4):727–34.

[107] Kawaguchi Y, Shirai Y. Fatigue evaluation of type 316 stainless steel using positron annihilation lineshape analysis and β^{+}-γ coincidence positron lifetime measurement. J Nucl Sci Technol 2002;39(10):1033–40.

[108] Maeda N, Nakamura N, Uchida M, Ohta Y, Yoshida K. Application of positron annihilation line-shape analysis to fatigue damage for nuclear plant materials. Nucl Eng Des 1996;167(2):169–74.

[109] Asoka-Kumar P, Hartley JH, Howell RH, Sterne PA, Akers D, Shah V, et al. Direct observation of carbon-decorated defects in fatigued type 304 stainless steel using positron annihilation spectroscopy. Acta Mater 2002;50(7):1761–70.

[110] Hori F, Oshima R. Positron annihilation study in the early stage of fatigue in type 304 stainless steel. Phys Status Solidi (A) Appl Res 2002;191(2):409–17.

[111] Holzwarth U, Schaaff P. On the non-destructive detection of fatigue damage in industrial aluminium alloys by positron annihilation. J Mater Sci 2007;42(14):5620–8.

[112] Tomáš I, Kovářík O, Kadlecová J, Vértesy G. Optimization of fatigue damage indication in ferromagnetic low carbon steel. Meas Sci Technol 2015;26(9).

[113] Kikuchi H, Ara K, Kamada Y, Kobayashi S. Effect of microstructure changes on Barkhausen noise properties and hysteresis loop in cold rolled low carbon steel. IEEE Trans Magn 2009;45(6):2744–7.

[114] Kasai N, Koshino H, Sekine K, Kihira H, Takahashi M. Study on the effect of elastic stress and microstructure of low carbon steels on Barkhausen noise. J Nondestr Eval 2013;32(3):277–85.

[115] Teschke M, Vasquez JR, Lücker L, Walther F. Characterization of damage evolution on hot flat rolled mild steel sheets by means of micromagnetic parameters and fatigue strength determination. Materials 2020;13(11).

[116] Yamaura S, Furuya Y, Watanabe T. The effect of grain boundary microstructure on Barkhausen noise in ferromagnetic materials. Acta Mater 2001;49(15):3019–27.
[117] Dijkstra LJ, Wert C. Effect of inclusions on coercive force of iron. Phys Rev 1950;79(6):979–85.
[118] Astie B, Degauque J. Influence of the dislocation structures on the magnetic and magnetomechanical properties of high-purity iron. IEEE Trans Magn 1981;17(6):2929–31.
[119] Scherpereel DE, Kazmerski LL, Allen CW. The magnetoelastic interaction of dislocations and ferromagnetic domain walls in iron and nickel. Metall Mater Trans B 1970;1(2):517–24.
[120] Deng Y, Li Z, Chen J, Qi X. The effects of the structure characteristics on Magnetic Barkhausen noise in commercial steels. J Magn Magn Mater 2018;451:276–82.
[121] Baldev R, Jayakumar T, Moorthy V, Vaidyanathan S. Characterisation of microstructures, deformation, and fatigue damage in different steels using magnetic Barkhausen emission technique. Russ J Nondestr Test 2001;37(11):789–98.
[122] Lindgren M, Lepistö T. Application of a novel type Barkhausen noise sensor to continuous fatigue monitoring. NDT E Int 2000;33(6):423–8.
[123] Lindgren M, Lepistö T. Effect of cyclic deformation on Barkhausen noise in a mild steel. NDT E Int 2003;36(6):401–9.
[124] Soultan M, Kleber X, Chicois J, Vincent A. Mechanical Barkhausen noise during fatigue of iron. NDT E Int 2006;39(6):493–8.
[125] Palma ES, Mansur TR, Silva Jr SF, Alvarenga Jr A. Fatigue damage assessment in AISI 8620 steel using Barkhausen noise. Int J Fatigue 2005;27(6):659–65.
[126] Sagar SP, Parida N, Das S, Dobmann G, Bhattacharya DK. Magnetic Barkhausen emission to evaluate fatigue damage in a low carbon structural steel. Int J Fatigue 2005;27(3):317–22.
[127] Morishita K, Gilanyi A, Sukegawa T, Uesaka T, Miya K. Magnetic non-destructive evaluation of accumulated fatigue damage in ferromagnetic steels for nuclear plant component. J Nucl Mater 1998;258–263(PART 2 B):1946–52.
[128] Gao Z, Chen ZJ, Jiles DC, Biner S. Variation of coercivity of ferromagnetic material during cyclic stressing. IEEE Trans Magn 1994;30(6):4593–5.
[129] Gilanyi A, Morishita K, Sukegawa T, Uesaka M, Miya K. Magnetic nondestructive evaluation of fatigue damage of ferromagnetic steels for nuclear fusion energy systems. Fusion Eng Des 1998;42(1–4):485–91.
[130] Chen ZJ, Strom A, Jiles DC. Micromagnetic surface measurements for evaluation of surface modifications due to cyclic stress. IEEE Trans Magn 1993;29(6):3031–3.
[131] Grimberg R, Leitoiu S, Bradu BE, Savin A, Andreescu A. Magnetic sensor used for the determination of fatigue state in ferromagnetic steels. Sens Actuators, A 2000;81(1):371–3.
[132] De Backer F, Schoss V, Maussner G. Investigations on the evaluation of the residual fatigue life-time in austenitic stainless steels. Nucl Eng Des 2001;206(2–3):201–19.
[133] Nagy PB. Fatigue damage assessment by nonlinear ultrasonic materials characterization. Ultrasonics 1998;36(1–5):375–81.
[134] Oruganti RK, Sivaramanivas R, Karthik TN, Kommareddy V, Ramadurai B, Ganesan B, et al. Quantification of fatigue damage accumulation using non-linear ultrasound measurements. Int J Fatigue 2007;29(9–11):2032–9.
[135] Cantrell JH, Yost WT. Nonlinear ultrasonic characterization of fatigue microstructures. Int J Fatigue 2001;23(SUPPL. 1):487–90.
[136] Kumar A, Adharapurapu RR, Jones JW, Pollock TM. In situ damage assessment in a cast magnesium alloy during very high cycle fatigue. Scr Mater 2011;64(1):65–8.
[137] Kumar A, Torbet CJ, Pollock TM, Wayne Jones J. In situ characterization of fatigue damage evolution in a cast Al alloy via nonlinear ultrasonic measurements. Acta Mater 2010;58(6):2143–54.
[138] Shui G, Kim JY, Qu J, Wang YS, Jacobs LJ. A new technique for measuring the acoustic nonlinearity of materials using Rayleigh waves. NDT E Int 2008;41(5):326–9.
[139] Jhang KY. Applications of nonlinear ultrasonics to the NDE of material degradation. IEEE Trans Ultrason Ferroelectr Freq Control 2000;47(3):540–8.
[140] Ogi H, Suzuki N, Hirao M. Noncontact ultrasonic spectroscopy on deforming polycrystalline copper: Dislocation damping and acoustoelasticity. Metall Mater Trans A 1998;29(12):2987–93.
[141] Ohtani T, Nishiyama K, Yoshikawa S, Ogi H, Hirao M. Ultrasonic attenuation and microstructural evolution throughout tension-compression fatigue of a low-carbon steel. Mater Sci Eng, A 2006;442(1–2 SPEC. ISS.):466–70.
[142] Ohtani T, Ogi H, Minami Y, Hirao M. Ultrasonic attenuation monitoring of fatigue damage in low carbon steels with electromagnetic acoustic resonance (EMAR). J Alloy Compd 2000;310(1–2):440–4.
[143] Liu JH, Li GL, Hao XY, Zeng DB, Sun ZH. Ultrasonic measurement of fatigue damage of nodular cast iron. Mater Lett 2001;50(4):194–8.
[144] Yamagishi H, Fukuhara M. Degradation behavior of moduli in extruded pure magnesium during low- to giga-scale cyclic tension fatigue. Acta Mater 2012;60(12):4759–67.
[145] Granato A, Lücke K. Theory of mechanical damping due to dislocations. J Appl Phys 1956;27(6):583–93.
[146] Granato A, Lücke K. Application of dislocation theory to internal friction phenomena at high frequencies. J Appl Phys 1956;27(7):789–805.
[147] Kenderian S, Berndt TP, Green Jr RE, Djordjevic BB. Ultrasonic monitoring of dislocations during fatigue of pearlitic rail steel. Mater Sci Eng, A 2003;348(1–2):90–9.

Paper III

Hardness Measurements as a Technique for Measuring Accumulated Fatigue Damage

Journal Paper
International Journal of Structural Integrity
*June 2022, doi:*10.1108/IJSI-04-2022-0061

Paper IV

Nonlinear Fatigue Life Prediction Model Based on the Theory of the S-N Fatigue Damage Envelope

Journal Paper
Fatigue & Fracture of Engineering Materials & Structures
March 2022, Volume 45, Pages 1480-1493

Received: 21 December 2021 | Revised: 27 January 2022 | Accepted: 10 February 2022

DOI: 10.1111/ffe.13680

ORIGINAL ARTICLE

FFEMS Fatigue & Fracture of Engineering Materials & Structures WILEY

Nonlinear fatigue life prediction model based on the theory of the S-N fatigue damage envelope

Fredrik Bjørheim | **Dimitrios G. Pavlou** | **Sudath C. Siriwardane**

Department of Mechanical and Structural Engineering and Materials Science, University of Stavanger, Stavanger, Norway

Correspondence
Fredrik Bjørheim, Department of Mechanical and Structural Engineering and Materials Science, University of Stavanger, Stavanger N-4036, Norway.
Email: fredrik.bjorheim@uis.no

Abstract

A nonlinear model is proposed in light of the theory of isodamage curves, to assess the cumulative fatigue damage under multistage loading. The isodamage curves were developed through the theory of the S-N fatigue damage envelope, proposed by Pavlou. The adopted functional form of the fatigue damage is a commonly accepted general form. In the present work, a stress function for the fatigue life exponent is derived with the aid of the S-N curve only. In the proposed nonlinear model, no adjusting parameters are necessary for fatigue damage estimation. The fatigue life prediction of the derived model is compared with experimental results of various alloys and existing models. The comparison is made for C35, C45, Al-2024-T42, 15HM, A336 GR 5, and A387 GR22 for two-stage loading high-low and low-high, and Al 6082-T6 for multistage loading.

KEYWORDS

fatigue damage envelope, fatigue life, isodamage, nonlinear damage model, variable amplitude loading

1 | INTRODUCTION

The commonly applied damage rule, first proposed by Palmgren[1] and popularized by Miner,[2] does not properly account for variable amplitude loading (VAL). The model is applied through a linear summation of the consumed life fraction per stress amplitude, where it is assumed that failure occurs when the summation reaches unity. However, the model is inherently flawed, due to its negligence regarding the perspective of loading sequence,[3] consequently resulting in failure commonly occurring at a sum lower than unity for decreasing load amplitude histories but higher than unity for their increasing amplitude counterparts.[4] This is due to the fact that the fatigue damage accumulation material mechanisms are nonlinear. In fact, if the applied stress amplitude were reduced from high to low fatigue loading, a crack might have initiated in the initial stress amplitudes, which would not have initiated for the equivalent percentage for the subsequent low amplitude fatigue loading.[5]

Despite the shortcomings of Miner's rule, it is still commonly recommended in both Eurocode[6] and DNVGL.[7] This is due to the perspective that an accumulation model is required to design for VAL, that it is

generally simple to follow, and that the formula yields acceptable life prediction for uniform random loading histories.[8–11] The inherent error or uncertainty in Miner's rule for decreasing load amplitude spectra could result in catastrophic consequences. However, it is commonly accounted for through the application of a Design Fatigue Factor, used in conjunction with a design S-N curve which already has a low probability of failure (2.3% in DNVGL),[12,13] resulting in a more conservative design due to the application of Miner's rule.

This highlights the need for further research within the field regarding damage accumulation, at which several attempts have been made both from the viewpoint of theoretical approaches or reflections regarding the S-N curve and regarding the measurement of fatigue damage.[14–24]

Examples of this might be such as the double linear damage rule (DLDR), developed by Manson et al.,[25–27] on the basis of the suggestion by Grover,[28] which shows good agreement with experimental results. The principle in Manson's work is to apply two linear damage rules, which were first categorized as crack initiation and propagation but later categorized as Phase I and Phase II. This arises from the perspective that no measurable cracks could be observed after the phase of initiation had been surpassed, whereas a difference between the phases was recognized.

Another example might be the isodamage lines. The theory of isodamage lines is based on the assumption that the S-N curve has a damage state of 100%, whereas the damage state for a given number of cycles and stress amplitudes falls on straight lines and can, therefore, be related to the next stress amplitude.

Subramanyan[29] proposed a set of straight isodamage lines which converge toward the knee point in an S-Log(N) diagram. Moreover, this model can then determine an equivalent n/N_f for the subsequent stress amplitude. The model implies that the number of cycles required to induce a certain level of damage increases with a reduction in stress amplitude and vice versa, thus being able to capture the loading sequence effect of high to low and low to high. An interesting paper which experimentally confirms the theory of isodamage lines for Al-2024-T42 is that by Pavlou,[30] in which isodamage curves were experimentally derived through the correlation of damage evolution with the evolution of surface hardness.

In contrast to Subramanyan, Hashin and Rotem proposed a set of isodamage lines which converge toward the intercept of the S-Log(N) curve with the stress axis.[31] The effectiveness of this model was criticized in Hectors and De Waele.[15] Most of the researchers have found that Subramanyan is the more favorable of the two theories. However, both models have been found to be slightly non-conservative.

Rege and Pavlou proposed a one-parameter nonlinear fatigue damage accumulation model, based on the concept of isodamage curves.[32] The objective was to reduce the non-conservatism of the model proposed by Subramanyan. It was successfully achieved for low to high two-stage loading, whereas, for high to low amplitude loading, little difference was observed.

Aeran et al. demonstrated the importance of a model which is based on the commonly available S-N curves.[33,34] This arose from the perspective that several damage models, depending on additional material parameters, had been proposed. This, in turn, resulted in the models not being readily applicable. Thus, they proposed a damage model based on the commonly applied S-N curves, in conjunction with a damage transfer concept to account for loading sequence. The damage model simply depends on the parameter N_f, commonly found in traditional S-N curves, whereas the transfer concept also depends on the related stress amplitudes.

Mesmacque et al. proposed a sequential law.[35] The sequential law does not depend on more than the full range of the S-N curve, which it is suggested can be found by the limited dataset of commonly used S-N curves through the Wöhler curve modeling proposed by Kohout and Vechet.[36] The model has, for instance, been adopted in research to estimate the remaining fatigue life of railway bridges.[37] However, even though the study showed a better estimation in comparison to the Miner's rule, a significant deviation from the real fatigue life was observed.

Presenting a function of evaluating the damage envelope and developing a simple tool for damage estimation and life prediction, which depends only on the readily available S-N curves, are the major objectives of this paper. The theory of the S-N fatigue damage envelope proposed by Pavlou[38] is adopted, and a generally accepted damage function formalism for damage evolution is utilized to develop the new damage model. The proposed model can be used for any metallic material, with any type of loading, and it depends only on the general S-N curve.

2 | THE CONCEPT OF THE FATIGUE DAMAGE ENVELOPE

The fatigue damage envelope proposed by Pavlou is based on the hypothesis that the area bounded by the stress and cycles' axes and the S-N curve provides a fatigue damage map for the material. However, in contrast to Subramanyan and Hashin and Rotem's common methodologies for isodamage lines, the proposed

isodamage curves in Pavlou's theory are not straight lines converging only at the knee point or at the ultimate stress S_u at the stress axis, as can be seen in Figure 1A,B, respectively. In fact, the isodamage curves proposed[38] are curved and converge at both the knee point and at the ultimate stress, as can be seen in Figure 2. The argument for the isodamage curve, in contrast to the isodamage straight line, originates from the fact that the S-N curve has a damage state of $D=1$, as in failure, whereas both the S and the N axes have a damage state of $D=0$. Consequently, it should be assumed that no damage is accumulated when the number of cycles is $n=0$, and the same follows for the scenario where the stress amplitude is equal (or beneath) the fatigue limit. It should be mentioned here that the stress-axis and the cycles-axis are the normalized quantities presented in Equations 1 and 2.

$$\sigma_i^* = \frac{\sigma_i - S_e}{S_u - S_e} \quad 0 \le \sigma_i^* \le 1 \tag{1}$$

$$n_i^* = \frac{n_i}{N_e} \quad 0 \le n_i^* \le 1 \tag{2}$$

where σ_i is the applied stress amplitude, S_e is the fatigue endurance limit, S_u is the ultimate stress and N_e is the fatigue capacity at the knee-point stress, resulting in the normalized parameters σ_i^* and n_i^* both having values in the range of 0 to 1. A schematical representation of the damage accumulation path under four-stage loading history is shown in Figure 3. In fact, it can be seen that, for a subsequent stress amplitude, an equivalent normalized number of cycles has to be found.

The development of the curves can be performed through a heat transfer analysis in a finite element software, described in detail in Pavlou's paper.[38]

3 | NONLINEAR FATIGUE DAMAGE FUNCTION

An increase in the number of loading cycles by dn/n causes an increase in damage dD/D. Taking this concept into account, a generally accepted formulation for damage function D is based on the solution of the following differential equation:

$$\frac{dD}{D} = q(\sigma, m)\frac{dn}{n} \tag{3}$$

where $q(\sigma, m)$ is a parameter affected by the stress amplitude σ and the material properties m.

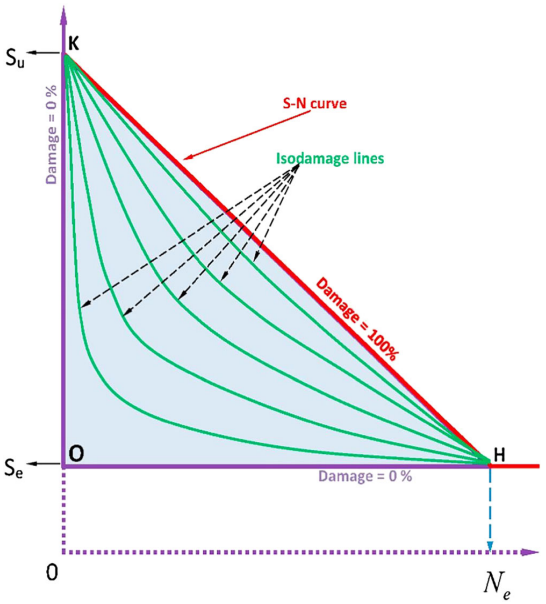

FIGURE 2 The isodamage lines within the S-N fatigue damage envelope. Reprinted from Pavlou[38] with permission from Elsevier, © 2018 [Colour figure can be viewed at wileyonlinelibrary.com]

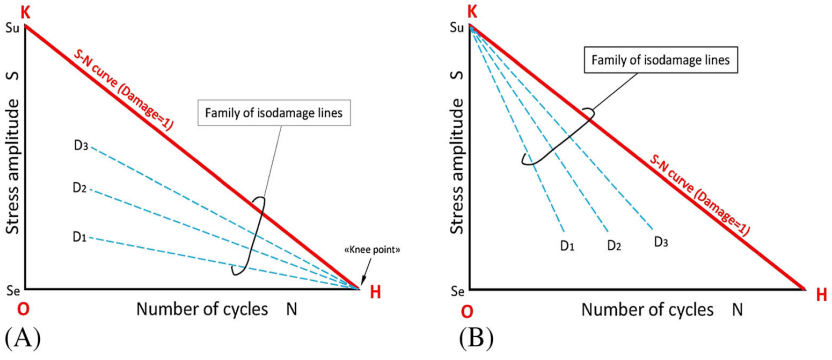

FIGURE 1 Isodamage lines converging: (A) at the knee point of the S-N curve, (B) at the S_u point. Reprinted from Pavlou[38] with permission from Elsevier, © 2018 [Colour figure can be viewed at wileyonlinelibrary.com]

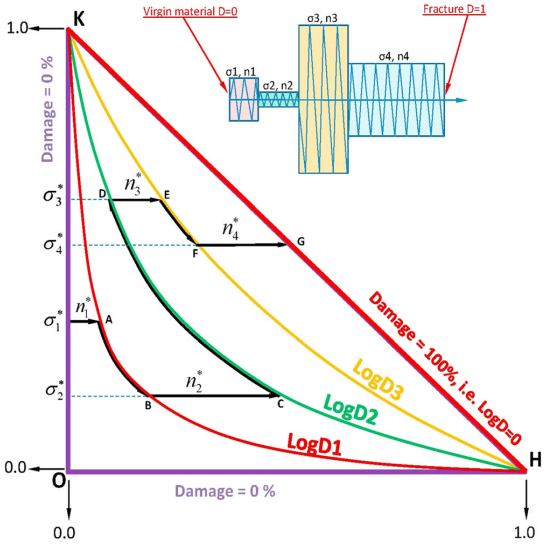

FIGURE 3 Schematical representation of the damage accumulation path under four-stage loading history. Reprinted from Pavlou[38] with permission from Elsevier, © 2018 [Colour figure can be viewed at wileyonlinelibrary.com]

The solution of Equation 3 yields

$$\mathrm{Log}(D) = q(\sigma, m)\mathrm{Log}(n) + C \tag{4}$$

where C is the integration parameter.

Taking into account the condition $D = 1$ for $n = N_f$, Equation 4 yields

$$C = -q(\sigma, m)Log(N_f) \tag{5}$$

With the aid of the above equation, Equation 4 can be written as follows:

$$\mathrm{Log}(D) = q(\sigma, m)\left(\mathrm{Log}(n) - Log(N_f)\right) \tag{6}$$

or

$$D = \left(\frac{n}{N_f}\right)^{q(\sigma,m)} \tag{7}$$

The exponent $q(\sigma, m)$ is accepted to be a function of the stress amplitude by all the existing research.[9,15,16,39] Both the final expression of the function $q(\sigma, m)$ and the number of material parameters m with their respective values depends upon the theoretical or experimental method which is adopted to develop a function, as there are both theoretical and experimental methods of defining damage. As the theoretical approach proposed by Pavlou[38] is adopted herein, the governing parameters for the resulting expression with its material parameters are related to the nature of the S-N curve. According to the theoretical background of the model, the S-N damage envelope[38] demonstrates the effect of the fatigue mechanisms, in damage accumulation in macroscopic level.

4 | DAMAGE ACCUMULATION UNDER MULTISTAGE LOADING

The nonlinear fatigue damage model in Equation 7 can be used to estimate the damage accumulation under multistage loading. For the sake of simplicity, Equation 7 will be initially applied to estimate the damage accumulation due to a two-stage loading history shown in Figure 4A.

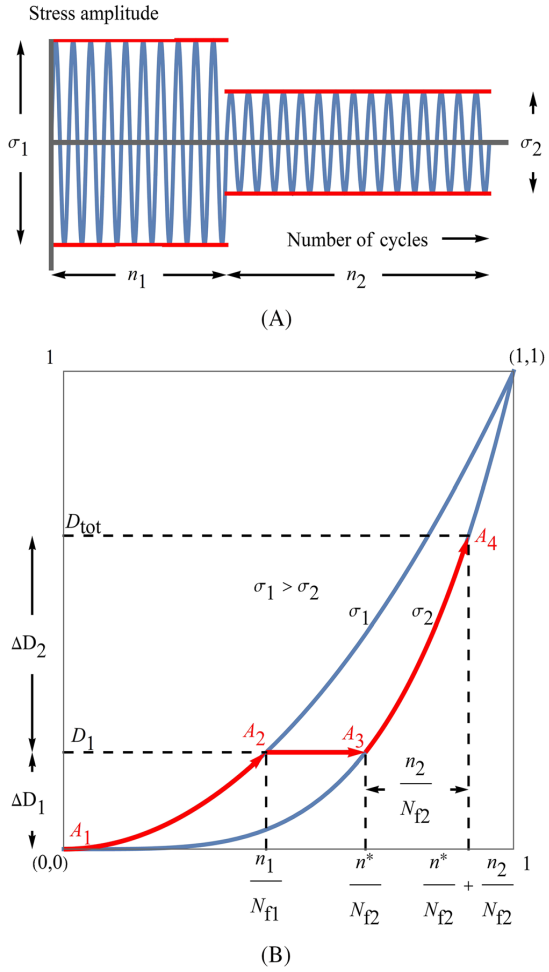

FIGURE 4 (A) Two-stage loading history and (B) damage accumulation path during two-stage loading history [Colour figure can be viewed at wileyonlinelibrary.com]

The damage accumulation during the first loading block (σ_1, n_1) is demonstrated by the path $A_1 \rightarrow A_2$ in Figure 4B. When the second loading block (σ_2, n_2) starts, damage D_1 has already been accumulated by the first loading block (σ_1, n_1). Therefore, the damage accumulation path for the second block (σ_2, n_2) starts from the point A_3 that corresponds to damage D_1. The damage accumulation path $A_3 \rightarrow A_4$ for the loading block (σ_2, n_2) lies on the isostress curve σ_2 and corresponds to the normalized number of cycles n_2/N_{f2} (see Figure 4B).

According to Equation 7, the total damage accumulation after the two loading blocks is

$$D_{tot} = \left(\frac{n^*}{N_{f2}} + \frac{n_2}{N_{f2}} \right)^{q(\sigma_2, m)} \tag{8}$$

The ratio n^*/N_{f2} corresponds to the starting point A_3 of the damage path $A_3 \rightarrow A_4$ of the second loading block (σ_2, n_2). Point A_3 corresponds to the same damage as the end point A_2 of the damage path $A_1 \rightarrow A_2$ of the first loading block (σ_1, n_1).

Therefore,

$$D_1 = \left(\frac{n_1}{N_{f1}} \right)^{q(\sigma_1, m)} \quad \text{for point } A_2 \tag{9}$$

and

$$D_1 = \left(\frac{n^*}{N_{f2}} \right)^{q(\sigma_2, m)} \quad \text{for point } A_3 \tag{10}$$

A combination of Equations 9 and 10 yields

$$\frac{n^*}{N_{f2}} = \left(\frac{n_1}{N_{f1}} \right)^{\frac{q(\sigma_1, m)}{q(\sigma_2, m)}} \tag{11}$$

With the aid of the above equation, Equation 8 yields

$$D_{tot} = \left(\left(\frac{n_1}{N_{f1}} \right)^{\frac{q(\sigma_1, m)}{q(\sigma_2, m)}} + \frac{n_2}{N_{f2}} \right)^{q(\sigma_2, m)} \tag{12}$$

The above equation can be generalized for multistage loading:

$$D_{tot} = \left(\left(\cdots \left(\left(\left(\frac{n_1}{N_{f1}} \right)^{\frac{q(\sigma_1, m)}{q(\sigma_2, m)}} + \frac{n_2}{N_{f2}} \right)^{\frac{q(\sigma_2, m)}{q(\sigma_3, m)}} + \frac{n_3}{N_{f3}} \right)^{\frac{q(\sigma_3, m)}{q(\sigma_4, m)}} + \cdots + \frac{n_{k-1}}{N_{f(k-1)}} \right)^{\frac{q(\sigma_{k-1}, m)}{q(\sigma_k, m)}} + \frac{n_k}{N_{f(k)}} \right)^{q(\sigma_k, m)} \tag{13}$$

According to the authors' knowledge, the existing nonlinear models in the literature commonly propose exponent ratios $q(\sigma_i, m)/q(\sigma_{i+1}, m)$ instead of exponent function $q(\sigma, m)$. The existing exponent ratios can be utilized only for the case that $D_{tot} = 1$, from which the following formulation can result:

$$\left(\cdots \left(\left(\left(\frac{n_1}{N_{f1}} \right)^{\frac{q(\sigma_1, m)}{q(\sigma_2, m)}} + \frac{n_2}{N_{f2}} \right)^{\frac{q(\sigma_2, m)}{q(\sigma_3, m)}} + \frac{n_3}{N_{f3}} \right)^{\frac{q(\sigma_3, m)}{q(\sigma_4, m)}} + \cdots + \frac{n_{k-1}}{N_{f(k-1)}} \right)^{\frac{q(\sigma_{k-1}, m)}{q(\sigma_k, m)}} + \frac{n_k}{N_{f(k)}} = 1 \tag{14}$$

Equation 14 is useful for estimating the remaining fatigue life $n_k/N_{f(k)}$ up to failure, but it is not capable of fatigue damage estimation or structural health monitoring for $D < 1$. Exponent $q(\sigma, m)$, instead of exponent's ratio $q(\sigma_i, m)/q(\sigma_{i+1}, m)$, has been proposed in Pavlou's phenomenological fatigue damage rule[30] and in the one-parameter fatigue model of Rege and Pavlou.[32] In the present work, an exponent function $q(\sigma, m)$ that does not contain any adjusting parameter is proposed for the first time. The new proposed function $q(\sigma, m)$ herein is based on the isodamage curves of the S-N fatigue damage envelope[38] and needs only the S-N curve of the material.

5 | QUANTIFICATION OF FATIGUE DAMAGE ENVELOPE RESULTS AND PROPOSED DAMAGE MODEL

The model is developed through quantification of the results found in a paper by Pavlou.[38] The selected S-N curve for analysis can be seen in Figure 5, which shows the simplified example of how damage mapping is performed. The variables of the axes are specified for the abscissa in Equation 1 and the ordinate in Equation 2.

The results provided by Pavlou included both the points and an equation to fit to the points, resulting in the following plot seen in Figure 6. For the sake of demonstration, an isostress line for $\sigma^* = 0.5$ can also be seen in the figure, in which each intersection between the damage curves and the isostress line determines a cycle ratio for each level of damage for the specific stress amplitude. Such an evaluation was performed from a normalized stress of 0.1 to 0.9 with a step size of 0.1. After the cycle ratios per damage level had been determined for the evaluated normalized stress levels, the damage curves were interpolated with the functional formalism as presented in Equation 7 to determine the stress dependent exponent. The resulting damage curves, where the ratio n/N_e has been normalized to n/N_f, can be seen in Figure 7.

The exponent in Equation 7 was then plotted as a function of normalized stress amplitude, with the objective of finding a relation with the normalized stress through curve interpolation, as can be seen in Figure 8. It was found that the best interpolation function was in the form as presented in Equation 15.

$$q(\sigma^*, m) = \frac{a}{\sigma^*} \tag{15}$$

where the parameter a was found to be $a = 6$, whereas σ^* is the normalized stress, as previously presented in Equation 1. Therefore,

$$q(\sigma, m) = \frac{a(S_u - S_e)}{(\sigma - S_e)} \tag{16}$$

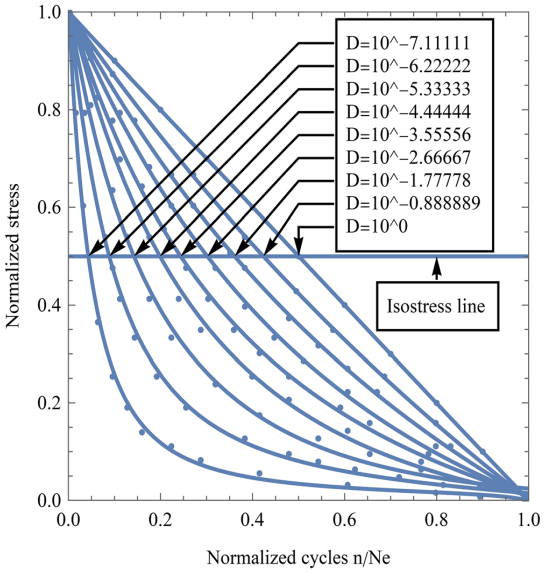

FIGURE 6 Method to develop the isostress damage curves [Colour figure can be viewed at wileyonlinelibrary.com]

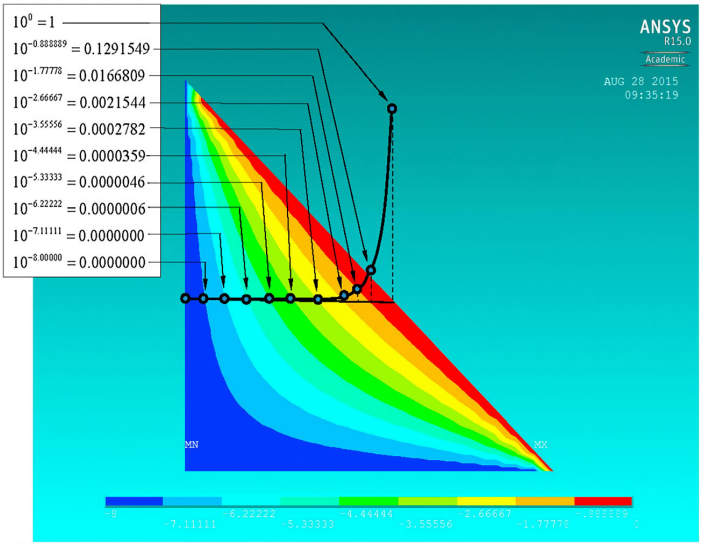

FIGURE 5 Isodamage curves including the damage value for each curve. Reprinted from Pavlou[38] with permission from Elsevier, © 2018 [Colour figure can be viewed at wileyonlinelibrary.com]

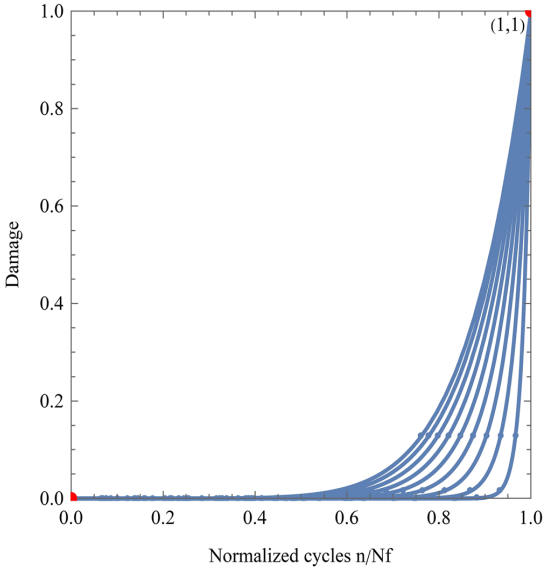

FIGURE 7 Isostress curves with the normalized quantity n/N_f [Colour figure can be viewed at wileyonlinelibrary.com]

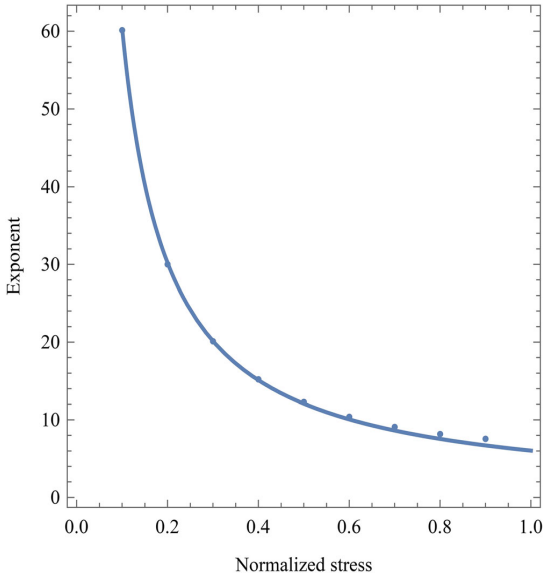

FIGURE 8 Damage exponent as a function of normalized stress amplitude [Colour figure can be viewed at wileyonlinelibrary.com]

inserting Equation 16 into Equation 7, the following nonlinear fatigue damage model can be obtained:

$$D = \left(\frac{n}{N_f}\right)^{\frac{a(S_u - S_e)}{\sigma_1 - S_e}} \tag{17}$$

6 | IMPLEMENTATION AND VERIFICATION OF THE PROPOSED MODEL

The proposed model was verified and compared with other models for the following materials C45,[40] C35,[29] 15HM, A387 GR 22, A336 GR 5,[41] and Al-2024-T42[30] for two-stage loading, and Al 6082-T6[42] for multistage loading. The models adopted for the comparison are the Palmgren-Miner's rule,[1,2] Aeran,[33] Rege and Pavlou,[32] and Mesmacque.[35] Within the results used for verification, both two-stage loading and the results obtained for multistage loading were adopted. Therefore, it is practical to separate this section into two subsections regarding the two categories of results.

Throughout the verification and comparison section, the parameter "experimental remaining life" is the measured number of cycles in the last loading block before failure, whereas the parameter "calculated remaining life" is the estimated number of cycles in the last loading block before failure. For two-stage loading, the "experimental remaining life" is the measured number of cycles n_2 of the second block up to failure (Figure 4A) under the stress amplitude σ_2. The calculated remaining life is determined by Equation 12 for $D_{tot} = 1$, that is, $n_2 = N_{f2}\left(1 - \left(n_1/N_{f1}\right)^{q(\sigma_1,m)/q(\sigma_2,m)}\right)$. Further information regarding the loading histories can be found in the respective references.

6.1 | Verification and comparison of the model for two-stage loading

6.1.1 | C45 steel

C45 steel is a medium carbon steel, known to have a high wear resistance and good quenching and tempering capabilities. C45 steel is commonly applied for such items as bolts, fasteners, shafts, crankshafts, bigger gears, car parts and structures.[43–45] The material was in the normalized condition, and the cyclic loading was rotating bending, fully reversed stress-controlled two-stage loading. The mechanical properties of the material are as follows: yield strength $\sigma_y = 371.7$ MPa, ultimate tensile strength $S_u = 598.2$ MPa and the knee-point stress $S_e = 262.8$ MPa. The cyclic stress amplitudes applied were 331.5 MPa and 284.4 MPa, where both high-low and low-high loading were used, resulting in the high to low loading sequence being 331.5–284.4 MPa, whereas the low to high loading sequence was 284.4–331.5 MPa. The results obtained from the comparison for both the high-low and low-high loading sequences can be seen in Figure 9. The solid line

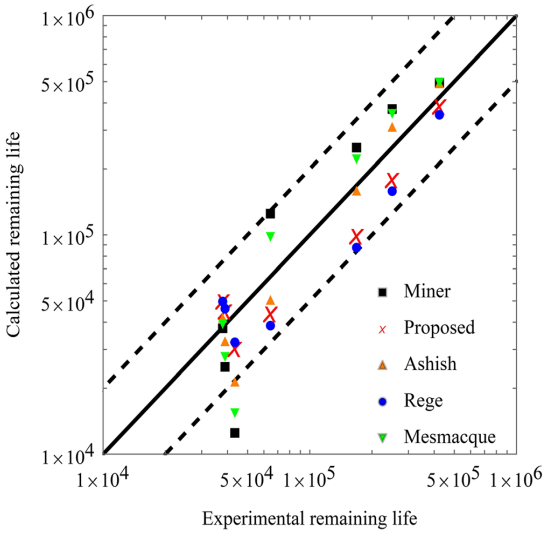

FIGURE 9 Comparison of calculated and experimental remaining life for C45 steel two-block loading [Colour figure can be viewed at wileyonlinelibrary.com]

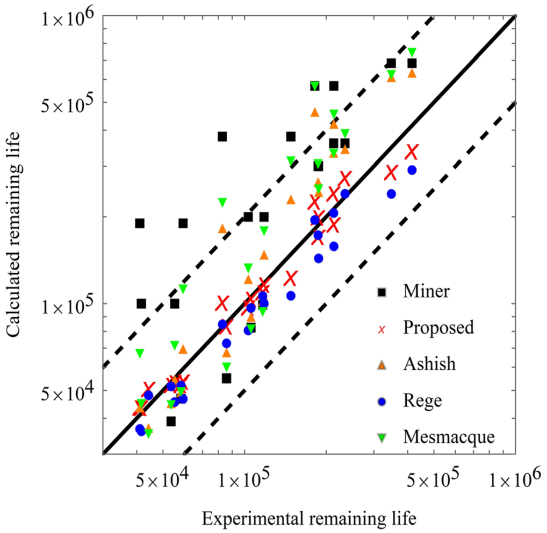

FIGURE 10 Comparison of calculated and experimental remaining life for C35 steel two-block loading [Colour figure can be viewed at wileyonlinelibrary.com]

refers to ideal conformity of the results, whereas the dotted lines represent a scatter band with a coefficient of two.

6.1.2 | C35 steel

C35 steel is also a medium carbon steel, with slightly less carbon (0.35%–0.39%) than the C45 steel, resulting in a reduction in hardness, although its application areas are within the same domain. The mechanical properties of the specimens are yield strength $\sigma_y = 324$ MPa, ultimate tensile strength $S_u = 458$ MPa and knee-point stress $S_e = 255$ MPa. The specimens were ground in the longitudinal direction, and no heat treatment was given. The tests were performed as two-stage block loading, under cantilever rotating beam fatigue, with stress-controlled conditions, at 3000 rpm = 50 Hz. Stress amplitudes of 373, 353, 334, 294, and 275 were used, in various combinations, for two-stage block loading for both high-low and low-high. The results obtained from the comparison for both the high-low and low-high loading can be seen in Figure 10. The solid line refers to ideal conformity of the results, whereas the dotted lines represent a scatter band with a coefficient of two.

6.1.3 | 15HM, A387 GR 22, and A336 GR 5

These different steels are commonly used in the electrical power and petroleum chemistry industries under high temperature and pressure. For such items as steam heater coils, plates for boiler drums and pressurized vessels, forgings and bars for boiler parts, pressurized vessels and turbines and pipelines of superheated steam, 15HM (13CrMo4-5) is commonly applied.[46–48] Meanwhile, A387 GR 22 (10CrMo9-10) is commonly used in seamless pipes for steam conditions reaching high temperatures, such as pressurized parts of boilers powered by fossil fuels and heat recovery system generators.[49,50] A336 GR 5 can also be found to be applicable in the same domain.[51] The specimens were all fatigued under stress controlled fully reversed ($R = -1$) tension compression loading, at 20 Hz in room temperature (21°C). Each type of material was tested under the two-stage block loading sequences of high-low and low-high. The stress amplitudes 375 MPa and 400Mpa were adopted for 15HM steel, 475 MPa and 525 MPa for A387 GR 22, and 375 and 425 MPa for A336 GR5. The results obtained from the comparison for both the high-low and low-high loading can be seen in Figure 11. The solid line refers to ideal conformity of the results, whereas the dotted lines represent a scatter band with a coefficient of two.

6.1.4 | Al-2024-T42

Al-2024-T42 is an aluminum-copper-magnesium-manganese, which is solution heat treated and naturally aged to a substantially stable condition. Al-2024 is

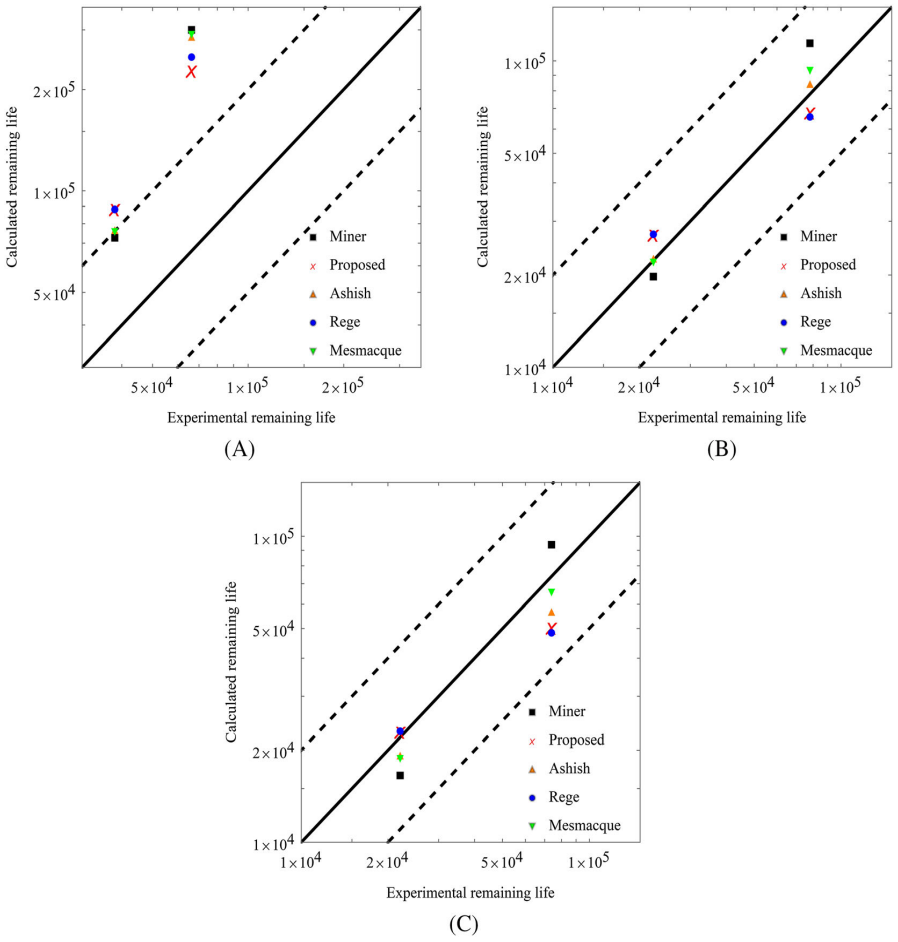

FIGURE 11 Comparison of calculated and experimental remaining life for (A) 15HM, (B) A387 GR22, and (C) A336GR5 subjected to two-block loading [Colour figure can be viewed at wileyonlinelibrary.com]

commonly used in such items as airframes, wing tension members, shear webs and ribs, due to the requirement for high strength to weight ratio in conjunction with good fatigue performance.[52–54] The Al-2024-T42 was fatigued under fully reversed ($R = -1$) uniaxial tension compression, with a frequency of 25 Hz at stress amplitudes of 150 and 200 MPa, from high to low and low to high, resulting in 150–200 and 200–150 MPa loading. However, it is well known that aluminum alloys do not exhibit a clear knee-point stress.[55,56] Therefore, it was decided to adopt a knee point of 0 MPa. The results obtained from the comparison for both the high-low and low-high loading can be seen in Figure 12. The solid line refers to ideal conformity of the results, whereas the dotted lines represent a scatter band with a coefficient of two.

6.2 | Verification and comparison of the model for multistage loading

6.2.1 | Al-6082-T6

Al-6082-T6 is a high-strength aluminum-magnesium-silicon alloy, which is solution heat treated and then artificially aged at a temperature of about 170–200°C.[54,57] The 6082 alloy has similar characteristics to those of the commonly used 6061 alloy. In the T6 condition, the alloy will also have slightly higher mechanical properties and will provide good machinability. Al-6082 is commonly adopted for such items as rods, bars, machining stock, structural profiles and seamless tubing.[58,59] The specimens were acquired as plates of 8 mm thickness, which were machined to dog bone specimens. Thereafter, the

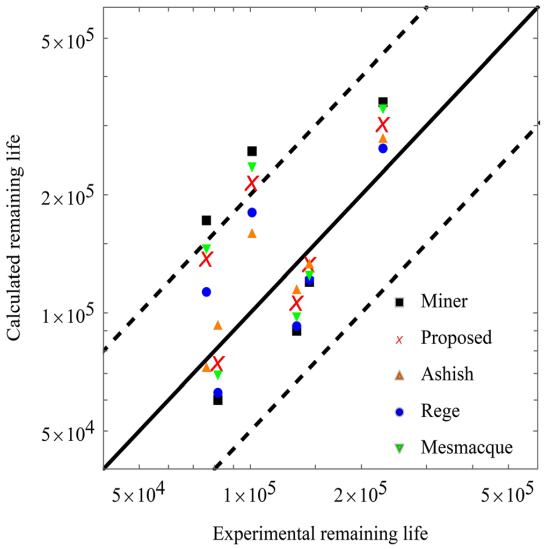

FIGURE 12 Comparison of calculated and experimental remaining life for Al-2024-T42 subjected to two-block loading [Colour figure can be viewed at wileyonlinelibrary.com]

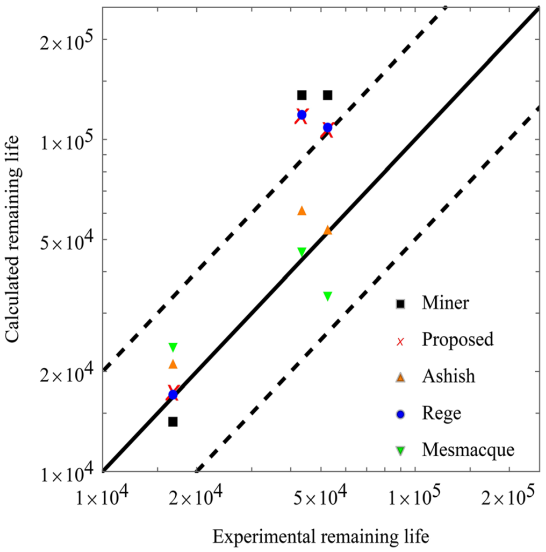

FIGURE 13 Comparison of calculated and experimental remaining life for Al-6082-T6 subjected to multilevel block loading [Colour figure can be viewed at wileyonlinelibrary.com]

specimens were subjected to uniaxial constant amplitude fatigue. The mechanical properties of the material are as follows: yield stress $\sigma_y = 347$ MPa, ultimate tensile stress $S_u = 370$ MPa, whereas the fatigue knee point S_e again is defined as 0, due to the common fatigue curve seen in aluminum alloys. The maximum stresses which were used in the various blocks are 240, 260, 280, and 305 MPa in the low-high and high-low staircase loading, with the addition of random loading in the sequence 280, 305, 260, and 240 MPa. The results obtained from the comparison for the three aforementioned scenarios can be seen in Figure 13. The solid line refers to ideal conformity of the results, whereas the dotted lines represent a scatter band with a coefficient of two.

7 | DISCUSSION

The proposed model is inherently simple to follow for practicing engineers, and both an estimation of the intermediate damage level and a prediction of remaining fatigue capacity can be performed. To carry out an analysis using the proposed model, the only requirement is the commonly used S-N or Wöhler curves, readily available in standards, which can, alternatively, be developed for the specific material or detail category if desired. From the results, it can be seen that the model generally obtains good to somewhat conservative results as regards the C35 and the C45 materials, which are ferritic pearlitic low-carbon steels. Furthermore, for the materials A387 Grade 22 and A336 GR 5, it was found that the model would provide good estimations, well within the scatter bands plotted with a coefficient of two. However, none of the models provided very good results for the 15 HM stainless steel. The results which deviate the most are those for the high to low loading, and the researcher who published the results stated that the specimen experienced early activation of Lüders bands,[41] resulting in a concentration of crystallographic defects, which accelerates the fatigue damage process. However, the results for the low to high loading are also non-conservative for the proposed and all compared models. For the material Al-2024-T42, with the assumption that the fatigue knee-point stress is set as zero, the model also has reasonable accuracy. However, for Al-6082-T6 with the same assumption, under multilevel block loading, the model has a result which is very accurate for a load increase test, whereas the load reduction (at the dashed line) and random loading (outside the dashed line) resulted in fairly non-conservative estimations. It should be highlighted that the proposed damage function herein is simply validated for cyclic loading with stepwise variable amplitude in order to check the effectiveness of the model to consider the material memory effect and to address the effect of the loading sequence in fatigue life prediction. The proposed function can also be implemented to random (irregular) service loading with the aid of a counting method (e.g., Rainflow method). However, even with the aid of a counting method,

direct implementation of the proposed model to irregular loading spectra yields numerical error accumulation in long loading histories. To this end, a multilinear damage summation technique for utilizing nonlinear models in spectrum loading and a new counting method has recently been proposed by Pavlou[9] and can be adopted by the proposed damage function.

In fact, it can also be considered to be a framework for how to develop fatigue damage accumulation formulas through the theory of the S-N fatigue damage envelope. This is from the perspective that, herein, a general, simplistic form of an S-N curve and a triangular envelope, as presented in Figure 5, was adopted, with a generally accepted formulation for damage, as presented in Equation 7, to develop a damage function. However, material specific, detail category specific or environmentally specific S-N curves might also be investigated, by applying the method explained herein in conjunction with the theory of the S-N fatigue damage envelope proposed by Pavlou.[38]

Furthermore, a short discussion regarding the theory of the S-N fatigue damage envelope is appropriate here. During the analysis of the isodamage curves proposed by Pavlou, it was found that, if the abscissa were transformed to the parameter n/N_f in contrast to n/N_e, but the ordinate was maintained as the normalized stress in accordance with Equation 1, the isodamage curves would be as presented in Figure 14. It can be seen that, within the domain of high amplitude low cycle fatigue, the Palmgren–Miner rule might be somewhat accurate,

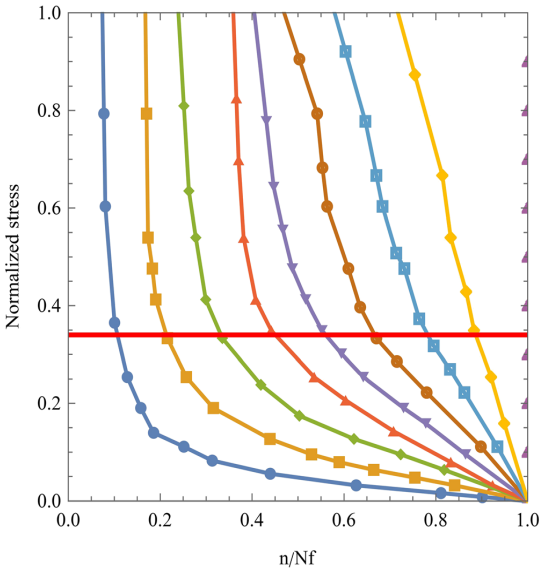

FIGURE 14 normalized isodamage curves [Colour figure can be viewed at wileyonlinelibrary.com]

whereas it will vastly deviate within the domain of low amplitude high cycle fatigue. This is from the perspective that, within the domain of high cycle fatigue, the majority of the fatigue life is spent in the initiation stage, whereas low cycle fatigue is dominated by crack propagation.[60,61] This means that, for the high-low fatigue loading transition, a crack might be initiated in the high amplitude loading, which could have taken nearly the entire fatigue capacity for the low amplitude fatigue loading. However, for the low-high transition, the low amplitude fatigue loading region might all have been spent on crack initiation, which would have occurred within the few first cycles within the high amplitude fatigue loading, thus resulting in the commonly accepted phenomenon of the linear damage rule, namely that the sum of the cycle ratios will be greater than unity for low-high loading but less than unity for high-low loading.[14] Furthermore, regarding the higher normalized stress amplitudes, Dowling specified that "the sequence effects do not occur if all of the levels cause significant plastic straining, which is consistent with the observation that the initiation period is short in the low cycle region."[62] In this regard, C35, for instance, can be considered, with material parameters of yield strength $\sigma_y = 324\,\text{MPa}$, ultimate tensile strength $S_u = 458\,\text{MPa}$ and knee-point stress $S_e = 255\,\text{MPa}$. The consequence is a cyclic stress amplitude equivalent to the yield strength of the material, resulting in a normalized stress of $\sigma^* = 0.34$. It can be seen from the figure that, if all stress amplitudes are higher than a normalized stress of 0.34, the relation between various stress amplitudes will, for the most part, behave linearly, where the deviation from the linear behavior will increase with n/N_f. Thus, it can be seen that the theory proposed by Pavlou clearly demonstrates the variable amplitude relation which has been documented by researchers.

For the derivation of the functional form of q in Equation 16, and the derived value of a in Equation 15, the usual engineering S-N curve which is demonstrated by a straight line passing the ultimate stress *Su* and the knee-point *Se* is used for the sake of simplicity. The corresponding triangular damage envelope in Figure 5[38] has been derived in terms of the normalized parameters of Equations 1 and 2. Therefore, the derivation of the damage map within the envelope of Figure 5 and the corresponding isodamage lines are universal. Since the derived function q in Equation 16 and the parameter a in Equation 15 are based on the isodamage lines of the universal triangular damage envelope, they include the material properties *Su*, *Se*, and *Ne* of any material and are universal too. Of course, Finite Element analysis can be performed for the specific S-N curve of each material and the function q considering the detailed nature of the S-N curve can be carried out. However, it seems that

Equation 16 is simple for engineering applications and provides sufficient accuracy in fatigue life prediction.

Almost all the known nonlinear rules are based on concepts of the rules of Manson-Halford,[27] Subramanyan,[29] Hashin-Rotem,[31] and so on. The majority of the existing damage accumulation rules provide only ratios of damage exponents $q(\sigma_i,m)/q(\sigma_{i+1},m)$, and they cannot propose the function $q(\sigma,m)$. Therefore, they can only predict the duration of the last loading block before failure $D=1$, but they cannot estimate the real-time accumulated damage at any stage ($D<1$) during loading. On the other hand, they are not valid for both HCF and LCF because some of the models (Figure 1) assume isodamage lines converging at the knee point of the S-N curve and they are valid only for large number of loading cycles (HCF), and other models assume isodamage lines converging at the *Su* point and they are valid for high stress amplitude (LCF). The proposed fatigue model has the following advantages versus the existing models: (a) It is based on nonlinear isodamage lines that take into account the damage map of the whole S-N damage envelope (Figure 2) and it is valid for all the fatigue stages, both HCF and LCF, and (b) it proposes a nonlinear exponent function $q(\sigma,m)$ instead of damage exponent ratios $q(\sigma_i,m)/q(\sigma_{i+1},m)$ and has the capability for estimation of the fatigue damage accumulation at any stage of the loading history.

8 | CONCLUSIONS

a. A new nonlinear fatigue damage accumulation model is proposed in light of the theory of the S-N fatigue damage envelope, proposed by Pavlou. Consequently, the expression is dependent on the readily available S-N curves only.
b. The resulting damage function was verified in experimental results and compared with other models for several materials, indicating good fatigue damage estimation.
c. A general framework for how to adopt the theory of the S-N curve to develop damage functions for general and case-specific S-N curves has been presented.
d. The theory of the S-N fatigue damage envelope has been discussed and compared in regard to commonly accepted relations within the fatigue damaging process.

ACKNOWLEDGEMENT

The authors are grateful for the financial support provided by the Norwegian Ministry of Education during this project. Furthermore, the group wishes to thank the publisher for allowing the reuse of figures.

AUTHOR CONTRIBUTIONS

Fredrik Bjørheim: Conceptualization, methodology, formal analysis, visualization, and writing-original draft. **Dimitrios G. Pavlou:** Conceptualization, methodology, formal analysis, writing-review and editing, and supervision. **Sudath C. Siriwardane:** Methodology, formal analysis, writing-review and editing, and supervision.

DATA AVAILABILITY STATEMENT

The data that support the findings of this study are available on request from the corresponding author. The data are not publicly available due to privacy or ethical restrictions.

REFERENCES

1. Die PA, von Kugellagern L. *Zeitschrift Des Vereines Deutscher Ingenieure*. 1924;58(14):339-341.
2. Miner MA. Cumulative damage in fatigue. *J Appl Mech*. 1945; 12(3):A159-A164.
3. Jang J, Khonsari MM. On the prediction of fatigue life subjected to variable loading sequence. *Fatigue Fract Eng Mater Struct*. 2021;44(11):2962-2974.
4. Peng Z, Huang H-Z, Zhu S-P, Gao H, Lv Z. A fatigue driving energy approach to high-cycle fatigue life estimation under variable amplitude loading. *Fatigue Fract Eng Mater Struct*. 2016; 39(2):180-193.
5. Li ZX, Ko JM, Chan THT. Modelling of load interaction and overload effect on fatigue damage of steel bridges. *Fatigue Fract Eng Mater Struct*. 2001;24(6):379-390.
6. Eurocode 3. Design of steel structures-Part 1–9: Fatigue, NS-EN 1993-1-9:2005+NA:2010
7. DNVGL, RP-C203: fatigue design of offshore steel structures, 2014
8. Carpinteri A, Vantadori S, Łagoda T, Karolczuk A, Kurek M, Ronchei C. Fatigue assessment of metallic components under uniaxial and multiaxial variable amplitude loading. *Fatigue Fract Eng Mater Struct*. 2018;41(6):1306-1317.
9. Pavlou D. A deterministic algorithm for nonlinear, fatigue-based structural health monitoring. *Comput Aided Civ Inf Eng*. 2021;1-23.
10. Singh A. The nature of initiation and propagation S-N curves at and below the fatigue limit. *Fatigue Fract Eng Mater Struct*. 2002;25(1):79-89.
11. He L, Akebono H, Sugeta A, Hayashi Y. Cumulative fatigue damage of stress below the fatigue limit in weldment steel under block loading. *Fatigue Fract Eng Mater Struct*. 2020; 43(7):1419-1432.
12. Lotsberg I. *Fatigue design of marine structures*. New York NY: Cambridge University Press; 2016.
13. Ciavarella M, D'antuono P, Papangelo A. On the connection between Palmgren-Miner rule and crack propagation laws. *Fatigue Fract Eng Mater Struct*. 2018;41(7):1469-1475.
14. Fatemi A, Yang L. Cumulative fatigue damage and life prediction theories: a survey of the state of the art for homogeneous materials. *Int J Fatigue*. 1998;20(1):9-34.
15. Hectors K, De Waele W. Cumulative damage and life prediction models for high-cycle fatigue of metals: a review. *Metals*. 2021;11(2):204-235.

16. Santecchia E, Hamouda AMS, Musharavati F, et al. A review on fatigue life prediction methods for metals. *Adv Mater Sci Eng*. 2016;2016:9573524.
17. Bjørheim F, Siriwardane SC, Pavlou D. A review of fatigue damage detection and measurement techniques. *Int J Fatigue*. 2022;154:106556.
18. Xia F-L, Zhu S-P, Liao D, Dantas R, Correia JAFO, De Jesus AMP. Isodamage curve-based fatigue damage accumulation model considering the exhaustion of static toughness. *Eng Fail Anal*. 2020;115:104575.
19. Zhu S-P, Hao Y-Z, de Oliveira Correia JAF, Lesiuk G, de Jesus AMP. Nonlinear fatigue damage accumulation and life prediction of metals: a comparative study. *Fatigue Fract Eng Mater Struct*. 2019;42(6):1271-1282.
20. Meneghetti G, Ricotta M, Atzori B. A synthesis of the push-pull fatigue behaviour of plain and notched stainless steel specimens by using the specific heat loss. *Fatigue Fract Eng Mater Struct*. 2013;36(12):1306-1322.
21. Zhu SP, Lei Q, Wang QY. Mean stress and ratcheting corrections in fatigue life prediction of metals. *Fatigue Fract Eng Mater Struct*. 2017;40(9):1343-1354.
22. Sun B, Yang L, Guo Y. A high-cycle fatigue accumulation model based on electrical resistance for structural steels. *Fatigue Fract Eng Mater Struct*. 2007;30(11):1052-1062.
23. Gao K, Liu G. Nonlinear time-varying fatigue reliability analysis based on the improved toughness exhaustion model. *Fatigue Fract Eng Mater Struct*. 2021;44(12):3482-3498.
24. Teng Z, Wu H, Boller C, Starke P. Thermodynamic entropy as a marker of high-cycle fatigue damage accumulation: example for normalized SAE 1045 steel. *Fatigue Fract Eng Mater Struct*. 2020;43:2854-2866.
25. Manson SS, Nachtigall AJ, Ensign CR, Freche JC. Further investigation of a relation for cumulative fatigue damage in bending. *J Eng Ind*. 1965;87(1):25-35.
26. Manson SS. Interfaces between fatigue, creep, and fracture. *Int J Fract Mech*. 1966;2(1):327-363.
27. Manson SS, Halford GR. Practical implementation of the double linear damage rule and damage curve approach for treating cumulative fatigue damage. *Int J Fract*. 1981;17(2):169-192.
28. Grover HJ. An observation concerning the cycle ratio in cumulative damage. In: Subcommittee V, ed. *West Conshohocken*. PA: ASTM International; 1960:120-124.
29. Subramanyan S. A Cumulative Damage Rule Based on the Knee Point of the S-N Curve. *J Eng Mater Technol*. 1976;98(4):316-321. doi:10.1115/1.3443383
30. Pavlou DG. A phenomenological fatigue damage accumulation rule based on hardness increasing, for the 2024-T42 aluminum. *Eng Struct*. 2002;24(11):1363-1368.
31. Hashin Z, Rotem A. A cumulative damage theory of fatigue failure. *Mater Sci Eng A*. 1978;34(2):147-160.
32. Rege K, Pavlou DG. A one-parameter nonlinear fatigue damage accumulation model. *Int J Fatigue*. 2017;98:234-246.
33. Aeran A, Siriwardane SC, Mikkelsen O, Langen I. A new nonlinear fatigue damage model based only on S-N curve parameters. *Int J Fatigue*. 2017;103:327-341.
34. Aeran A, Siriwardane SC, Mikkelsen O, Langen I. An accurate fatigue damage model for welded joints subjected to variable amplitude loading. *IOP Conf Ser: Mater Sci Eng*. 2017;276:012038.
35. Mesmacque G, Garcia S, Amrouche A, Rubio-Gonzalez C. Sequential law in multiaxial fatigue, a new damage indicator. *Int J Fatigue*. 2005;27(4):461-467.
36. Kohout J, Věchet S. A new function for fatigue curves characterization and its multiple merits. *Int J Fatigue*. 2001;23(2):175-183.
37. Siriwardane S, Ohga M, Dissanayake R, Taniwaki K. Application of new damage indicator-based sequential law for remaining fatigue life estimation of railway bridges. *J Constr Steel Res*. 2008;64(2):228-237.
38. Pavlou DG. The theory of the S-N fatigue damage envelope: generalization of linear, double-linear, and non-linear fatigue damage models. *Int J Fatigue*. 2018;110:204-214.
39. Pavlou DG. Loading sequence effects on fatigue damage accumulation of offshore structures: a deterministic approach. In: *Paper presented at: Proceedings of the International Conference on Offshore Mechanics and Arctic Engineering - OMAE2017*.
40. Shang D-G, Yao W-X. A nonlinear damage cumulative model for uniaxial fatigue. *Int J Fatigue*. 1999;21(2):187-194.
41. Socha G. Prediction of the fatigue life on the basis of damage progress rate curves. *Int J Fatigue*. 2004;26(4):339-347.
42. Aid A, Amrouche A, Bouiadjra BB, Benguediab M, Mesmacque G. Fatigue life prediction under variable loading based on a new damage model. *Mater Des*. 2011;32(1):183-191.
43. Satish GJ, Madhusudhana HK, Nishant BH, Kottursheттar BB. Optimising cutting parameters in boring operation for C45 steel. *IOP Conf Ser: Mater Sci Eng*. 2020;872:012080.
44. Faur AS, Popa MS, Sattel S. Aproaches upon the influence of a new tap drill geometry on C45 steel processing. *Acta Techn Napocens Ser: Appl Math Mech Eng*, [S.l.], v. 59, n. 4, dec. 2016: 393-398. ISSN 2393–2988. Available at: https://atna-mam.utcluj.ro/index.php/Acta/article/view/809
45. Selvam MD, Senthil P. Investigation on the effect of turning operation on surface roughness of hardened C45 carbon steel. *Austr J Mech Eng*. 2016;14(2):131-137.
46. Pietryka I, Golański G, Jasak J, Słania J, Urbańczyk P, Wieczorek P. Degradation of microstructure and mechanical properties of 15HM steel after 420,000 hours of service. *Adv Mater Sci Eng*. 2014;14(4):5-11.
47. Jackiewicz D, Kachniarz M, Rożniatowski K, et al. Temperature resistance of magnetoelastic characteristics of 13CrMo4-5 constructional steel. *Acta Phys Polon A*. 2015;127:614-616.
48. Gwoździk M. Characterization of oxide layers formed on 13CrMo4-5 steel operated for a long time at an elevated temperature. *Arch Metall Mater*. 2015;60:1783-1788.
49. Westin EM, Schnitzer R, Ciccomascolo F, Maderthoner A, Grönlund K, Runnsjö G. Austenitic stainless steel bismuth-free flux-cored wires for high-temperature applications. *Weld World*. 2016;60(6):1147-1158.
50. Hattingh DG, van Zyl C. Temperature distribution for a friction taper stud weld in thick wall 10CrMo910 steel. *R&D Journal*. 2012;28:37-45.
51. Dietrich L, Socha G. Accumulation of damage in A336 GR5 structural steel subject to complex stress loading. *Strain*. 2012;48(4):279-285.
52. Jefferson TB, Woods G, James FLAWF. *Metals and How to Weld Them*. 2nded. James F. Lincoln Arc Welding Foundation: Cleveland, Ohio; 1962.

53. Alcoa. Alloy 2024 sheet and plate—excellent fatigue properties-consistent performance. Accessed May 26, 2021. https://web.archive.org/web/20060827072154/http://www.alcoa.com/mill_products/catalog/pdf/alloy2024techsheet.pdf
54. Hatch JE. *Aluminum: Properties and Physical Metallurgy*. 1sted. Materials Park: Materials Park: ASM International; 1984.
55. Kaleva O, Orelma H, Petukhov D. Parameter estimation of a high-cycle fatigue model combining the Ottosen-Stenström-Ristinmaa approach and Lemaitre-Chaboche damage rule. *Int J Fatigue*. 2021;147:106153.
56. Brighenti R, Carpinteri A. A notch multiaxial-fatigue approach based on damage mechanics. *Int J Fatigue*. 2012;39:122-133.
57. Ericsson M, Sandström R. Influence of welding speed on the fatigue of friction stir welds, and comparison with MIG and TIG. *Int J Fatigue*. 2003;25(12):1379-1387.
58. Moreira PMGP, de Jesus AMP, Ribeiro AS, de Castro PMST. Fatigue crack growth in friction stir welds of 6082-T6 and 6061-T6 aluminium alloys: a comparison. *Theor Appl Fract Mech*. 2008;50(2):81-91.
59. Hydro. Alloy 6082. https://www.hydro.com/Document/Index?name=Alloy%206082.pdf&id=560720. Accessed 27.05, 2021.
60. Murakami Y, Miller KJ. What is fatigue damage? a view point from the observation of low cycle fatigue process. *Int J Fatigue*. 2005;27(8):991-1005.
61. Chowdhury P, Sehitoglu H. Mechanisms of fatigue crack growth—a critical digest of theoretical developments. *Fatigue Fract Eng Mater Struct*. 2016;39(6):652-674.
62. Dowling NE. Fatigue failure predictions for complicated stress-strain histories. T. & A.M. Report no. 337. Department of theoretical and applied mechanics university of Illinois; 1971.

How to cite this article: Bjørheim F, Pavlou DG, Siriwardane SC. Nonlinear fatigue life prediction model based on the theory of the S-N fatigue damage envelope. *Fatigue Fract Eng Mater Struct*. 2022;1-14. doi:10.1111/ffe.13680

Paper V

S-N Based Fatigue Damage Modelling of Offshore Structures: Recent damage accumulation models and the way forward

Conference Paper
8th European Congress on Computational Methods in Applied Sciences and Engineering
ECCOMAS 2022
Oslo, Norway

Paper VI

Tension Testing of Additively Manufactured Specimens of 17-4 PH Processed by Bound Metal Deposition

Conference Paper
3rd Conference of Computational Methods in Offshore Technology,
COTech 2021
Stavanger, Norway

Tension testing of additively manufactured specimens of 17-4 PH processed by Bound Metal Deposition

To cite this article: F Bjørheim and I M La Torraca Lopez 2021 *IOP Conf. Ser.: Mater. Sci. Eng.* **1201** 012037

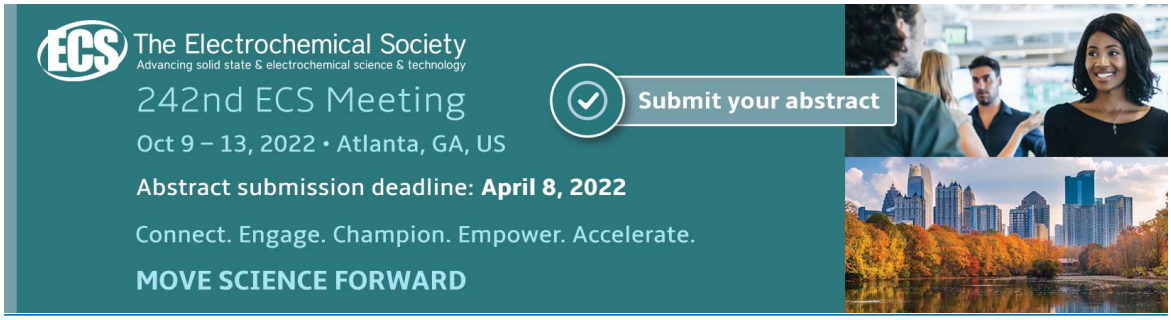

Tension testing of additively manufactured specimens of 17-4 PH processed by Bound Metal Deposition

F Bjørheim* and I M La Torraca Lopez

Department of Mechanical and Structural Engineering and Materials Science, University of Stavanger, Norway

*Corresponding author: fredrik.bjorheim@uis.no

Abstract. In contrast to the traditional ways of subtractive manufacturing, additive manufacturing (AM), also known as 3D printing, adapts computer-aided design to iteratively build the component or part layer by layer. The technology has recently gained a high momentum, both within academia, but also within the industrial sector. However, it is common that parts produced by AM will have more defects than parts produced by traditional methods. The objective of this paper is to investigate a new method of additive manufacturing, namely the bound metal deposition method (BMD). This method seemed promising from the perspective that the metal is not iteratively being melted, similar to such as welding. In fact, the part is first printed, then washed, for then to be sintered. Consequently, avoiding the complex thermal histories/cycles. It was found that the material will exhibit anisotropic behaviour, and have a mesh of crack like defects, related to the printing orientation.

1. Introduction

Additive manufacturing (AM), often called 3-D printing can be defined as the process that fabricates complex or customized solid free form parts using computer aided design (CAD). The process consists of iteratively adding layer by layer of materials, in contrast to conventional methods of subtractive manufacturing (e.g., cutting, drilling, grinding and machining) [1].

AM is changing both the way products are designed and manufactured, and has been used in many industries, such as automotive, aerospace, energy, oil and gas, health care, industrial and remanufacture industries, amongst others [2].

Some of the advantages worth mentioning regarding AM technology might be such as design freedom, the possibility of fabricating complicated geometries with complex internal structures, which are difficult if not impossible to build using traditional manufacturing techniques [3]. Furthermore, mass customization, as in producing a number of customized parts can be as cost-effective as mass production of identical parts. This from the perspective of the design freedom, that the manufacturing process is not dependent on such as molds and tooling [4]. Fast prototyping, the part or component can be produced directly from the computer aided design (CAD) software, with the addition of developing the printing pattern for the component. Consequently, reducing the need of many of the conventional processing steps and expensive tooling [5]. Another advantage worth mentioning is higher material efficiency, or waste minimization. This from the perspective that material is iteratively added in contrast to subtraction as per traditional methods [6]. In addition, parts can be manufactured on site by the method of AM, reducing the storage space of spare parts needed on site [5]

The advantages of the additively manufacturing process has resulted in a high interest from the industry. Examples of this might be such as Equinor [7] where the goal is to be able to reduce downtime

due to failure of production critical parts. They propose this can be performed by having a digital inventory and drones. In fact, a part could then be printed locally by a manufacturer, for then to be sent to the offshore facility with drones. Consequently, resulting in a "just-in-time" production of spare parts. Another example/motivation for additive manufacturing might be such as the reduction of weight in the aerospace industry [8]. The energy industry is also interested in the additive manufacturing of parts, due to such as fast prototyping, as the development of gas turbines involves trial and error. Thus, fast prototyping accelerates gas turbine development. Additionally, both the aerospace and energy sectors are commonly using complex parts, such as sophisticated air-cooling channels, which can easily be produced in the additive manufacturing process [9].

There is a large selection of metal AM technologies, which often include the melting of powder or wire feedstock using various energy or heat sources [10, 11]. The most accepted or alternatively most used methods for AM might be categorized as powder bed fusion (PBF) and direct energy deposition (DED). It is commonly accepted that the PBF has a high precision, whereas DED has a better production speed. Furthermore, it should be mentioned that the manufacturing/production parameters will significantly affect the resulting part [5]. This from the perspective that both methods iteratively add layer by layer by iteratively melting new material on the previously placed layer.

An issue with the AM technology, is the challenge of controlling the properties of the final product [12]. The AM process is commonly having issues such as pores, voids, surface roughness, loss of alloying elements, cracking, delamination, residual stresses, deformation etc. This due to the complex thermal history, resulting from laser speed, laser energy, scanning path strategy and powder/layer thickness etc. [5, 13]. However, bound metal composition (BMD) is a relatively new technology, promising a significant reduction in cost, while producing quality parts [14]. Furthermore, the technology does not iteratively melt or sinter layer by layer, thus, removing the perspective of the complex thermal histories/cycles.

Herein, the method of bound metal deposition is adapted to produce monotonic tensile test specimens. Specimens were designed and tested in accordance with ASTM E8/E8M for tension testing. Various printing orientations were used, to investigate the directional dependence on the mechanical properties. Furthermore, samples were prepared for inspection with an optical light microscope. Anisotropic behavior was found from the tension testing, for then to be correlated with defects found during inspection of the polished samples with an optical light microscope. Furthermore, the findings are discussed in light of mechanical properties and fatigue, for then to propose further research.

2. Bound metal deposition

The method adapted for printing is the method named Bound Metal Deposition by Markforged and Desktop Metal (DM). The manufacturing process can be described to have four steps, namely; (a) printing, (b) debinding, (c) sintering and (d) post processing. (a) firstly, powder-filled wire of polymer-wax binder is heated up and extruded layer by layer to develop the generated and sliced geometry. (b) Thereafter, the printed specimen is put in a washer to go through a debinding process to partly remove the binder. (c) After debinding has been performed, the specimen will be sintered to both remove the remaining binder, and to bind the metal particles together, resulting in a solid metal part. The sintering process is performed through placing the specimen in a furnace, with a slow uniform heat development and subsequent cooling in an inert gas. (d) The last step is post processing, this might be such as machining or polishing to achieve a better surface finish in regard to fatigue capacity, or alternatively hot isostatic pressing (HIP) to reduce pore structure, or alter the microstructure [14, 15].

It should be mentioned that the methodology of BMD is a fairly new technology. However, some advantages to the printing technique might be such as:

1. The BMD technology is expected to be roughly 60% less expensive than similarly sized PBF system [16].
2. There are fewer safety concerns with the BMD technology, with no need for a dedicated operator or powder management system [14]

3. As the sintering process is performed after the geometry of the part has finished printing, it is believed that the final product will have a better microstructure with low to none residual stresses in comparison to similar methods. Consequently, achieving favourable mechanical properties.

2.1 Printing scheme/strategy

The printing strategy of the machine is commonly to build a wall surrounding the geometry, which can be defined by the user between 2-8 wall layers. The wall layers are simply lines surrounding the geometry, developing the perimeter of the specimen. However, it should be noted that successive layers will be placed directly above the previous, in the same direction, unless the cross-sectional area is changing with height. Furthermore, the internal part of the specimen is the remaining cross-sectional are after the wall has been placed. The internal area is filled with layers, where the layers alternate between ±45º for each layer.

3. Experimental work

The material which was used during the experimental work was 17-4 PH stainless steel, which is a heat treatable precipitation hardening martensitic stainless steel. Commonly used in situations where corrosion resistance is required, such as aerospace, petroleum and chemical industries [6, 16].

As previously mentioned, the method for printing is by the BMD method, where the specimens were produced at the University of Stavanger by the use of a Markforged Metal X BMD printer. The printed specimens were tension tested to determine the mechanical properties as follows: Ultimate strength (UTS), yield tensile strength (YTS), Young's modulus (E) and elongation at break (%). Thereafter, the obtained results were compared to the documentation provided by Markforged for AM 17-4 PH stainless steel in the "as-sintered" condition. Furthermore, the printed specimens were inspected by the use of an optical light microscope, with the objective of determining the cause of the observed variation in mechanical properties.

3.1 Sample manufacturing

Specimens were designed in accordance with the ASTM E8/E8M subsize specimen, and can be seen in Figure 1 [17]. Thereafter, they were printed using a Markforged Metal X printer, which has a maximum build volume of 300x220x180mm, by the use of 17-4 PH stainless steel wire, supplied by Markforged. All the specimens were printed with 8 wall/perimeter layers, whereas the remaining internal section is printed with the alternating ±45º pattern. Subsequently, the specimens produced were washed, for then to be sintered to achieve the "as-sintered" condition. Herein, the step of post processing is skipped, other than removing the support structure.

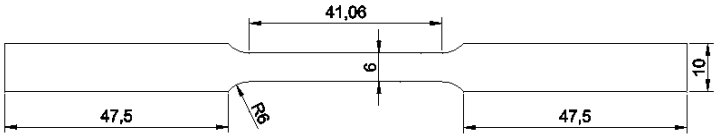

Figure 1. Specimen in accordance with ASTM E8/E8M, in mm.

A total of 9 specimens were manufactured, where three specimens were produced for three different printing directions. The first group consists of horizontally oriented specimens, which were called XY-flat. These specimens were built after 68 successive layers. The second group was rotated 90 degrees in relation to the x axis, consequently result in the need for a support structure while printing. These specimens were called XY-sided, and were built after 100 layers. The third group contained vertically printed specimens, which were called ZX. These specimens were built after 1175 layers. The build direction of the specimens XY-flat, XY-sided and ZX can be seen in Figure 2 a), b) and c) respectively.

For the optical light microscope, two samples were produced, one bar which was built in the vertical direction (V) with the dimensions 10x10x50 mm, and one built in the horizontal direction (H) with the

dimensions 50x10x10 mm as shown in Figure 2 d). This to be able to inspect for defects in regard to the printing orientation.

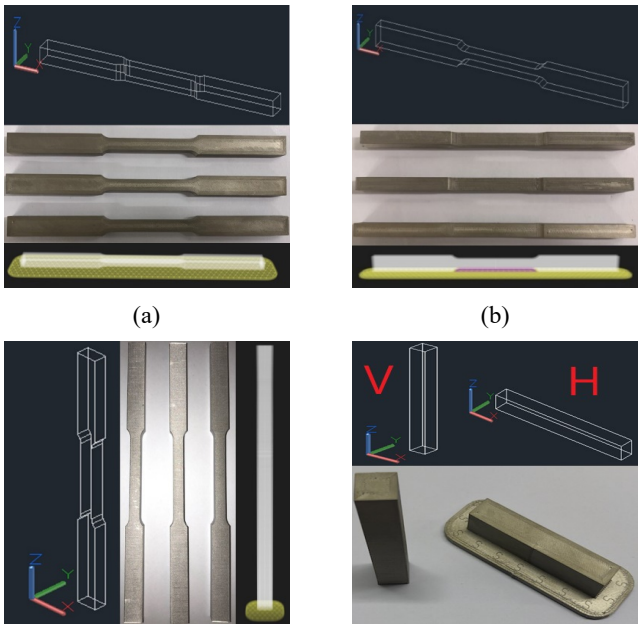

(a) (b)

(c) (d)

Figure 2. Printed specimens, (a) XY-flat, (b) XY-sided, (c) ZX, (d) vertical and horizontal print

3.2 Tension testing results

All the tension specimens were monotonically loaded until failure, in accordance with the standard ASTM E8/E8M. The resulting stress-strain curves for the specimens can be seen in Figure 4 and the fractured specimens can be observed in Figure 3. Furthermore, the resulting mechanical properties were tabulated, as can be seen in Table 1.

From the stress-strain curve presented in Figure 4, it can clearly be seen that most of the specimens (XY-sided and ZX) fail before any significant plasticity is achieved. Consequently, resulting in effectively a brittle failure, due to the choice of printing direction. In Figure 3, the various fractured specimens are presented. It can be seen that the XY-flat and ZX specimens commonly will fracture in the gauge length, whereas the XY-sided specimens will fail at the shoulder. This is believed to be due to defects being generated during the printing process in the shoulder for the XY-sided specimens. Furthermore, from the tabulated results, it can clearly be observed that the only specimens which have comparable mechanical properties to what is stated by Markforged, is the XY-flat specimens.

Figure 3. Fractured specimens

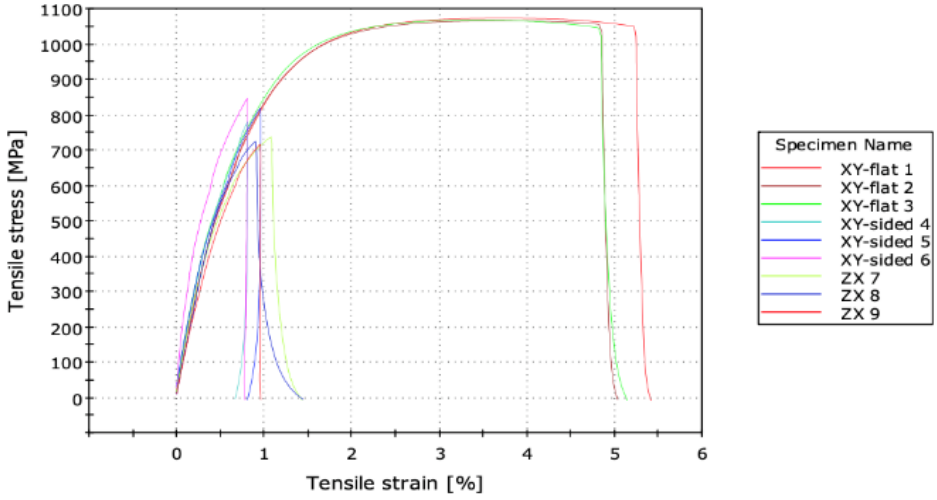

Figure 4. Stress-strain curves for the specimens

Table 1. Summary of mechanical properties

Specimen	0 2% Yield strength (MPa)	Ultimate tensile strength (MPa)	Young's modulus (GPa)	Elongation at break (%)
Markforged as-sintered [18]	800	1050	140	5
XY-flat 1	661,00	1072,00	136,74	5,24
XY-flat 2	764,30	1065,00	115,59	4,85
XY-flat 3	638,80	1067,00	161,53	4,84
XY-sided 4	699,80	780,80	135,54	0,81
XY-sided 5	637,60	817,50	145,63	0,96
XY-sided 6	613,30	846,70	286,87	0,80
ZX 7	579,40	737,70	139,73	1,09
ZX 8	656,60	725,50	128,68	0,91
ZX 9	610,10	717,20	123,83	0,95

3.3 Optical light microscope inspection

The specimens used for microscope inspection were the samples displayed in Figure 2 d). The specimens were cut using a Struers Discotom-5 machine. After cutting, the specimens were cleaned, rinsed and dried. The samples were prepared to be able to investigate both the top and side view of the vertical and horizontally printed part. The samples were iteratively polished, as follows:

1. 220 µm grit for 2 minutes.
2. Diamond suspension (9 µm) 3 minutes.
3. Diamond suspension (3 µm) 3 minutes
4. Chem OP-AA oxide polishing 2 minutes

The samples were cleaned between each of the aforementioned steps, by the use of an ultrasonic cleaner (Struers Lavamin machine) to remove any remaining particles from the previous step. The resulting images taken from the optical light microscope can be seen in Figure 6.

From the images presented, it can clearly be seen that the material exhibits a mesh of defects throughout the specimen. This mesh of defects also seems to be related to the printing scheme used by the machine. By observing the top view of the polished specimens (Figure 6 a) and c)), it can be seen that there are continuous lines, similar to the printing scheme/strategy previously mentioned. Figure 6 c) especially show how the walls or outer perimeter was developed with 8 layers, whereas the internal region has a 45º angle to the outer perimeter. It is also noted that each of these layers have a continuous defect/line between each of the printed perimeter or "walls".

Furthermore, by looking at the examples presented in Figure 7, where a representation is made in regard to how the walls are printed and how the internal filling is performed, a) and b) respectively, it can be seen that the area within the red squares have a similar shape to the defects found in Figure 6 b) and d). Consequently, strengthening the argument that the defects come due to the method of printing.

The defects which were found were estimated using the software Olympus stream essentials, where it was found that the shortest dimension of the triangular defects would commonly be on the range 22-33µm, whereas the longest dimension would commonly be on the range 39-86 µm. The square defect would commonly have a diagonal length on the range of 66-83 µm.

Additionally, the surface roughness of the "as-printed" specimens, due to the iterative layers during the printing process can be observed in Figure 5. The measured distance from top to bottom was on the range 43-54µm. However, it should be noted that the surface condition mentioned here, is only in regard to the iterative layers placed, and the surface will not be as rough along the grooves of the roughness/layers presented here. As in the direction into or out of the picture.

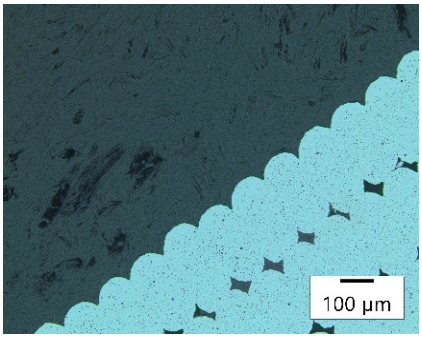

Figure 5. Surface condition

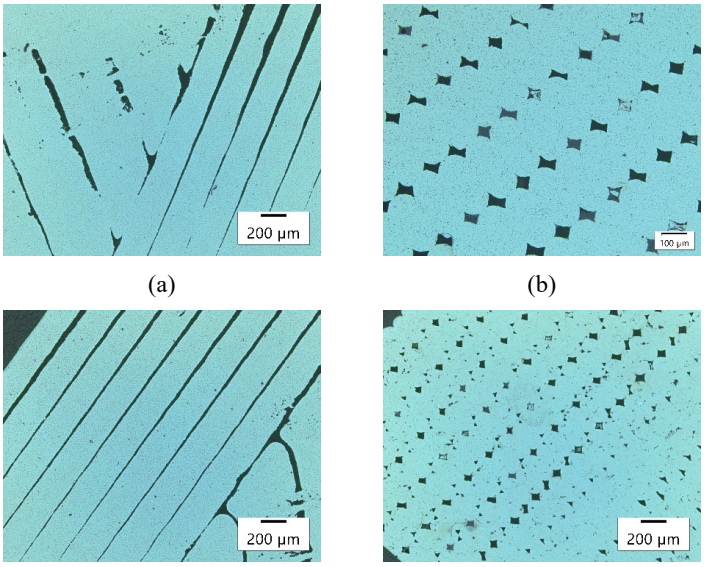

(a) (b)

(c) (d)

Figure 6. Images taken from optical light microscope, (a) top view vertical printed, (b) side view vertical printed, (c) top view of horizontal print, (d) side view of horizontal print

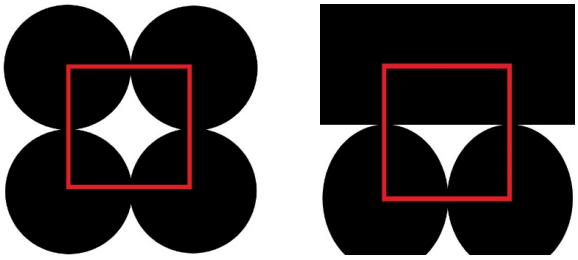

(a) (b)

Figure 7. Representations of defects found in the printed material, (a) square defect, (b) triangle defect

4. Discussion

4.1 Mechanical properties and defects

The specimens manufactured in the horizontal direction without any support (XY-flat) specimens, exhibited comparable ultimate tensile strength and elongation at break as listed by Markforged for the as-sintered condition. In contrast to the XY-flat printed specimens, both the XY-sided and ZX printed specimens exhibited worse mechanical properties than listed by Markforged for the as-sintered condition. Furthermore, the specimens XY-sided commonly fractured outside of the gauge length. This possibly due to a defect produced during the printing process.

The results obtained by tension testing the specimens clearly show that the build orientation of the specimens affects the resulting mechanical properties of the metal parts. Furthermore, during the light microscope inspection of the polished parts, it was found that there is a clear pattern of directional

defects which are directly correlated to the printing orientation. Consequently, resulting in the anisotropic behaviour observed in the experimental work.

Through the use of the images taken and presented in Figure 6, it can be seen that two defects commonly occur from the side view. One exhibits a shape similar to a diamond/square, whereas the other exhibits more a shape of a triangle, as is depicted in Figure 7. In fact, the defects within each specimen will be as follows in the reduced section:

1. Horizontally built flat (XY-flat): The outer wall will exhibit longitudinal defects as depicted in Figure 7 a), however, as the stress will act parallel to the length direction of the defect, minimal reduction of capacity is expected. The internally filled area will exhibit defects as presented in Figure 7 b), with a 45-degree angle to the applied loading direction. Furthermore, the grooves of the roughness presented in Figure 5 will also be parallel to the loading direction, consequently expecting it not to have a significant effect.
2. Horizontally built rotated (XY-sided): The outer wall, in the commonly failure region, will exhibit defects similar to the ones presented in Figure 7 a). However, at the shoulder of the specimen, the flaws will be perpendicular to the loading direction, potentially describing the cause and location of failure. The surface at the shoulder section will also be rough, similar to the roughness shown in Figure 5, in the direction perpendicular to the applied stress. Furthermore, the interior will have similar flaws as the interior in the previously explained specimen, however rotated by 90 degrees. In the gauge length, the specimen will again have a similar defect mesh as presented for the previous specimen. This explains the reason why it failed at the shoulder.
3. Vertically built (ZX): The outer wall will exhibit flaws similar to Figure 7 a), throughout the entire specimen, which will also be perpendicular to the loading direction. In addition, the surface roughness of the section will be as presented in Figure 5, where the applied loading will act perpendicular to the roughness/grooves. Furthermore, the internal section of the specimen will have a mesh of defects as presented in Figure 7 b), where the applied loading will act perpendicular to the longest direction of the defects, which was on the range 39-86μm.

The mechanical properties and light microscopy inspection and the discussion herein coincide well. This from the perspective that the mechanical properties are easily explained by the defects observed within the material. From the defects observed, the ultimate tensile strength from best to worst should be 1. XY-flat, 2. XY-sided, 3. ZX, which is confirmed in Table 1.

4.2 Fatigue considerations

Herein, no fatigue tests were performed in regard to the BMD printing method. However, a general comment in regard to potential fatigue capacity should be made, considering some of the main industries motivating for additive manufacturing are such as automotive, aerospace, energy oil and gas, mentioned in the introduction. This from the perspective that automotive, aerospace and energy oil and gas industries all commonly have to consider dynamic loading.

From the tensile testing, it was clearly noted that the material exhibited anisotropic mechanical properties. Furthermore, during the inspection of the material with light microscopy, it was found that a mesh of defects, similar to cracks, were present. Consequently, resulting in that the following can be expected during fatigue loading:

1. The fatigue capacity will also be anisotropic.
2. The material/specimens might have a reasonable fatigue capacity for the specimens printed in the XY-flat orientation, however, both the XY-sided and ZX specimens are expected to have a very poor fatigue capacity. This from the crack's orientation to the applied cyclic loading.

4.3 Suggestions for further research

As previously mentioned, the printed specimens exhibited a fine mesh of defects, depending on the printing orientation of the specimen. Furthermore, the surface finish of the as-printed specimens was observed to be poor (rough surface). Therefore, it is believed that a post processing strategy might significantly improve the mechanical properties of the material. This might be such as:

1. Hot isostatic pressing (HIP) to reduce the size of the defects present in the specimen.
2. Machining the surface to achieve a smooth surface.

5. Conclusions

Herein, the method of BMD metal printing was assessed, in regards to printing direction, and defects present within the final product. Main activities and findings are presented as follows:

1. Specimens were manufactured by the BMD method with three different printing orientations, tension tested in accordance with ASTM E8/E8M and compared with the mechanical properties presented by Markforged.
2. Anisotropic behaviour in regard to the printing orientation was found.
3. Samples were prepared and inspected with the use of an optical light microscope, where a clear mesh of defects similar to cracks were noticed, and an estimated size was presented.
4. The mesh of defects was discussed and related to the mechanical properties.
5. Application of components printed by the BMD method was discussed in light of dynamic loading (fatigue) on the basis of the mechanical properties and defects found.
6. Suggestions for further research was proposed, as in the possibility of post processing to improve mechanical properties/behaviour.

Acknowledgement

The authors are grateful for the support provided by Jørgen Grønsund, Jan-Tore Jakobsen, Johan A. Thorkaas and Mats Ingdal during the experimental work.

References

[1] ASTM 2021 *Additive Manufacturing Overview*. [Online] [cited 09.09.2021]; Available from: https://www.astm.org/industry/additive-manufacturing-overview.html.
[2] Milewski J 2017Additive Manufacturing of Metals: From Fundamental Technology to Rocket Nozzles, Medical Implants, and Custom Jewelry. Additive Manufacturing of Metals,.
[3] Zadi-Maad A, Rohib R and Irawan A 2018 Additive manufacturing for steels: a review. *IOP Conf Series*: *Mater Sci Eng* **285**, 012028.
[4] Ngo T D, Kashani A, Imbalzano G, Nguyen K T Q and Hui D 2018 Additive manufacturing (3D printing): A review of materials, methods, applications and challenges. *Compos Part B*: Eng,. **143**, 172-96.
[5] DebRoy T, Wei H L, Zuback J S, Mukherjee T, Elmer J W, Milewski J O, et al., 2018 Additive manufacturing of metallic components – Process, structure and properties. *Progress Mater Sci* **92**, 112-24.
[6] Molaei R and Fatemi A 2019 Crack paths in additive manufactured metallic materials subjected to multiaxial cyclic loads including surface roughness, HIP, and notch effects. *Int J Fatigue* **124**, 558-70.
[7] Equinor. From designer's dream to production reality: Spare parts on the fly. [Online] 2021; Available from: https://www.equinor.com/en/magazine/fieldmade-3d-printing-spare-parts.html.
[8] Blakey-Milner B, Gradl P, Snedden G, Brooks M, Pitot J, Lopez E, et al., 2021 Metal additive manufacturing in aerospace: A review. *Mater Des.* **209**, 110008.
[9] Appleyard D 2015 Powering up on powder technology. Metal Powder Report,. **70**(6), 285-89.
[10] Herzog D, Seyda V, Wycisk E and Emmelmann C 2016 Additive manufacturing of metals. *Acta Materialia*. **117**, 371-392.
[11] Nezhadfar P D, Burford E, Anderson-Wedge K, Zhang B, Shao S, Daniewicz S R, et al., 2019 Fatigue crack growth behavior of additively manufactured 17-4 PH stainless steel: Effects of build orientation and microstructure. *Int J Fatigue* **123**, 168-79.

[12] Afkhami S, Dabiri M, Alavi S H, Björk T and Salminen A 2019 Fatigue characteristics of steels manufactured by selective laser melting. *Int J Fatigue* **122,** 72-83.
[13] Wang Z, Wu W, Qian G, Sun L, Li X and Correia J A F O 2019 In-situ SEM investigation on fatigue behaviors of additive manufactured Al-Si10-Mg alloy at elevated temperature. Engineering Fracture Mechanics,. **214**, 149-63.
[14] Markforged. Metal X System. [Online] [cited 2021 13.09.2021]; Available from: https://markforged.com/3d-printers/metal-x.
[15] Desktop-metal. Deep Dive: Bound Metal Deposition (BMD). [cited 2021 13.09.2021]; Available from: https://www.desktopmetal.com/resources/deep-dive-bmd.
[16] Watson, A., J. Belding, and B.D. Ellis, Characterization of 17-4 PH Processed via Bound Metal Deposition (BMD). 2020. Cham: Springer International Publishing.
[17] ASTM-International, ASTM E8 / E8M-21: Standard Test Methods for Tension Testing of Metallic Materials. 2021.
[18] Markforged. 17-4 PH Stainless Steel - Datasheet. [Online] 2021 15.09.2021]; Available from: https://markforged.com/materials/metals/17-4-ph-stainless-steel / https://static.markforged.com/downloads/17-4-ph-stainless-steel.pdf.